The Light Way Towards Bioactive and Antifouling Coatings

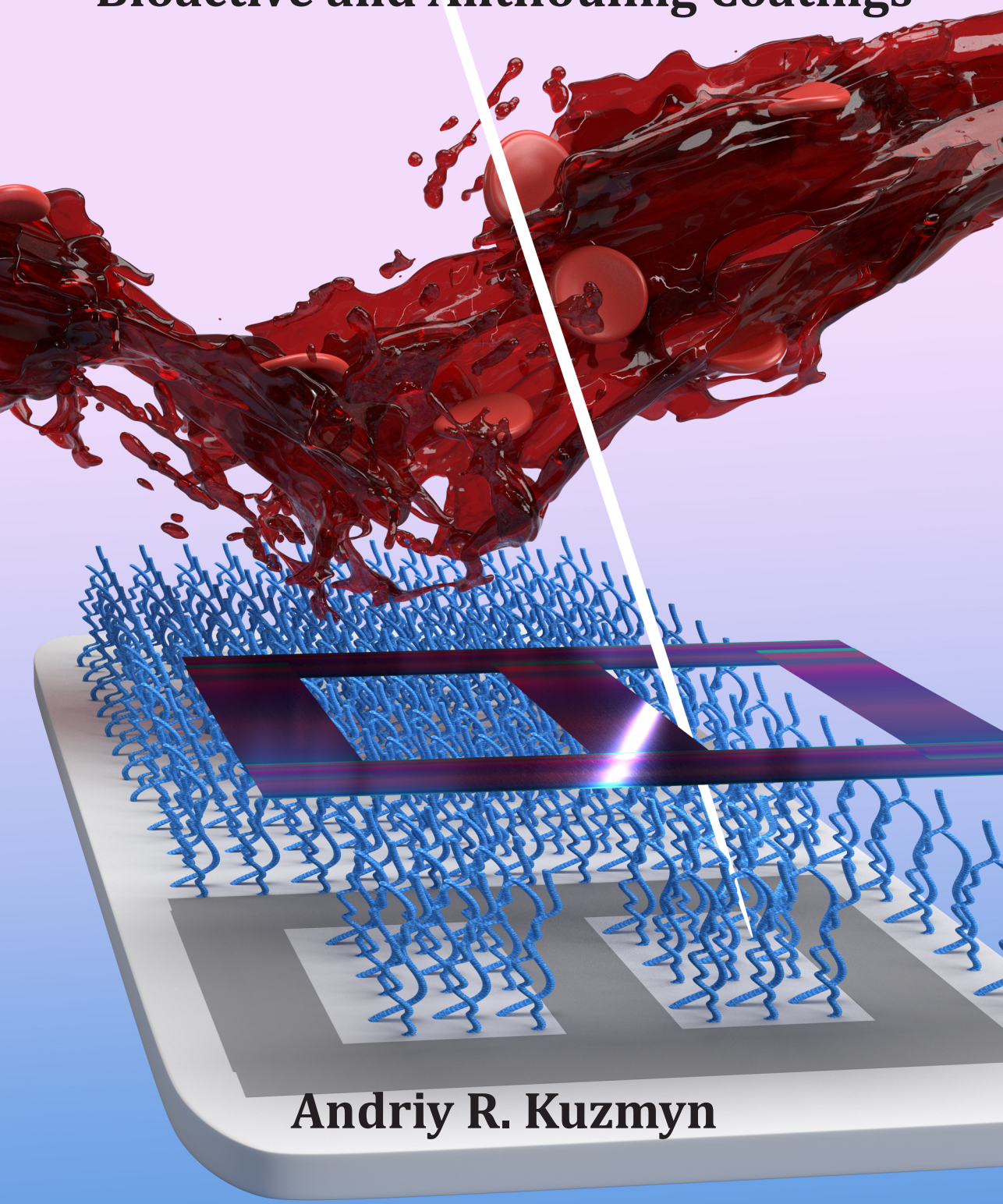

Andriy R. Kuzmyn

Prepositions

1. *N*-hydroxypropyl methacrylamide (HPMA) should be the central element in any antifouling polymer brush. (this thesis)
2. The energy- and atom-efficiency of PET-RAFT polymerizations, in combination with their robustness and options for reaction control, make them a hallmark for 21st-century chemistry. (this thesis)
3. Time is the main antagonist in the story, in which polymerization control is the protagonist.
4. The task of building a high-grafting density polymer brush by a "grafting to" approach is as challenging as constructing a dense rainforest from the fully grown trees.
5. Fitting of XPS spectra based on DFT calculations will save you from accidentally fitting a giraffe or elephant into the experimental data.
6. A good scientist is not defined by race, nationality, gender, or sexual orientation, but by the ability to dream, hope, learn and think creatively.
7. Those who forget the real world outside of the lab are deemed to live in an imaginary one.
8. The true nature of things is only understood in comparison.

Propositions belonging to the thesis entitled:

"The light way towards bioactive and antifouling coatings"

Andriy R. Kuzmyn

Wageningen, June 17, 2021

The Light Way Towards Bioactive and Antifouling Coatings

Andriy R. Kuzmyn

Thesis committee

Promotor

Prof. Dr H. Zuilhof

Professor of Organic Chemistry

Wageningen University & Research

Co-promotor

Dr J. Baggerman

CTO, Aquamarijn Micro Filtration BV, Zutphen

Other members

Prof. Dr J. van der Gucht, Wageningen University & Research

Dr S. de Beer, University of Twente

Prof. Dr A. Rosenhahn, Ruhr-Universität Bochum, Germany

Prof. Dr A. Laschewsky, Universität Potsdam, Germany

This research was conducted under the auspices of the Graduate School VLAG (Advanced studies in Food Technology, Agrobiotechnology, Nutrition and Health Sciences).

The Light Way Towards Bioactive and Antifouling Coatings

Andriy R. Kuzmyn

Thesis

submitted in fulfilment of the requirements of the degree of doctor

at Wageningen University

by the authority of the Rector Magnificus,

Prof. Dr A.P.J. Mol,

in the presence of the

Thesis Committee appointed by the Academic Board

to be defended in public

on Thursday 17 June 2021

at 11 a.m. in the Aula.

Andriy R. Kuzmyn

The light way towards bioactive and antifouling coatings,

166 pages.

PhD thesis, Wageningen University, Wageningen, the Netherlands (2021)

With references, with summary in English

ISBN: 978-94-6395-735-9

DOI: https://doi.org/10.18174/542757

Contents

Chapter 1

General Introduction

Protein Fouling

In a wide range of situations, surfaces will come into contact with solutions that contain proteins. Such situations may be everyday ones that are easy to see, such as evident from the growth of biofilms on ship hulls, or less obvious ones, such as protein adsorption on surfaces of the biosensor. In such situations, the proteins will non-specifically adsorb onto the surface in contact with the fluid. This process is also called *protein fouling* (Figure 1).[1-6] For examples related to human health, the biological fluid in this process may be blood that interacts with a biosensor's surface detecting pathogens or artificial valves in the heart.[7] The fluid may be a lymph or extracellular matrix that interacts with an artificial implant.[8] It also can be seawater, in which protein adsorption is the first step in the marine fouling process.[9-10] One might think that this simple protein adsorption process should not affect those devices' performance. However, in the case of biosensors, the biosensor that detects pathogens in the blood will typically have a problem distinguishing accurately between the pathogenic or biomarking molecule and any non-specifically adsorbed protein.[11] The lifetime and biocompatibility of, for example, artificial heart valves and implants are evidently affected by those randomly adsorbing proteins.[6, 12] The speed and fuel consumption of the ship sailing in the sea is strongly influenced by the aforementioned marine fouling.[13-15] Thus, protein fouling is a problem that prevents and hinders the performance of many biomedical and biotechnological devices.

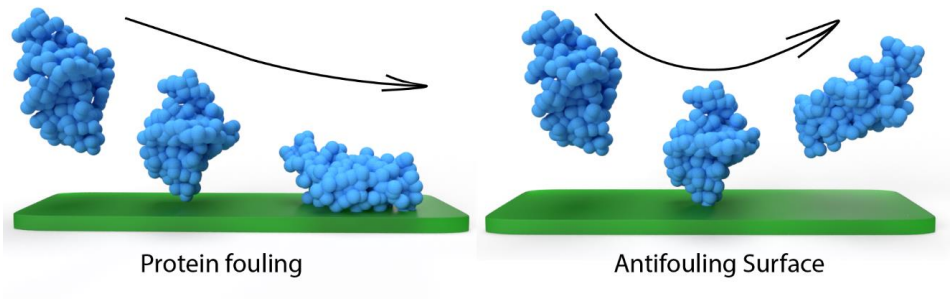

Figure 1. Schematic representation of protein fouling on surfaces and antifouling surfaces.

There is no simple or single answer to the question: *"Why proteins stick so well to almost any material?"*. The problem of protein fouling is complex because of the complex and widely different structures of proteins. The interactions between different types of proteins in

biological fluids and surfaces are dependent on numerous factors, such as charge, hydration, structure, and bioaffinity. The process of protein fouling is supported by different protein-protein interactions, e.g., generically via the Vroman effect,[16] but also in a steered manner via cascades of different biological responses, including thrombocytes and c-complement activation.[17-18] The interaction between proteins and a surface typically happens in aqueous solutions. Thus, the interactions with water molecules and the organization of water molecules on both the surface and on proteins are probable key puzzle pieces for the understanding of protein fouling. The protein may displace or interfere with a relatively structured layer of water close to the surface.[3-4, 19] This process likely constitutes a large component to the overall driving force for the first proteins to either adsorb or not adsorb onto the surface. Thus, one type of antifouling materials can be thought of as strongly binding water, making protein interference with it impossible—ultimately creating a water shield on the surface, additionally making the surface "invisible" for proteins. According to some studies, upon the approach of the protein towards the surface coated with the antifouling layer, the layer puts pressure on water molecules what creates a thermodynamically unfavorable osmotic penalty.[19-20] On the other hand, highly hydrophobic materials are also considered to have good antifouling properties. The antifouling mechanism there is based on those materials' property to reject water and consequently readily release any adsorbed proteins and cells.[21-22]

Antifouling Coatings

Antifouling coatings are layers that prevent the non-specific adsorption of proteins. For both the highly hydrophilic and hydrophobic surfaces, there are numerous approaches for creating antifouling coatings. The layers can be differentiated by chemical compositions based on hydrophilic molecules: dextrans,[23] proteins,[11] amino acids,[10, 24] oligoethylene oxides,[25-27] zwitterionic moieties,[5, 9, 28-32] and hydrophobic molecules: perfluoropolyethers[22] and polysiloxanes.[21] The layers can further be divided by their architectures: self-assembled monolayers (SAMs),[2] physadsorbed layers,[11, 23] and polymer brushes.[1, 5-6, 25-26, 32-42] The surface's passivation with single or multiple proteins solutions limits the nonspecific interactions. SAMs have proven to be highly effective in prevention fouling from single-protein solutions. However, they fail in contact with complex biological fluids.[6] The manifold of protein-protein interactions and cascades of bio-responses make searching for antifouling

coatings in biofluids challenging. The presence of "domino-like" systems in blood, plasma, and lymph turn the adsorption of one protein into the adsorption of tens or hundreds of proteins on the material. Thus, the creation of non-fouling surfaces is typically hard in static complex fluids, but within living environments it seems an almost herculean task. Currently, the coatings that are most effective in preventing protein fouling from complex biological media, eukaryotic, and bacterial cells are based on *polymer brushes*.[6, 12, 32, 37, 42]

Polymer Brushes

So, "What is a polymer brush?" All polymer brushes are constituted from surface-bound polymers. However, not every attached polymer to the surface yields a polymer brush. The polymer on the surface may be structured in three different regimes of conformations depending on the density of polymer chains: "pancake", "mushroom", and "brush".[43-44] The "pancake" and "mushroom" are the low-density regimes (Figure 2). The polymer chains usually are collapsed or in a coiled state where the individual polymer chains almost do not interact with each other and are close to the surface. The polymer "brush" regime, on the other hand, is a high-density system where all polymer chains are close to each other, with an overall orientation stretching upwards of individual chains. Many surface-bound polymer systems are labeled as polymer brushes, with disregard for the grafting density. However, since the biological effects, including protein fouling, are highly dependent on that density, it makes sense to distinguish these regimes clearly.[30] Therefore, in this thesis, the term "brush" will be used only for high-density polymer chain regimes.

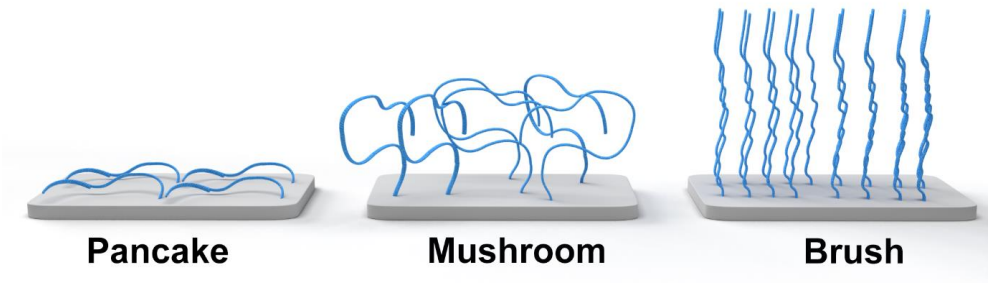

Figure 2. Schematic representation of different regimes of polymer on a surface.

Polymer brushes are typically synthesized in either of two different approaches, "grafting to" and "grafting from". The "grafting to" typically includes attaching the ready polymer to the surface. The straight-forward nature and one-step attachment advantages of this method

are balanced by commonly complex polymer syntheses and isolations and lower grafting densities accessible for this method. The polymer brushes are commonly synthesized by a "grafting from" approach that allows creating polymer systems with higher grafting densities and thicknesses. The polymer is grown from an initiator layer on the surface. Each polymer chain is like a tree in a dense rain forest, rising towards the sun. The initiator layer is serving as the seed for future chains of polymers. The growth of a monomorphic and well-structured polymer brushes layer from the surface requires a highly controlled polymerization technique. In practice, it requires as many as possible initiator seeds sprout to produce the trees with more or less the same height. Just like we rarely see a rain forest with trees that all have the same height, finding the right instrument on a nano level to achieve this is a challenge on its own. The currently best instruments to achieve this are surface-initiated controlled radical polymerizations, such as atom transfer radical polymerization (ATRP),[1, 5-6, 12, 25, 35, 38] reversible addition−fragmentation chain-transfer polymerization (RAFT),[45-48] and their derivative techniques. Those polymerizations create polymers with a low polydispersity ($M_w/M_n < 1.5$), also on a surface.[28, 49-50] Thus, most polymer chains grew from the surface have similar heights, thereby creating a low-roughness coating. Despite being commonly applied in industry, the traditional free radical polymerization does not allow us to achieve the livingness or control over the polymerization provided by ATRP and RAFT, and surface-initiated variants thereof yield highly polydisperse and typically thin (< 10 nm) coatings: without control, no success.[51]

Controlled Living Polymerizations

Polymerization is the process of reacting individual molecules together to form polymer chains.[52] The polymer may be created via two main polymerization reactions: step-growth or chain-growth.[53] In step-growth polymerizations monomers combine to larger units at each step, which then again couple to (increasingly larger) reactive moieties to form a longer polymer molecule; in chain-growth polymerization, monomers add to the growing polymer chains with an active center such as a free radical. To see how these can be turned into well-controlled polymerization reactions, let us compare uncontrolled free-radical polymerizations with its controlled variants. In free-radical polymerizations, four main stages can be distinguished: initiation, propagation, termination, and chain transfer. (Figure 3) During the initiation, the active center of polymerization is created. As the initiator($I^{\bullet}$) – "locomotive" is

the first carriage in a long train. The propagation stage includes adding the monomers (M) – "passenger carriages" to the train – polymer (P_n, P_m). The termination is a process in which the addition of new monomers to the chain is stopped, and the active center of polymerization is deactivated. It may happen due to the connection of two radical chains, interactions with impurities, or radical disproportionation. This termination process is eventually inevitable. This termination thus has to be outcompeted by chain transfer steps. Chain transfer occurs when the radical is transferred from a growing chain to a solvent, monomer, initiator, or another polymer chain. Free-radical polymerization is the most commonly applied polymerization technique to create polymers. However, it provides only poor control over the final polymer's polydispersity and its molecular weight, and uncontrolled chain terminations and chain transfer reactions are the main causes of this. In the controlled variant of living polymerizations, such as ATRP or RAFT, chain termination is reduced to a minimal level. In contrast, chain transfer is now actually made intrinsic to chain elongation, yielding entirely different polymerization kinetics.

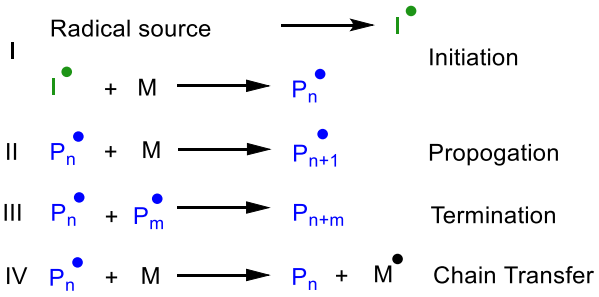

Figure 3. Schematic depiction of free radical polymerization.

Atom transfer radical polymerization (ATRP) is a reversible-deactivation radical polymerization. This technique was independently discovered by Mitsuo Sawamoto[54] and by Krzysztof Matyjaszewski and Jin-Shan Wang.[49] At the heart of this polymerization is a reversible complex between alkyl halides (in further stages macromolecular halides) and a transition-metal catalyst (Figure 4). The transition-metal catalyst acts as a halogen atom carrier in a reversible redox process, creating a transient radical species that will transfer a radical species to a monomer and start a polymerization. The high degree of control over polydispersity and molecular weight of the final polymer allows applying this technique to create polymer brushes. The polymer brushes can be grown from halogen-terminated self-

assembled monolayers with readily abstractable halogen atoms. The polymerization proceeds with vinyl or acrylic monomers and a transition-metal ligand complex as catalyst.

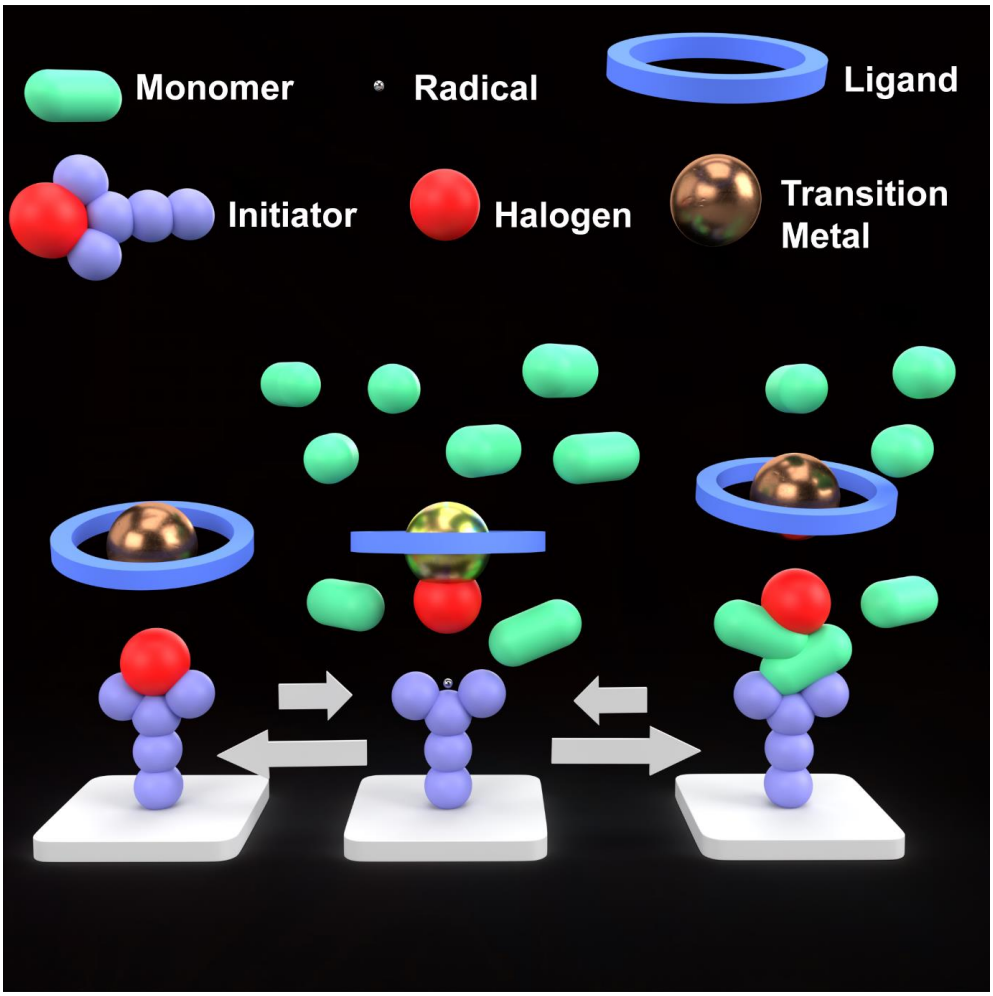

Figure 4. Schematic depiction of the ATRP mechanism on a surface.

Reversible addition-fragmentation chain transfer (RAFT) polymerization applies a chain-transfer agent (typically containing a thiocarbonylthio moiety) to achieve control over molecular weight and polydispersity during a free-radical polymerization.[55-56] The polymerization was discovered in the Commonwealth Scientific and Industrial Research Organisation (CSIRO) team of scientists led by David Solomon and Ezio Rizzardo.[57] The RAFT polymerization utilizes thiocarbonylthio compounds as chain-transfer agents or RAFT agents to achieve control over the polydispersity and molecular weight of the final polymer. In this

type of polymerization, the initiator and monomer are present as in traditional free-radical polymerizations. RAFT polymerization mechanism starts with creating radical species similar to the free radical polymerization step I (Figure 5). Following the addition of the radical species to the RAFT agent (chain transfer agent, CTA), the radical species enter an equilibrium between active and dormant species (steps III and V). The RAFT agent regulates the processes that typically affect the control and livingness of polymerization (chain terminations and chain transfer reactions). The free radical from the initiator or growing chain is transferred to the chain transfer agent creating the main RAFT equilibrium (step V, Figure 5).[58] The RAFT polymerization was applied to synthesize polymer brushes by immobilization of the RAFT agent on the surface.[47, 59] The further introduction of photoredox systems to ATRP and RAFT polymerizations allows conducting photo-triggered controlled polymerizations.

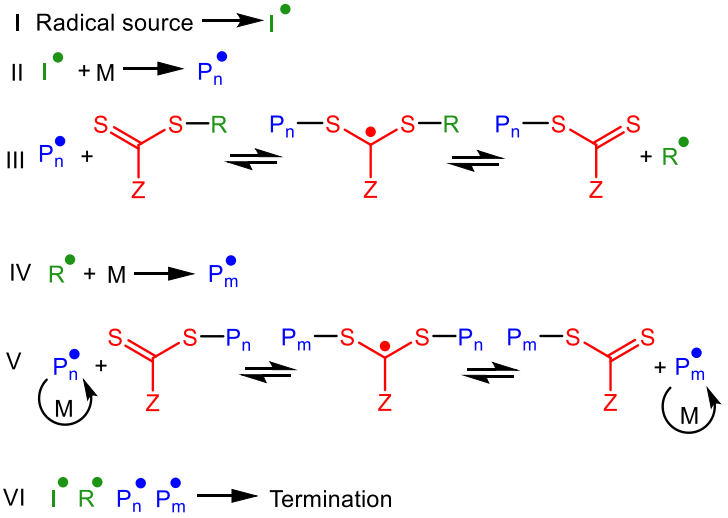

Figure 5. Proposed Mechanism of Reversible Addition−Fragmentation Chain Transfer Polymerization.[28]

Surface-initiated light-triggered controlled polymerization

After being around for about two decades in thermally induced variations, in the last decade also light-induced variants of ATRP and RAFT have been developed. The introduction of photo-triggered controlled/living polymerizations transforms the polymer synthesis into likely one of the most tolerant and versatile chemical reactions feasible: it has the potential to offer user-friendly, atom-and energy-efficient syntheses with precise molecular weight

control, yet allows the inclusion of an extremely wide range of reactants in several distinct stages of the process, to allow highly diverse compositions of the growing polymer chains.[60-62] One of the main advantages of this technique is use of light as an on and off switch of the polymerization.[61-62] Typically, the polymerization catalyst is activated by exposure to light. This aspect opens the route for creating complex 3D nanostructures. Solar energy is the most widely available energy source on Earth and the most common energy source and regulator in nature. Most biopolymers are created utilizing visible spectrum solar light directly or indirectly. Most photo-triggered controlled polymerizations resemble traditional ATRP and RAFT processes. Typically, those processes utilize the same initiators or chain transfer agents such as alkyl halides (ATRP) or thiocarbonylthios (RAFT). The photocatalyst in this process is a transition metal complex, or the more eco-friendly options like organic dye molecules, such as methylene blue, fluorescein, rhodamine 6G, Nile red, and eosin Y.[63] The mechanism of photo-triggered controlled polymerizations can be divided into two categories: bond cleavage or energy transfer processes, and photoredox processes. In the first case, the temporally excited state species (typically: radicals) are created. In the second, single electron transfer is the triggering process for polymerization.[63-64]

Surface-initiated Photoinduced Electron Transfer-Reversible Addition–Fragmentation Chain Transfer Polymerization (SI-PET-RAFT)

The combination of RAFT agents and photoredox catalysis introduced PET-RAFT technology. The photo-triggered nature of this polymerization allows easy control of reactions by turning the light source on/off.[63-64] The RAFT agent provides the opportunity to regulate the molecular weight and polydispersity of the final polymer. Furthermore, the use of heavy metal-free catalysts yields tools for green polymer synthesis. The immobilization of the RAFT agent on the surface thus presents a route for applying RAFT and PET-RAFT techniques of polymerization to surfaces, and the creation of polymer brushes by those methods.[45, 47] The mechanism of this polymerization is similar to traditional RAFT polymerization with the addition of a photocatalyst that initiates the polymerization. The excitation of the photocatalyst under visible-light illumination triggers an electron transfer to the thiocarbonylthio moiety and starts the RAFT polymerization.[64] SI-PET-RAFT mechanism can be further demonstrated in the example of Eosin Y(EY) as photocatalyst and triethylamine(TEA) as co-catalyst. (Figure 6) The EY and TEA systems can initiate a free radical

polymerization under light in an oxygen-containing environment. The electronically excited state of EY (EY*) was previously demonstrated to be capable of readily accepting an electron (*i.e.*, photo-induced electron transfer or PET). TEA or any other tertiary amine can act as an electron donor able to transfer an electron to EY* to produce an EY radical anion.[63-65] Despite the relative complexity of the PET-RAFT mechanism, the polymerization can be easily applied for a wide range of applications, including polymer brush synthesis due to its robust oxygen tolerance and a widely available cheap catalyst.

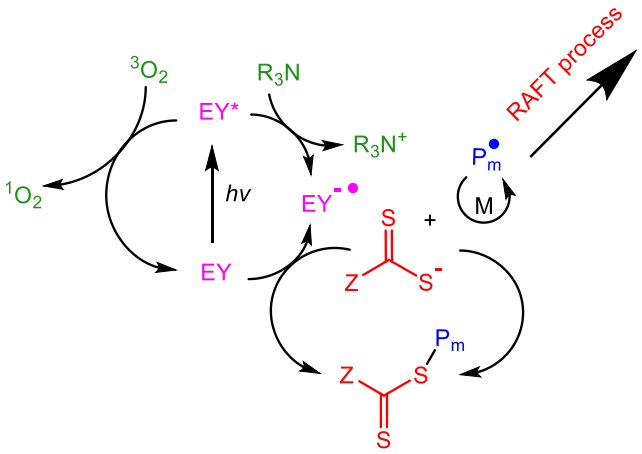

Figure 6. General scheme of the proposed mechanism of SI-PET-RAFT. [66-67]

Antifouling Polymer brushes

As indicated above, water-binding polymer brushes provide significant potential as antifouling coatings. As 'best in their class' examples, polymer brushes based on *N*-(2-hydroxypropyl) methacrylamide, oligo(ethylene glycol) methacrylate, and zwitterionic methacrylic monomers (carboxybetaine, sulfobetaine, and phosphocholine, methacrylate and methacrylamide derivatives) and their derivatives have shown an unparalleled resistance against protein fouling from complex biological fluids, such as blood serum, and media containing eukaryotic and bacterial cells (Figure 7). Yet, some differences are worthwhile to note. Oligoethylene glycol-based polymer brushes have shown effective resistance towards biological fluids, with the non-specific adsorption onto those surfaces from blood plasma in the range from 10 - 50 pg·mm^2.[6, 26] Moreover, the use of polymerizations with a relatively good living character allows for smooth polymer brushes and chain end biofunctionalization

with the preservation of most antifouling properties. The main drawbacks of the oligo(ethylene glycol) based polymer brush coatings are the lack of functional groups, low loading biofunctionalization, and the long-term instability of the layers.

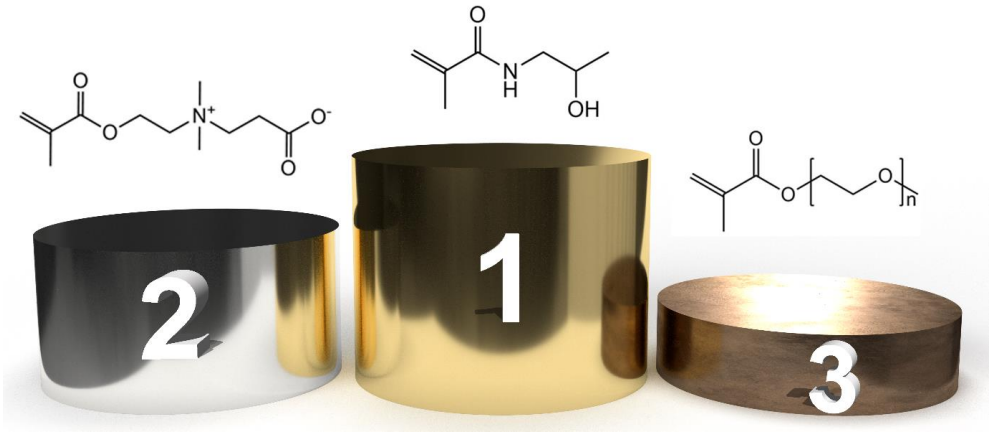

Figure 7. Main chemical types of antifouling monomers arranged by resistance to non-specific protein adsorption of corresponding polymer brushes.

Zwitterionic-based poly(carboxybetaine) and poly(sulfobetaine) brushes show an even better resistance against protein fouling, with even full blood serum fouling down to the range of 10 - 30 pg·mm^{-2}.[5-6, 35] Their strong affinity towards water is theorized to be one of the main reasons for their antifouling properties. Besides this, the possibility of biofunctionalization, by applying the trivial technique of NHS/EDS active esters (in case of carboxybetaines),[5, 32] or via charge-neutral alkyl azide-based sulfobetaines,[29] have shown these classes to function well in the creation of bioactive interfaces.

Finally, the best antifouling performance was observed for *N*-(2-hydroxypropyl) methacrylamide (HPMA) and some of its derivatives, effectively reaching the limit of detection of highly sensitive techniques such as SPR in protein fouling in the range from 3 - 10 pg·mm^{2}.[6, 35, 37, 42] It can be said that the success of these HPMA brushes is somewhat of a riddle: where the theory behind the success of zwitterionic brushes is well developed, it seems counterintuitive that HPMA would equal this, or even be slightly better in a direct comparison.[29] However successful in its antifouling characteristics, there is a drawback to these HPMA-based brushes, as the biofunctionalization of these polymer brushes is complex due to the lack of an easily activated group. Thus, the combination of HPMA with

carboxybetaine in random polymer brushes comes to mind, and this combination was shown to be an excellent platform for creating biointerfaces for biosensors and biomedical devices.[32, 68-69]

Thesis outline

Polymer brushes based on zwitterionic, *N*-(2-hydroxypropyl) methacrylamide, and oligo(ethylene glycol) methacrylate derivatives can function as excellent coatings to prevent protein fouling from various biological fluids. However, to be applicable in a truly wide range of biomedical and biotechnological applications, it is crucial that they can be prepared in a simple and robust manner and that they allow for a flexible and preferably easy-to-apply biofunctionalization. This thesis aims to develop new approaches in the creation of antifouling coatings and their biofunctionalization.

In chapter 2, hierarchical bioactive surfaces were created by visible-light-induced surface-initiated living radical polymerization employing tris[2-phenylpyridinato-C2,N]-iridium(III) as a photocatalyst. Hierarchical antifouling diblock copolymer structures were grown consisting of *N*-(2 hydroxypropyl)-methacrylamide (first block) and carboxybetaine methacrylate (second block). The living nature of the polymerization allowed after attachment of the first block the reinitiation of polymerization with the second biofunctionalizable block, and also to create a patterned layer by building controlled biofunctionalized spots onto a uniform and the generically antifouling underlayer. Despite the well-controlled nature of this approach, it still requires an inert atmosphere and minor degassing, which prompted us to introduce the PET-RAFT technique for the creation of antifouling coatings in the following chapters.

Chapter 3 describes our work towards an easy, robust, and environmentally friendly method of creating antifouling coatings in an aqueous environment, i.e., under atmospheric conditions without any prior degassing and using heavy-metal catalysts. This new method for synthesizing antifouling polymer brushes hinges on a novel surface-initiated photoinduced electron transfer–reversible addition-fragmentation chain transfer (SI-PET-RAFT) polymerization with Eosin Y and triethanolamine as catalysts. This technique was applied to the preparation of polymer brushes derived from three different monomers: oligo(ethylene glycol) methacrylate, *N*-(2-hydroxypropyl)methacrylamide, and carboxybetaine methacrylamide. The polymer brushes demonstrated excellent antifouling properties when exposed to either single-protein solutions or to complex biological matrices, such as diluted bovine serum.

The work in chapter 3, however, still required a well-defined initiator layer to start the brush growth from. While this works fine in an academic research lab, it hampers the easy

transferability towards larger-scale applications. Therefore, in chapter 4 we describe the approach of PET-RAFT polymerization to be extended in the synthesis of a surface-bound bottlebrush polymer. This polymer is constructed with a poly-L-lysine backbone and *N*-(2-hydroxypropyl)methacrylamide side chains, with the latter containing 5% carboxybetaine methacrylamide monomers that eventually allow for additional (bio)functionalization in solution or after surface immobilization. This approach allowed the one-step creation of antifouling and biofunctional surfaces, and both are discussed in detail.

Chapter 5 further explores the possibilities of SI-PET-RAFT polymerization for creating antifouling polymer brushes on gold surfaces. We have further explored this polymerization's livingness for the creation of diblock and random copolymer brushes based on *N*-(2-hydroxypropyl)methacrylamide and carboxybetaine methacrylamide monomers. It will allow the functionalization of those brushes with biologically active moieties.

Finally, chapter 6 aims to place the obtained results in a broader context and provides recommendations for further research.

References

1. Baggerman, J.; Smulders, M. M. J.; Zuilhof, H., Romantic Surfaces: A Systematic Overview of Stable, Biospecific, and Antifouling Zwitterionic Surfaces. *Langmuir* **2019,** *35* (5), 1072-1084.

2. Chapman, R. G.; Ostuni, E.; Takayama, S.; Holmlin, R. E.; Yan, L.; Whitesides, G. M., Surveying for Surfaces that Resist the Adsorption of Proteins. *Journal of the American Chemical Society* **2000,** *122* (34), 8303-8304.

3. Le-Clech, P., Protein Fouling. In *Encyclopedia of Membranes*, Drioli, E.; Giorno, L., Eds. Springer Berlin Heidelberg: Berlin, Heidelberg, 2015; pp 1-2.

4. Le-Clech, P., Protein Fouling Mechanisms. In *Encyclopedia of Membranes*, Drioli, E.; Giorno, L., Eds. Springer Berlin Heidelberg: Berlin, Heidelberg, 2015; pp 1-2.

5. Jiang, S.; Cao, Z., Ultralow-Fouling, Functionalizable, and Hydrolyzable Zwitterionic Materials and Their Derivatives for Biological Applications. *Advanced Materials* **2010,** *22* (9), 920-932.

6. de los Santos Pereira, A.; Rodriguez-Emmenegger, C.; Surman, F.; Riedel, T.; Alles, A. B.; Brynda, E., Use of Pooled Blood Plasmas in the Assessment of Fouling Resistance. *RSC Advances* **2014,** *4* (5), 2318-2321.

7. Jones, M. I.; McColl, I. R.; Grant, D. M.; Parker, K. G.; Parker, T. L., Protein Adsorption and Platelet Attachment and Activation, on TiN, TiC, and DLC Coatings on Titanium for Cardiovascular Applications. *Journal of Biomedical Materials Research* **2000,** *52* (2), 413-421.

8. Wang, Z.; Yan, Y.; Qiao, L., Protein Adsorption on Implant Metals with Various Deformed Surfaces. *Colloids and Surfaces B: Biointerfaces* **2017,** *156*, 62-70.

9. Yu, Y.; Cirelli, M.; Li, P.; Ding, Z.; Yin, Y.; Yuan, Y.; de Beer, S.; Vancso, G. J.; Zhang, S., Enhanced Stability of Poly(3-sulfopropyl methacrylate potassium) Brushes Coated on Artificial Implants in Combatting Bacterial Infections. *Industrial & Engineering Chemistry Research* **2019,** *58* (47), 21459-21465.

10. Huang, N.-P.; Michel, R.; Voros, J.; Textor, M.; Hofer, R.; Rossi, A.; Elbert, D. L.; Hubbell, J. A.; Spencer, N. D., Poly(l-lysine)-g-poly(ethylene glycol) Layers on Metal Oxide Surfaces: Surface-Analytical Characterization and Resistance to Serum and Fibrinogen Adsorption. *Langmuir* **2001,** *17* (2), 489-498.

11. Homola, J.; Dostálek, J.; Chen, S.; Rasooly, A.; Jiang, S.; Yee, S. S., Spectral Surface Plasmon Resonance Biosensor for Detection of Staphylococcal Enterotoxin B in Milk. *International Journal of Food Microbiology* **2002,** *75* (1), 61-69.

12. Rodriguez-Emmenegger, C.; Avramenko, O. A.; Brynda, E.; Skvor, J.; Alles, A. B., Poly(HEMA) Brushes Emerging as a New Platform for Direct Detection of Food Pathogen in Milk Samples. *Biosensors and Bioelectronics* **2011,** *26* (11), 4545-4551.

13. Hakim, M. L.; Nugroho, B.; Nurrohman, M. N.; Suastika, I. K.; Utama, I. K. A. P., Investigation of Fuel Consumption on an Operating Ship due to Biofouling Growth and Quality of Anti-fouling Coating. *IOP Conference Series: Earth and Environmental Science* **2019,** *339*, 012037.

14. Koschitzki, F.; Wanka, R.; Sobota, L.; Koc, J.; Gardner, H.; Hunsucker, K. Z.; Swain, G. W.; Rosenhahn, A., Amphiphilic Dicyclopentenyl/Carboxybetaine-Containing Copolymers for Marine Fouling-Release Applications. *ACS Applied Materials & Interfaces* **2020,** *12* (30), 34148-34160.

15. Townsin, R. L., The Ship Hull Fouling Penalty. *Biofouling* **2003,** *19* (sup1), 9-15.

16. Vroman, L.; Adams, A. L.; Fischer, G. C.; Munoz, P. C., Interaction of High molecular Weight Kininogen, Factor XII, and Fibrinogen in Plasma at Interfaces. *Blood* **1980,** *55* (1), 156-159.

17. Wei, Q.; Becherer, T.; Angioletti-Uberti, S.; Dzubiella, J.; Wischke, C.; Neffe, A. T.; Lendlein, A.; Ballauff, M.; Haag, R., Protein Interactions with Polymer Coatings and Biomaterials. *Angewandte Chemie International Edition* **2014,** *53* (31), 8004-8031.

18. Horbett, T. A., The Role of Adsorbed Proteins in Animal Cell Adhesion. *Colloids and Surfaces B: Biointerfaces* **1994,** *2* (1), 225-240.

19. Banerjee, I.; Pangule, R. C.; Kane, R. S., Antifouling Coatings: Recent Developments in the Design of Surfaces That Prevent Fouling by Proteins, Bacteria, and Marine Organisms. *Advanced Materials* **2011,** *23* (6), 690-718.

20. Jeon, S. I.; Andrade, J. D., Protein—surface Interactions in the Presence of Polyethylene Oxide: II. Effect of Protein Size. *Journal of Colloid and Interface Science* **1991,** *142* (1), 159-166.

21. Zhang, H.; Chiao, M., Anti-fouling Coatings of Poly(dimethylsiloxane) Devices for Biological and Biomedical Applications. *Journal of Medical and Biological Engineering* **2015,** *35* (2), 143-155.

22. Molena, E.; Credi, C.; De Marco, C.; Levi, M.; Turri, S.; Simeone, G., Protein Antifouling and Fouling-release in Perfluoropolyether Surfaces. *Applied Surface Science* **2014,** *309*, 160-167.

23. O'Shannessy, D. J.; Brigham-Burke, M.; Peck, K., Immobilization Chemistries Suitable for Use in the BIAcore Surface Plasmon Resonance Detector. *Analytical Biochemistry* **1992,** *205* (1), 132-136.

24. Li, W.; Liu, Q.; Liu, L., Amino Acid-based Zwitterionic Polymers: Antifouling Properties and Low Cytotoxicity. *Journal of Biomaterials Science, Polymer Edition* **2014,** *25* (14-15), 1730-1742.

25. Kuzmyn, A. R.; de los Santos Pereira, A.; Pop-Georgievski, O.; Bruns, M.; Brynda, E.; Rodriguez-Emmenegger, C., Exploiting End Group Functionalization for the Design of Antifouling Bioactive Brushes. *Polymer Chemistry* **2014,** *5* (13), 4124-4131.

26. Rodriguez Emmenegger, C.; Brynda, E.; Riedel, T.; Sedlakova, Z.; Houska, M.; Alles, A. B., Interaction of Blood Plasma with Antifouling Surfaces. *Langmuir* **2009,** *25* (11), 6328-6333.

27. Pereira, A. d. l. S.; Rodriguez-Emmenegger, C.; Surman, F.; Riedel, T.; Alles, A. B.; Brynda, E., Use of pooled blood plasmas in the assessment of fouling resistance. *RSC Advances* **2014,** *4* (5), 2318-2321.

28. Perrier, S., 50th Anniversary Perspective: RAFT Polymerization—A User Guide. *Macromolecules* **2017,** *50* (19), 7433-7447.

29. Lange, S. C.; van Andel, E.; Smulders, M. M. J.; Zuilhof, H., Efficient and Tunable Three-Dimensional Functionalization of Fully Zwitterionic Antifouling Surface Coatings. *Langmuir* **2016,** *32* (40), 10199-10205.

30. Ahmed, S. T.; Leckband, D. E., Protein Adsorption on Grafted Zwitterionic Polymers Depends on Chain Density and Molecular Weight. *Advanced Functional Materials* **2020,** *30* (30), 2000757.

31. Nguyen, A. T.; Baggerman, J.; Paulusse, J. M. J.; van Rijn, C. J. M.; Zuilhof, H., Stable Protein-Repellent Zwitterionic Polymer Brushes Grafted from Silicon Nitride. *Langmuir* **2011,** *27* (6), 2587-2594.

32. Lísalová, H.; Brynda, E.; Houska, M.; Víšová, I.; Mrkvová, K.; Song, X. C.; Gedeonová, E.; Surman, F.; Riedel, T.; Pop-Georgievski, O.; Homola, J., Ultralow-Fouling Behavior of Biorecognition Coatings Based on Carboxy-Functional Brushes of Zwitterionic Homo- and Copolymers in Blood Plasma: Functionalization Matters. *Analytical Chemistry* **2017,** *89* (6), 3524-3531.

33. Krause, J. E.; Brault, N. D.; Li, Y.; Xue, H.; Zhou, Y.; Jiang, S., Photoiniferter-Mediated Polymerization of Zwitterionic Carboxybetaine Monomers for Low-Fouling and Functionalizable Surface Coatings. *Macromolecules* **2011,** *44* (23), 9213-9220.

34. Rana, D.; Matsuura, T., Surface Modifications for Antifouling Membranes. *Chemical Reviews* **2010,** *110* (4), 2448-2471.

35. Rodriguez-Emmenegger, C.; Brynda, E.; Riedel, T.; Houska, M.; Šubr, V.; Alles, A. B.; Hasan, E.; Gautrot, J. E.; Huck, W. T. S., Polymer Brushes Showing Non-Fouling in Blood Plasma Challenge the Currently Accepted Design of Protein Resistant Surfaces. *Macromolecular Rapid Communications* **2011,** *32* (13), 952-957.

36. Vaisocherová-Lísalová, H.; Surman, F.; Víšová, I.; Vala, M.; Špringer, T.; Ermini, M. L.; Šípová, H.; Šedivák, P.; Houska, M.; Riedel, T.; Pop-Georgievski, O.; Brynda, E.; Homola, J., Copolymer Brush-Based Ultralow-Fouling Biorecognition Surface Platform for Food Safety. *Analytical Chemistry* **2016,** *88* (21), 10533-10539.

37. van Andel, E.; Lange, S. C.; Pujari, S. P.; Tijhaar, E. J.; Smulders, M. M. J.; Savelkoul, H. F. J.; Zuilhof, H., Systematic Comparison of Zwitterionic and Non-Zwitterionic Antifouling Polymer Brushes on a Bead-Based Platform. *Langmuir* **2019,** *35* (5), 1181-1191.

38. de los Santos Pereira, A.; Riedel, T.; Brynda, E.; Rodriguez-Emmenegger, C., Hierarchical Antifouling Brushes for Biosensing Applications. *Sensors and Actuators B: Chemical* **2014,** *202*, 1313-1321.

39. Pop-Georgievski, O.; Rodriguez-Emmenegger, C.; Pereira, A. d. l. S.; Proks, V.; Brynda, E.; Rypáček, F., Biomimetic Non-fouling Surfaces: Extending the Concepts. *Journal of Materials Chemistry B* **2013,** *1* (22), 2859-2867.

40. Thissen, H.; Gengenbach, T.; du Toit, R.; Sweeney, D. F.; Kingshott, P.; Griesser, H. J.; Meagher, L., Clinical Observations of Biofouling on PEO Coated Silicone Hydrogel Contact Lenses. *Biomaterials* **2010,** *31* (21), 5510-5519.

41. Vaisocherová, H.; Ševců, V.; Adam, P.; Špačková, B.; Hegnerová, K.; de los Santos Pereira, A.; Rodriguez-Emmenegger, C.; Riedel, T.; Houska, M.; Brynda, E.; Homola, J., Functionalized Ultra-low Fouling Carboxy- and Hydroxy-functional Surface Platforms: Functionalization Capacity, Biorecognition Capability and Resistance to Fouling from Undiluted Biological Media. *Biosensors and Bioelectronics* **2014,** *51*, 150-157.

42. Vorobii, M.; de los Santos Pereira, A.; Pop-Georgievski, O.; Kostina, N. Y.; Rodriguez-Emmenegger, C.; Percec, V., Synthesis of Non-fouling poly[N-(2-hydroxypropyl)methacrylamide] Brushes by Photoinduced SET-LRP. *Polymer Chemistry* **2015,** *6* (23), 4210-4220.

43. Michalek, L.; Barner, L.; Barner-Kowollik, C., Polymer on Top: Current Limits and Future Perspectives of Quantitatively Evaluating Surface Grafting. *Advanced Materials* **2018,** *30* (21), 1706321.

44. Zoppe, J. O.; Ataman, N. C.; Mocny, P.; Wang, J.; Moraes, J.; Klok, H.-A., Surface-Initiated Controlled Radical Polymerization: State-of-the-Art, Opportunities, and Challenges in Surface and Interface Engineering with Polymer Brushes. *Chemical Reviews* **2017,** *117* (3), 1105-1318.

45. Li, M.; Fromel, M.; Ranaweera, D.; Rocha, S.; Boyer, C.; Pester, C. W., SI-PET-RAFT: Surface-Initiated Photoinduced Electron Transfer-Reversible Addition–Fragmentation Chain Transfer Polymerization. *ACS Macro Letters* **2019,** *8* (4), 374-380.

46. Lueckerath, T.; Strauch, T.; Koynov, K.; Barner-Kowollik, C.; Ng, D. Y. W.; Weil, T., DNA–Polymer Conjugates by Photoinduced RAFT Polymerization. *Biomacromolecules* **2019,** *20* (1), 212-221.

47. Zamfir, M.; Rodriguez-Emmenegger, C.; Bauer, S.; Barner, L.; Rosenhahn, A.; Barner-Kowollik, C., Controlled Growth of Protein Resistant PHEMA Brushes via S-RAFT Polymerization. *Journal of Materials Chemistry B* **2013,** *1* (44), 6027-6034.

48. Zhou, J.; Ye, L.; Lin, Y.; Wang, L.; Zhou, L.; Hu, H.; Zhang, Q.; Yang, H.; Luo, Z., Surface Modification PVA Hydrogel with Zwitterionic via PET-RAFT to Improve the Antifouling Property. *Journal of Applied Polymer Science* **2019,** *136* (24), 47653.

49. Wang, J.-S.; Matyjaszewski, K., Controlled/"Living" Radical Polymerization. Atom Transfer Radical Polymerization in the Presence of Transition-Metal Complexes. *Journal of the American Chemical Society* **1995,** *117* (20), 5614-5615.

50. Goodman, D.; Kizhakkedathu, J. N.; Brooks, D. E., Molecular Weight and Polydispersity Estimation of Adsorbing Polymer Brushes by Atomic Force Microscopy. *Langmuir* **2004,** *20* (8), 3297-3303.

51. Hyun, J.; Chilkoti, A., Surface-Initiated Free Radical Polymerization of Polystyrene Micropatterns on a Self-Assembled Monolayer on Gold. *Macromolecules* **2001,** *34* (16), 5644-5652.

52. Jenkins, A. D.; Kratochvíl, P.; Stepto, R. F. T.; Suter, U. W., Glossary of Basic Terms in Polymer Science (IUPAC Recommendations 1996). *Pure and Applied Chemistry* **1996,** *68* (12), 2287-2311.

53. Cowie, J. M. G.; Arrighi, V., *Polymers Chemistry and Physics of Modern Materials, Third Edition*. CRC Press: 2007.

54. Kato, M.; Kamigaito, M.; Sawamoto, M.; Higashimura, T., Polymerization of Methyl Methacrylate with the Carbon Tetrachloride/Dichlorotris-(triphenylphosphine)ruthenium(II)/Methylaluminum Bis(2,6-di-tert-butylphenoxide) Initiating System: Possibility of Living Radical Polymerization. *Macromolecules* **1995,** *28* (5), 1721-1723.

55. Yeole, N., Thiocarbonylthio Compounds. *Synlett* **2010,** *2010* (10), 1572-1573.

56. Moad, G.; Rizzardo, E.; Thang, S. H., Radical addition–fragmentation chemistry in polymer synthesis. *Polymer* **2008,** *49* (5), 1079-1131.

57. Rizzardo, E.; Solomon, D. H., On the Origins of Nitroxide Mediated Polymerization (NMP) and Reversible Addition–Fragmentation Chain Transfer (RAFT). *Australian Journal of Chemistry* **2012,** *65* (8), 945-969.

58. Werner, M.; Oliveira, J. C. A.; Meiser, W.; Buback, M.; Mata, R. A., Critical Assessment of RAFT Equilibrium Constants: Theory Meets Experiment. *Macromolecular Theory and Simulations* **2020,** *29* (5), 2000022.

59. Gurbuz, N.; Demirci, S.; Yavuz, S.; Caykara, T., Synthesis of Cationic N-[3-(dimethylamino)propyl]methacrylamide Brushes on Silicon Wafer via Surface-initiated RAFT Polymerization. *Journal of Polymer Science Part A: Polymer Chemistry* **2011,** *49* (2), 423-431.

60. Yeow, J.; Chapman, R.; Gormley, A. J.; Boyer, C., Up in the Air: Oxygen Tolerance in Controlled/Living Radical Polymerisation. *Chemical Society Reviews* **2018,** *47* (12), 4357-4387.

61. Chen, M.; Zhong, M.; Johnson, J. A., Light-Controlled Radical Polymerization: Mechanisms, Methods, and Applications. *Chemical Reviews* **2016,** *116* (17), 10167-10211.

62. Pan, X.; Tasdelen, M. A.; Laun, J.; Junkers, T.; Yagci, Y.; Matyjaszewski, K., Photomediated Controlled Radical Polymerization. *Progress in Polymer Science* **2016,** *62*, 73-125.

63. Xu, J.; Shanmugam, S.; Duong, H. T.; Boyer, C., Organo-photocatalysts for Photoinduced Electron Transfer-reversible Addition–fragmentation Chain Transfer (PET-RAFT) Polymerization. *Polymer Chemistry* **2015,** *6* (31), 5615-5624.

64. Phommalysack-Lovan, J.; Chu, Y.; Boyer, C.; Xu, J., PET-RAFT Polymerisation: Towards Green and Precision Polymer Manufacturing. *Chemical Communications* **2018,** *54* (50), 6591-6606.

65. Bagheri, A.; Bainbridge, C. W. A.; Engel, K. E.; Qiao, G. G.; Xu, J.; Boyer, C.; Jin, J., Oxygen Tolerant PET-RAFT Facilitated 3D Printing of Polymeric Materials under Visible LEDs. *ACS Applied Polymer Materials* **2020,** *2* (2), 782-790.

66. Figg, C. A.; Hickman, J. D.; Scheutz, G. M.; Shanmugam, S.; Carmean, R. N.; Tucker, B. S.; Boyer, C.; Sumerlin, B. S., Color-Coding Visible Light Polymerizations To Elucidate the Activation of Trithiocarbonates Using Eosin Y. *Macromolecules* **2018,** *51* (4), 1370-1376.

67. Nomeir, B.; Fabre, O.; Ferji, K., Effect of Tertiary Amines on the Photoinduced Electron Transfer-Reversible Addition–Fragmentation Chain Transfer (PET-RAFT) Polymerization. *Macromolecules* **2019,** *52* (18), 6898-6903.

68. Kotlarek, D.; Vorobii, M.; Ogieglo, W.; Knoll, W.; Rodriguez-Emmenegger, C.; Dostálek, J., Compact Grating-Coupled Biosensor for the Analysis of Thrombin. *ACS Sensors* **2019,** *4* (8), 2109-2116.

69. Kotlarek, D.; Curti, F.; Vorobii, M.; Corradini, R.; Careri, M.; Knoll, W.; Rodriguez-Emmenegger, C.; Dostálek, J., Surface plasmon resonance-based aptasensor for direct monitoring of thrombin in a minimally processed human blood. *Sensors and Actuators B: Chemical* **2020,** *320*, 128380.

Chapter 2

Bioactive Antifouling Surfaces by Visible-Light-Triggered Polymerization

Kuzmyn, A. R., Nguyen, A. T., Zuilhof, H., & Baggerman, J. (2019). Bioactive Antifouling Surfaces by Visible-Light-Triggered Polymerization. Advanced Materials Interfaces, 6(12), 1900351. https://doi.org/10.1002/admi.201900351

Abstract

Hierarchical bioactive surfaces are created by visible-light-induced surface-initiated living radical polymerization employing tris[2-phenylpyridinato-C2,*N*]iridium(III) as a photocatalyst. The hierarchical antifouling diblock copolymer structures consist of *N*-(2-hydroxypropyl)-methacrylamide (first block) and carboxybetaine methacrylate (second block). The living nature of the polymerization is shown by a linear increase in layer thickness (as measured by atomic force microscopy) and reinitiation of the polymerization to create a patterned second block of polymer. The chemical structure of the brushes is confirmed by X-ray photoelectron spectroscopy and attenuated total reflection Fourier transform infrared spectroscopy measurements. The block copolymer brushes demonstrate excellent antifouling properties when exposed to single-protein solutions or to bovine serum. The second carboxy betaine block of the hierarchical antifouling structures can effectively be biofunctionalized with an anti-fibrinogen antibody. The coated surfaces show a high affinity and specificity to fibrinogen, while preventing non-specific adsorption from other proteins in bovine serum.

Introduction

Bioactive surfaces have an indispensable role in a variety of biomedical applications such as biosensing, tissue engineering, and bioimplants.[1] Those surfaces optimally display immobilized bioactive molecules that can interact with cells, proteins or other active biological elements of interest.[2] Nevertheless, many bioactive surfaces exposed to complex biological media have difficulties curbing the non-specific adoption of proteins.[3] Therefore, practical application of such bioactive layers requires the incorporation of antifouling layers.[4]

Different strategies are employed for creating such antifouling coatings, including functional self-assembled monolayers (SAMs),[5] polymer layers by "grafting-to" methods,[6-7] and polymer brushes by "grafting-from" methods.[8-13] For example, oligo(ethyleneglycol)-terminated alkyl SAMs are able to resist or decrease fouling from single-protein solutions.[14] Also poly(ethyleneglycol) (PEG) polymer-coated surfaces obtained by grafting-to methods show significant resistance to non-specific protein adsorption.[15] Nevertheless, neither of these approaches is able to fully prevent fouling from complex biological matrices such as blood plasma or serum.[16-17] In contrast, polymer brushes created by grafting-from methods have demonstrated remarkable resistance to biofouling from complex biological matrices, especially those based on zwitterionic polymers,[18-19] such as polycarboxybetaines based on

the corresponding methacrylate/amide (CBMA),[12, 20] polysulfobetaines from their methacrylate/amide precursor (SBMA),[9, 21-22] but also formally uncharged polymer brushes derived from *N*-(2-hydroxypropyl) methacrylamide (HPMA).[10, 23]

Surface-initiated atom transfer radical polymerization (SI-ATRP) is the most frequently used approach for creating antifouling polymer brush coatings.[10, 13, 24] However, SI-ATRP is a thermal reaction that requires a rigorous control over oxygen-free reaction conditions, which makes the reaction difficult to scale up and only provides uniform coatings. In response, new and easy-to-use approaches towards versatile polymer brush coatings were developed,[25-26] such as activator regenerated by electron transfer (ARGET)[12, 27] and initiators for continuous activator regeneration (ICAR).[28] In addition, light-induced polymerizations have been developed, so as to allow spatial and temporal control over the surface coating.[29] For example, surface-initiated photoinduced single-electron transfer living radical polymerization reactions (SET-LRP)[23] and surface-initiated photoiniferter-mediated polymerization (SI-PIMP)[8, 20] have been used to create antifouling polymer brushes. However, those techniques utilize UV light that is not suitable for all types of monomers, as it may trigger uncontrolled photopolymerizations. Recently, a new technique was introduced for surface-initiated visible-light-triggered living radical polymerization (LT-LRP) mediated by transition metal-based photoredox chemistry, e.g. by iridium complexes.[30-33] This method requires only a small amount of catalyst and allows to create, in a highly controlled manner, complex patterns of polymer brushes using visible light.[32, 34]

A good bioactive antifouling layer balances two objectives, namely, maximizing immobilization of bioreceptors and minimizing the non-specific adsorption of proteins.[4, 35] However, a significant amount of immobilized bioreceptors itself increases the non-specific adsorption of proteins, due to fouling nature of bioreceptors on their own, as well as due to the changes in brush structure.[36-37] In contrast, a low amount of immobilized bioreceptors might decrease the biosensing capabilities of the bioactive surfaces, but better maintains the antifouling properties of the polymer brushes. The balance between these two factors determines the performance of antifouling bioactive surfaces, i.e. robust antifouling behavior and efficient capture of analytes.

The effective biofunctionalization of polymer brushes without impairing antifouling properties still poses a challenge. The two main methods used for post-polymerization

biofunctionalization of antifouling polymer brushes are chain-end modification[24, 38-39] and side-chain modification.[10, 40] The latter method can be achieved using three different approaches via homopolymers with reactive side chains,[18] copolymers with both reactive and unreactive side chains,[36] or thirdly, diblock copolymer brushes with only the upper block being functionalized.[39] The immobilization of the bioactive elements on the chain end of polymer brushes allows to largely preserve the structure of the brush and its antifouling properties. However, the quantity of immobilized bioactive molecules is significantly lower than with side-chain functionalization. The side-chain modification approach is typically based on activating functional groups of the side chains of (co)polymer brush. This approach allows reactive groups to react with biomolecules to immobilize a large quantity of biomolecules along the chain, while still maintaining significant antifouling. Two recent examples led us to our current work. First, the combination of a sulfobetaine with a clickable but still zwitterionic sulfobetaine, which allows fully three-dimensional loading of biomolecules.[21] Second, a random copolymer brush of *N*-(2-hydroxypropyl) methacrylamide (HPMA) and carboxybetaine methacrylamide (CBMAA), in which the latter could be bioconjugated via the use of activated ester reactions.[37] While both aspects highlight important facets in particular high loading of bioactive moieties, the first approach starts to display loss of antifouling properties upon high degrees of loading, while the second impairs the structure of the brush causing changes in the hydrodynamic properties of the polymer chains, crosslinking of lateral chains, and steric hindrance. Diblock copolymer brushes with only the upper block modification might constitute a compromise approach that allows to immobilize a significant number of biomolecules where they can most readily interact with the biomarkers of interest (i.e. near the outside of the brush), and simultaneously nearly fully preserves the lower block of the antifouling polymer brush structure and consequently the antifouling properties of whole system.[41-42]

Herein, we introduce a robust and facile method for the formation of temporally and spatially tuned antifouling bioactive polymer brushes using LT-LRP. With this method we synthesized for the first time biofunctional antifouling diblock copolymer brushes based on *N*-(2-hydroxypropyl) methacrylamide (HPMA) at the bottom of the brush, and carboxybetaine methacrylate (CBMA) at the top. The resulting brushes were characterized extensively by X-ray Photoelectron Spectroscopy (XPS), Atomic Force Microscopy (AFM), attenuated total reflection Fourier-transform infrared spectroscopy (ATR-FTIR), and scanning Auger

microscopy (AES). The bottom poly(HPMA) block was chosen because it seems to yield the best antifouling properties of the routinely studied brushes,[10, 40, 43] while the poly(CBMA) brushes display high antifouling properties even after significant functionalization.[18, 40] We outline that the $Ir(ppy)_3$-mediated light-triggered surface-initiated living radical polymerization allows for well-controlled polymerization conditions and for further reinitiation from poly(HPMA) brush. Moreover, we show that this technique yields spatial control over the brush formation and biofunctionalization.[32] The antifouling character, as studied by fluorescence microscopy, is verified in single protein solutions and also in complex biological media. Finally, we demonstrate selective capture by antibody functionalized poly(CBMA) in complex media, which indicates the application potential of these block copolymer brushes.

Results and discussions

The method employed to create hierarchical bioactive antifouling diblock copolymer brushes consists of four consecutive steps including LT-LRP (Scheme 1). From an initiator-coated silicon nitride surface poly(HPMA) brushes are grown via LT-LRP. Subsequently, a chain extension was performed from the poly(HPMA)-coated surfaces with a protected carboxybetaine derivative. The carboxybetaine monomer was chosen for the second block because of the exceptional antifouling properties of the CBMA-based polymer brushes and for the well-explored synthetic pathways of biofunctionalization of those brushes.[18] A tert-butyl ester-protected carboxybetaine methacrylate-based poly(CBMA-tBu) was utilized, as direct polymerization of carboxy betaine monomers did not succeed (see below).[44] Thirdly, deprotection of the protected carboxyl groups in the poly(CBMA-tBu) polymer yielded the carboxybetaine polymer and, finally, bioactive moieties were coupled to the CBMA block via NHS/EDC activation of the carboxyl groups.

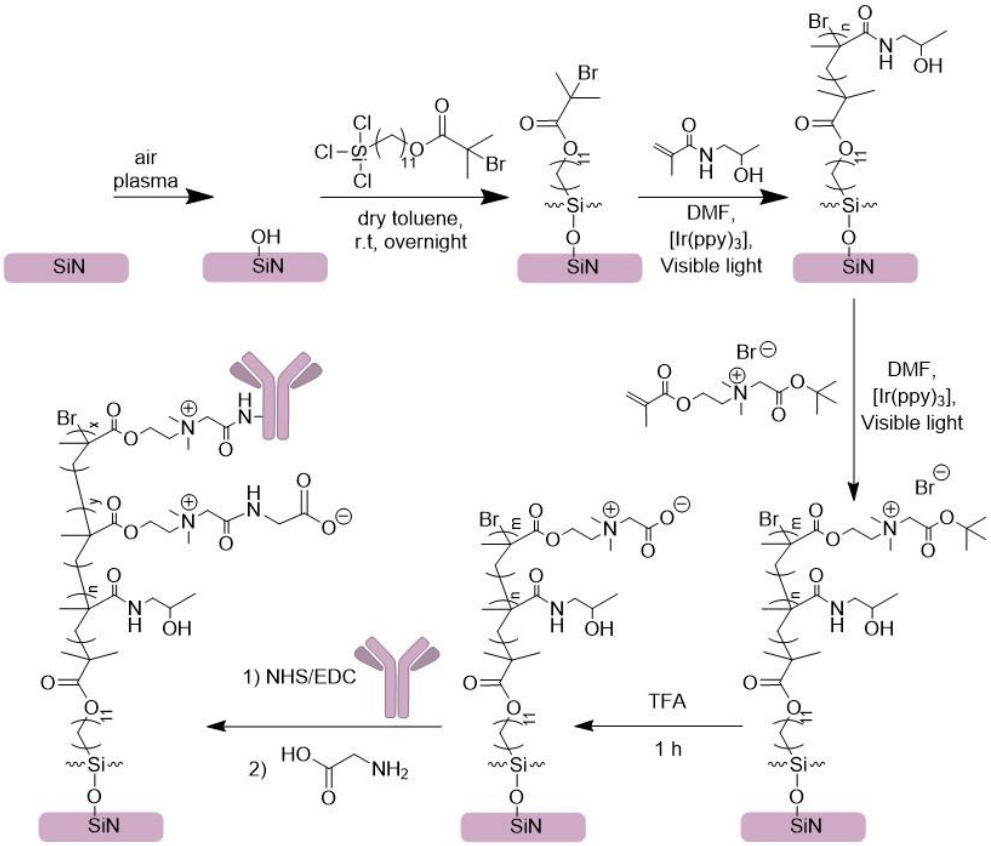

Scheme 1. Schematic depiction of the method to create hierarchical bioactive surfaces. Poly(CBMA)-poly(HPMA)-diblock brushes are grown from an initiator SAM on silicon nitride via LT-LRP, and subsequently biofunctionalized via further activation of the carboxyl groups of poly(CBMA) polymer block.

Visible light-triggered polymerization of poly(HPMA) brushes. The poly(HPMA) brushes of different thickness were grown from self-assembled monolayers of 11-(trichlorosilyl)undecyl-2-bromo-2-methylpropanoate by LT-LRP. The selected trichlorosilane self-assembled monolayers have been previously reported as suitable for anchoring of polymer brushes.[23, 45-46] The successful grafting of the initiator monolayer was confirmed by XPS. The XPS narrow-scan spectrum of the C1s region (Figure S1a, Supporting Information) shows three peaks. The peak at 285.0 eV is attributed to the carbon atoms in the alkyl backbone of the initiator, and the peaks at 286.7 and 289.3 eV are assigned to the carbon atoms adjacent to the ester [C-O] and bromide [C-Br], and

the carbon from the carbonyl group, respectively. The observed ratio between [C-C/H] : [C-O] : [C-Br] : [C=O] peaks is 12.1 : 1.0 : 1.1 : 0.8, which corresponds to the theoretically expected ratio of 12 : 1 : 1 : 1. Also, the experimentally obtained spectrum corresponds well to a simulated XPS spectrum (Figure S2, Supporting Information) based on the core orbital energy levels calculated by density functional theory (DFT).[47-48] In addition, peaks of the bromine end-group were found at 71 eV in the XPS Br3d narrow-scan spectrum (Figure S1b, Supporting Information), further confirming the presence of the initiator on the surface.

Poly(HPMA) brushes with different thicknesses were grown from the initiator-coated surfaces by LT-LRP utilizing $Ir(ppy)_3$ as a photocatalyst. The kinetics of the polymer brush growth – from 0 to ca. 80 nm – were followed by measuring by AFM the dry thickness of the polymer layer as function of the reaction time. The AFM topography images of brush-coated surfaces revealed homogeneous layers with an average roughness of *Rq* of 1.5 ± 0.3 nm (Figure S3a, Supporting Information). The thickness of the brush increased linearly in time, which confirms the controlled nature of the polymerization (Figure 1a and Table S1, Supporting Information). The polymerization proceeded faster using an LED (380 nm) average rate of polymerization 0.22 ± 0.01 $nm \cdot min^{-1}$ compared to a halogen lamp 0.16 ± 0.01 $nm \cdot min^{-1}$ (white light, see emission spectrum, Figure S4, Supporting Information). This could be caused by both the difference in intensity between these light sources and the higher absorption coefficient of $Ir(ppy)_3$ at 380 nm compared to that at visible light-wavelengths (see spectrum of light absorption, Figure S5, Supporting Information). The dependence of the polymerization rate on the light intensity was previously demonstrated by Hawker and coworkers.[31] A higher light intensity leads to an increased amount of excited photocatalyst and therefore to more activation of the polymerization initiator. The possibility of using a conventional broad-emission light source, such as a halogen lamp, confirms the ease of use and robustness of this approach for creating antifouling layers.

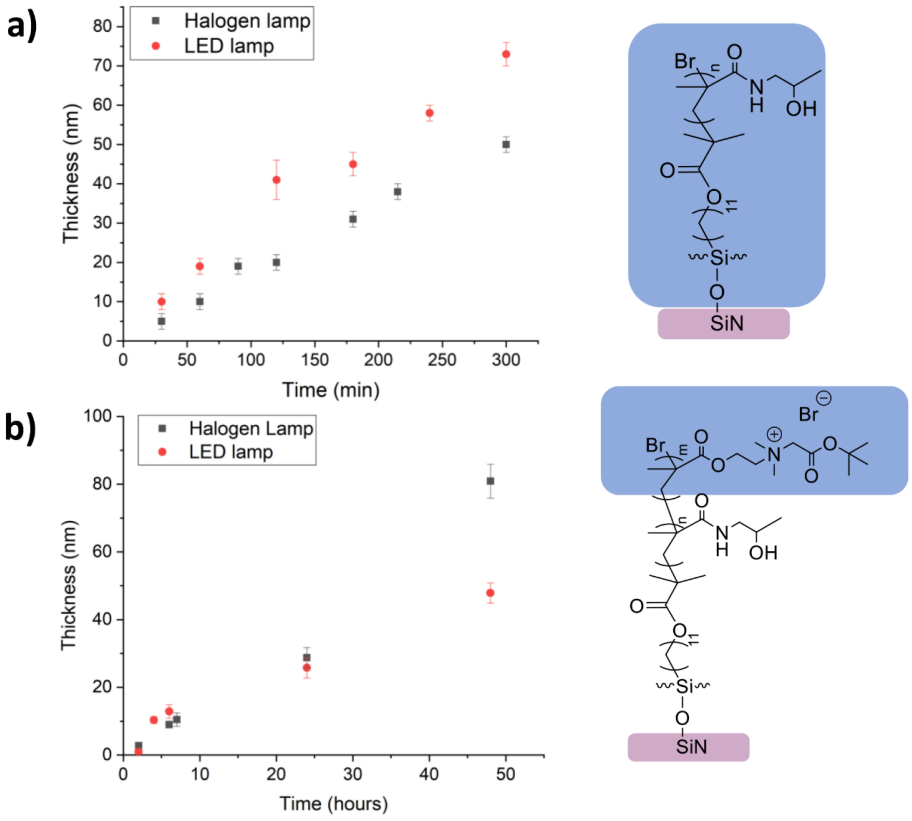

Figure 1. Dry thickness of polymer brushes as function of the polymerization time, as determined by AFM (a) for poly(HPMA), and (b) for poly(CBMA-tBu) grown from the poly(HPMA) macroinitiator thickness 20 nm.

The chemical structure of the synthesized poly(HPMA) brushes was confirmed by ATR-FTIR (Figure 2a). The FTIR spectrum of poly(HPMA) brushes with a thickness of 20 nm shows the typical broad stretching bands of hydroxyl (O-H) and amide (N-H) bonds around 3300 cm^{-1}. The C=O stretch (amide I) and the coupled N-H deformation and C-N stretch (amide II) bands of the secondary amide group are visible at 1650 cm^{-1} and 1530 cm^{-1}, respectively. The weak absorption at 1730 cm^{-1} corresponds to C=O stretching of the ester groups present in the initiator layer. These results are in good agreement with the expected chemical structure of poly(HPMA) on the surfaces.

The chemical structure was further confirmed by XPS. The wide-scan XPS spectrum shows – after the various washing steps – no residual iridium on the poly(HPMA)-coated surfaces (Figure S6, Supporting Information). The narrow-scan XPS C1s spectrum (Figure 2c), measured on poly(HPMA)-coated surface with a thickness of 20 nm, displays a broad peak at 285 eV with a shoulder between 286-287 eV, attributed to overlapping signals, and a smaller peak at 288 eV attributed to the carbonyl atom. The spectrum was deconvoluted by fitting it with four peaks centered at 285.0 eV assigned to C-H and C-C bound atoms, at 285.9 eV from the C-N atoms, at 286.6 eV from the C-O atoms, and at 287.9 eV from the C=O atoms. The ratio between [C-C/H] : [C-N] : [C-O] : [N-C=O] peaks is 3.8 : 1.1 : 1.1 : 1.0, which is in excellent agreement with the theoretically expected composition of the poly(HPMA) structure (4 : 1 : 1 : 1). Moreover, the C1s spectrum correlates well with the simulated C1s XPS spectrum obtained by DFT calculations (Figure S7, Supporting information).[47-48] The combination of AFM, XPS and IR data thus clearly confirm the presence of poly(HPMA) brushes on the initiator-coated surface.

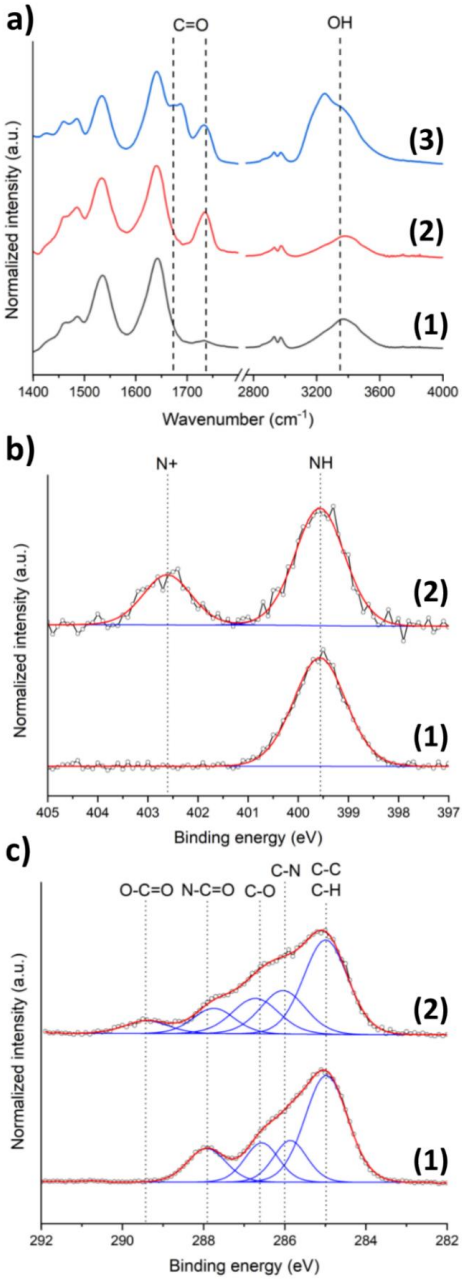

Figure 2. (a) ATR-FTIR spectra of (1) poly(HPMA) brushes with a thickness of 20 nm, (2) poly(HPMA)-poly(CBMA-tBu) copolymer with a total thickness of 30 nm, and (3) poly(HPMA)-poly(CBMA) copolymer thickness 30 nm. Narrow-range XPS spectra of the (b) N1s and (c) C1s regions for (1) poly(HPMA) brushes of 20 nm thickness, and (2) poly(HPMA)-poly(CBMA-tBu) copolymer of 30 nm thickness.

Introduction of second block of poly(CBMA-tBu) on poly(HPMA). The living nature of the LT-LRP polymerization should allow to grow a second polymer block from the poly(HPMA) brush macroinitiator. Initial attempts to grow polymer brushes of CBMA on poly(HPMA) by LT-LRP with $Ir(ppy)_3$ in mixtures of water, ethanol, methanol and DMF resulted in self-polymerization of the solution. Polymerization of CBMA in DMF or other non-protic polar solvents was not possible due to solubility issues of the monomer. Thus, a carboxyl-protected monomer, CBMA-tBu, was used for the synthesis of the second block. The AFM topography measurement confirmed an overall homogeneous layer without irregularities and pinholes and featuring a roughness of Rq = 1.2 ± 0.3 nm (Figure S4b, Supporting Information). The kinetics of growth of poly(CBMA-tBu) brush was again linear, thereby confirming that controlled nature of this polymerization step (Figure 1b and Table S2, Supporting Information). The rate of polymerization of CBMA-tBu monomer (halogen lamp 1.5 ± 0.2 $nm \cdot h^{-1}$ and LED lamp 1.1 ± 0.3 $nm \cdot h^{-1}$) is lower due to the charged nature of the monomer that causes repellence of the approaching monomer by the growing charged polymer brushes. This has been observed for this monomer before, showing also a slow polymerization rate with conventional ATRP.[49] Moreover, it was demonstrated previously that reinitiation is not effecting the polymerization rate by Hawker at al.[31-32] The chemical structure of the CBMA-tBu copolymer was confirmed by ATR-FTIR (Figure 2a) and XPS. In the ATR-FTIR spectrum of poly(CBMA-tBu)-poly(HPMA)-coated surfaces a strong ester-based C=O stretching peak appears at 1733 cm^{-1}, i.e. significantly different from the amide-based C=O peak at 1650 cm^{-1} observed for the poly(HPMA) block. The XPS N1s narrow scan (Figure 2b) shows an additional peak at 402.6 eV, which indicates the presence of positively charged nitrogen [N^+] in the chemical structure of the layer. The peak at 399.5 eV in those spectra corresponds to the neutral nitrogen [N-H] present in the poly(HPMA) layer below the second block. The relatively high intensity of the [N-H] peak, even with a 10 nm second poly(CBMA-tBu) block, is probably due to a relative low density of the latter. The charged nature of CBMA-tBu and bulky nature of tBu group in the monomer can cause the polymer chains to repel each other, which likely results in a lower density of the second block. Moreover, the XPS C1s narrow scan spectrum (Figure 2c) shows the appearance of a peak at 289.5 eV attributed to ester carbon atoms [O-C=O], and an increase in intensity of the peaks at

286.0 eV [C-N], and 286.7 eV [C-O]. The overall data demonstrate the successful growth of poly(CBMA-tBu) brushes from poly(HPMA) macroinitiator yielding poly(CBMA-tBu) layer as the second block of the copolymer.

In order to generate a zwitterionic CBMA polymer top block, the tert-butyl ester moieties of the poly(CBMA-tBu)-poly(HPMA) diblock polymer brush structures were deprotected by exposure to undiluted trifluoroacetic acid at room temperature for 1 h. The ATR-FTIR spectrum of the deprotected poly(CBMA)-block-poly(HPMA) shows the appearance of a new peak at 1670 cm^{-1} corresponding to the C=O stretching vibrations of the carboxylic acid groups. Also, an increase in the intensity of the hydroxyl stretching at 3200 cm^{-1} was observed. These changes indicate the occurrence of the carboxylic acid groups in the copolymer (Figure 2a). Moreover, the XPS wide-scan spectra (Figure S8, S9, Supporting Information). show a decrease of the carbon signals relative to the oxygen and nitrogen signals, which is in line with the loss of carbon due to the hydrolysis of the tert-butyl ester.

Patterning of poly(CBMA-tBu) brushes. An advantage of the LT-LRP approach is that it enables the formation of complex 3D-structured copolymer brush layers by using a mask and tuning the thickness of the different blocks. This was demonstrated by the growth of CBMA-tBu on poly(HPMA) with a patterning mask. From various observations, it became clear that the poly(CBMA-tBu) only grew in irradiated regions, whereas no growth was observed in regions without illumination. First, the resulting patterns could be easily observed with an optical microscope (Figure 3a), because the SiN surface changes its color in a regular fashion with a change of the thickness of the polymer brush layer on top. The dark pinkish stripes correspond to the thinner poly(HPMA) layer, the green to the poly(HPMA)-poly(CBMA-tBu) layer and the scratch (yellowish) in the middle of Figure 3a reveals the bare silicon nitride underneath, which was used as reference for the thickness evaluation. The 3D structure of corresponding layers was also confirmed by AFM studies of a uniformly coated poly(HMPA) layer onto which a pattern of locally grown poly(CBMA-tBu) was attached. Figure 3b shows a uniform poly(HPMA) layer thickness of 20 nm and a poly(HPMA)-poly(CBMA-tBu) layer thickness of 50 nm. The thickness of 20 nm for the poly(HPMA) layer corresponds to the thickness before patterning, which demonstrates that the second block only grew in the illuminated areas. Thirdly, the selective growth of the poly(CBMA-tBu) top block was further

confirmed by Auger intensity mapping of the nitrogen signal at 382 eV (Figure 3d). The different amount of neutral nitrogen [N-H] in patterned areas and non-patterned areas is shown by different intensities of red color.

This patterned growth thus also opened up the possibility of local biofunctionalization of the designed patterned layer, via the local immobilization of BSA-FITC on the surface. After deprotection (see above), the CBMA surfaces were biofunctionalized with BSA-FITC utilizing NHS/EDC active ester chemistry. Only fluorescence was observed in the CBMA-patterned areas, indicating that BSA-FITC was only present in these areas (Figure 3c). This approach enables the local biofunctionalization of antifouling surfaces, while the antifouling property in the non-functionalized areas is unaffected.

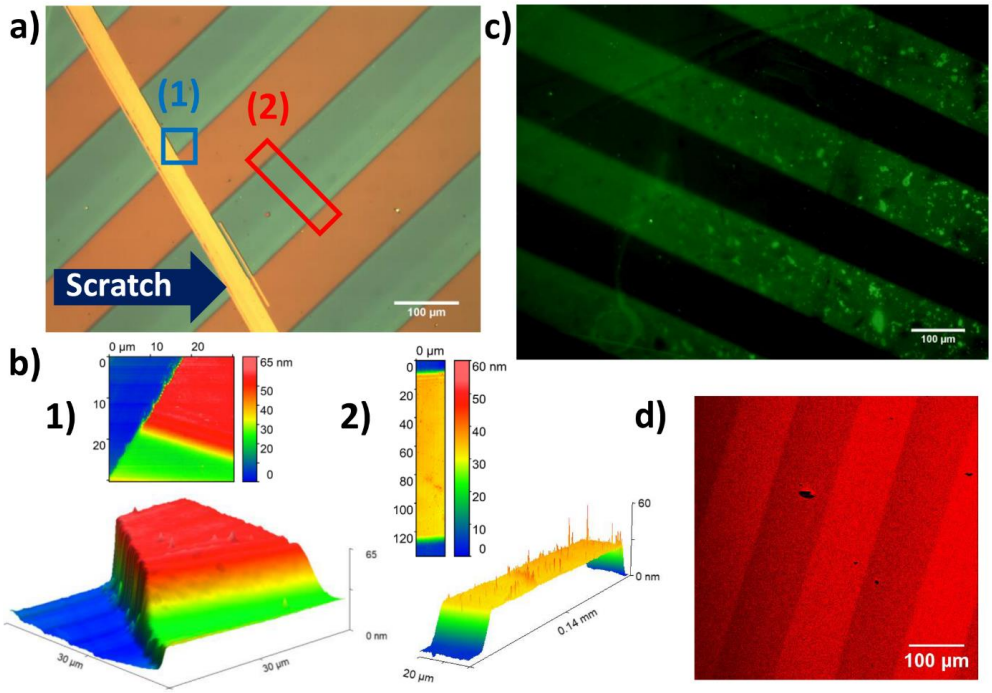

Figure 3. (a) Optical microscope image of line-patterned 30 nm thick poly(CBMA-tBu) layer on a uniformly coated 20 nm thick poly(HPMA) layer, with a scratch (orange bar) that was used as reference for the thickness measurement. (b) AFM topography of sections 1 and 2 in (a). (c) Fluorescence microscope image of a deprotected patterned poly(CBMA-tBu) layer with immobilized BSA-FITC. (d) Intensity mapping of the nitrogen Auger signal at 382 eV.

Biospecific capture with poly(CBMA)-poly(HPMA)-coated surfaces. To demonstrate the applicability of the poly(CBMA)-poly(HPMA)-coated surfaces for biosensing applications, anti-fibrinogen (AntiFbg) antibodies were immobilized on the surfaces. Fibrinogen (Fbg) was chosen as an analyte, since it also shows significant non-specific adsorption on non-modified surfaces and has been frequently used as a model protein for fouling determination. AntiFbg has strong affinity to the α-chain of human fibrinogen, allowing an efficient capture of fibrinogen. The immobilization of AntiFbg was achieved by activating the carboxylate groups along the CBMA chains using NHS/EDC chemistry and subsequently binding the antibody via active ester coupling. The design of bioactive surfaces requires to have not only high affinity to the analyte but also an excellent resistance to fouling from complex biological media. Therefore, poly(CBMA)-poly(HPMA)-coated surfaces were used with thicknesses of 20 nm and 10 nm for the HPMA and CBMA block, respectively. The thicknesses of these blocks were chosen to balance between antifouling performance of the bottom layer – for which typically > 15 nm brushes are required – and loading of bioactive elements and antifouling performance of the top layer.[50] A thicker second block allows for a higher loading of antibody but – since antibodies themselves are not antifouling, but rather: fouling - at the same time might reduce the fouling performance.

The coated surfaces were challenged by contacting them with fluorescent single-protein solutions of BSA-FITC, Fbg-Alexa647, and Str-FITC, respectively, and by a 10% biotinylated bovine serum (BS) solution in PBS for 15 min; this time is typically sufficient to assess the adsorption of proteins onto stable polymer brushes.[10] The fouling by biotinylated BS was detected by subsequent exposure to Str-FITC solution, which binds to the biotin residues of any fouling serum proteins present on the surface.[43] The fluorescence intensity of exposed bare SiN surfaces is high, due to the high non-specific adsorption of proteins from corresponding solutions (Figure 4a and Table S3, Supporting Information). The introduction of poly(HPMA) on the surface of SiN drastically lowers the intensity of fluorescence after exposure to biofouling solutions. This confirms that poly(HPMA) brushes synthesized by the LT-LRP technique preserve its original highly effective antifouling properties, as previously reported for poly(HPMA) brushes synthesized with ATRP and SET-LRP methods.[10, 23] The diblock copolymer structure of poly(HPMA) and poly(CBMA) also showed similarly high antifouling properties to both the three single-protein solutions and to the biotinylated

bovine serum solution. Both poly(HPMA) and poly(CBMA) are strongly hydrated polymers leading to their excellent antifouling properties.[10, 43, 51]

The bioactive antifouling surface was created by biofunctionalizing the second block of poly(HPMA)-poly(CBMA) with AntiFbg antibodies. The resulting surface was exposed as well to the different single-protein solutions and to the biotinylated bovine serum solution. The poly(HPMA)-poly(CBMA)-AntiFbg showed excellent resistance to the nonspecific adsorption

of Str-FITC, BSA-FITC and biotinylated serum proteins. In addition, it demonstrated the effective and specific capture of Fbg-Alexa647 from single protein solution (Figure 4a) compared polymer brush structures also indicated that a lower grafting density for the second layer may allow for a higher loading of antibody.[52]

We have further challenged the created AntiFbg-poly(CBMA)-poly(HPMA)-coated surfaces, for specific capture not only from single-protein solution but also from complex biological media, by exposing the surface to BS containing Fbg-Alexa647 (0.1 mg·mL^{-1}). Also, here the fouling from BS was detected by fluorescence from Str-FITC that labeled the adsorbed biotinylated BS proteins. The specific capture was detected by fluorescence from Fbg-Alexa647. On bare silicon nitride fluorescence was observed from both BS labeled with Str-FITC and Fbg-Alexa647 (Figure 4b). On bare silicon nitride fluorescence was observed from both BS labeled with Str-FITC and Fbg-Alexa647 (Figure 4b, Table S4). The bare silicon nitride has lower fluorescence intensities of protein adsorption from BS compared with the intensities observed for BS without Fbg-Alexa647 added. This is most likely due to the presence of Fbg-Alexa647 that also adsorbs on the surface and replaces some adsorbed BS proteins (Vroman effect). While on the poly(CBMA)-poly(HPMA)-coated surfaces nearly no fluorescence was observed from both the BS and Fbg (Figure 4b). However, on the AntiFbg functionalized block copolymer only fluorescence from the Fbg-Alexa647 was observed. The significant fluorescent signal of Fbg-Alexa647 as analyte and no signal from fouling of proteins attributed to BS on the surface that were exposed to BS containing Fbg-Alexa647 (0.1 mg·mL^{-1}). The fluorescence signal from Fbg-Alexa647 on the AntiFbg-poly(CBMA)-poly(HPMA)-coated surfaces is significantly higher ($P < 0.0001$) in case of capture from BS compared to that from single-protein solutions. A possible reason for this might be interaction of Fbg with other proteins present in the serum, in particular thrombin. This could cause dimerization of Fbg into fibrin dimers or oligomers, which can also be captured by AntiFbg on the surfaces.[53] Nevertheless, these results pave the way for the creation of

biosensors that recognize analytes selectively in different complex biological media.

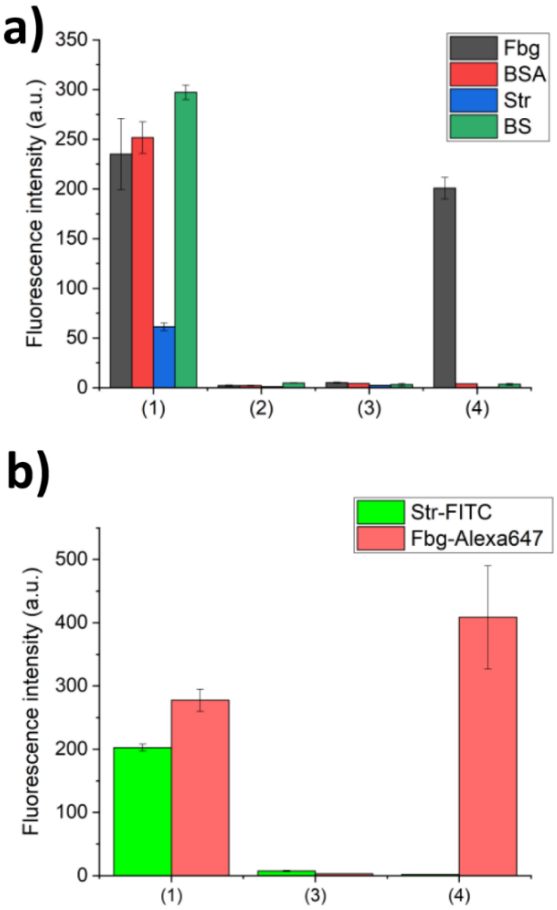

Figure 4. (a) Fluorescence intensities of Fbg-Alexa647 (0.1 mg·mL^{-1}), BSA-FITC (0.1 mg·mL^{-1}), Str-FITC (0.1 mg·mL-1), and Str-FITC labeled 10% diluted biotinylated bovine serum (BS) on (1) bare SiN (2), poly(HPMA), (3) poly(CBMA)-poly(HPMA), (4) AntiFbg-poly(CBMA)-poly(HPMA). (b) Fluorescence intensities of Fbg-Alexa647 (0.1 mg·mL^{-1}) in 10% diluted biotinylated bovine serum. The Str-FITC was used for labelling proteins from bovine serum labeled with fluorescent signal attributed to non-specific adsorption of proteins from bovine serum.

Conclusion

We designed a new approach to create bioactive polymer brush-coated surfaces using light-triggered living radical polymerization (LT-LRP). We demonstrated the potential of this approach to obtain patterned biospecific polymer brushes on top of an independently patternable non-fouling base layer. As an example in case, *N*-(2-hydroxypropyl)methacrylamide (HPMA, 1st block) and carboxybetaine methacrylate (CBMA, 2nd block) were grown successively from initiator-coated surfaces via LT-LRP with $Ir(ppy)_3$. The designed block copolymers showed excellent antifouling properties in single-protein solution of bovine serum albumin, streptavidin and fibrinogen, and also in diluted bovine serum medium. Furthermore, conjugation of anti-human fibrinogen antibody on the poly(HPMA)-poly(CBMA)-coated surfaces demonstrated the high selectivity of the bioreceptor to fibrinogen in complex biological medium without impairment of the proteins resistance. We thus envision that the strategy presented herein can be efficiently applied in highly sensitive biosensing devices, along several lines currently ongoing in our labs.

Experimental Section

Materials. All chemical reagents were used without further purification, unless otherwise specified. Tris[2-phenylpyridinato-C2,*N*]iridium(III) ($Ir(ppy)_3$), *N*,*N*-dimethylformamide (DMF), 2-(dimethylamino)ethyl methacrylate, tert-butyl bromoacetate, *N*-hydroxysuccinimide (NHS), *N*-(3-dimethylaminopropyl)-*N*-ethylcarbodiimide hydrochloride (EDC), and albumin fluorescein isothiocyanate conjugate from bovine serum (BSA-FITC) were purchased from Sigma-Aldrich, and *N*-(2-hydroxypropyl) methacrylamide (HPMA) from Polysciences, Inc. Fibrinogen from human plasma, Alexa Fluor™ 647 conjugate (Fbg-Alexa647), and mouse anti-fibrinogen monoclonal antibody (AntiFbg) were acquired from Thermo Fisher Scientific. Streptavidin-fluorescein isothiocyanate conjugate (Str-FITC) was purchased from BD Biosciences. 11-(Trichlorosilyl)undecyl 2-bromo-2-methylpropanoate was purchased from Gelest, Inc. Silicon substrates coated with 50 nm of LPCVD silicon nitride were acquired from Siltronix. Deionized water was produced with Milli-Q Integral 3 system Millipore, Molscheim, France (Milli-Q water). Bovine serum was obtained and biotinylated as previously described.[43]

2-tert-Butoxy-*N*-(2-(methacryloyloxy)ethyl)-*N*,*N*-dimethyl-2-oxoethanaminium (CBMA-tBu) monomer synthesis. The synthesis was performed as previously reported.[49] 2-(Dimethylamino)ethyl methacrylate (5.00 g, 31.8 mmol) and tert-butyl bromoacetate (8.68 g, 34.3 mmol) were reacted in acetonitrile (20 mL) for 24 h at 50 °C under Ar protection. Following the addition of ethyl ether (250 mL) to the reaction mixture, the product precipitated, and the obtained white crystals were isolated and dried under vacuum. The resulting CBMA-tBu monomer was immediately stored under argon protection at -20 °C.

^{1}H NMR (400 *MHz*) (D_2O) δ (ppm): 1.40 (s, 9H, -OC($\underline{CH_3}$)$_3$), 1.83 (*s*, 3H, CH_2=C($\underline{CH_3}$)COO-), 3.26 (*s*, 6H, -$CH_2N(\underline{CH_3})_2CH_2COO$-), 3.94 (*t*, 2H, *J* = 3 Hz, -$COOCH_2\underline{CH_2}N(CH_3)_2CH_2$-), 4.23 (*s*, 2H, $CH_2N(CH_3)_2\underline{CH_2}COO$-), 4.56 (*t*, 2H, *J* = 3 Hz, CH_2=$C(CH_3)COO\underline{CH_2}CH_2N(CH_3)_2$), 5.70 and 6.06 (*s*, 2H, $\underline{CH_2}$=$C(CH_3)COO$-). Yield: 90%. (See Supporting Information, Figure S11 for the NMR spectrum)

Light Source. A halogen lamp (see Supporting Information, Figure S4 for the emission spectrum) and an LED with maximum intensity at 380 nm (Intelligent LED Solutions product number: ILS-XO05-S380-0058-SC211-W2) were used. The light intensity of the halogen lamp was measured to be 3.5 μW/cm^2; the LED current was set at 700 mA, corresponding to a total radiometric power of 2.9 W, according to manufacturer specifications.

Formation of initiator-functionalized self-assembled monolayers (SAM). The substrates were rinsed with, acetone, absolute ethanol (EtOH) and Milli-Q water and blown dry under a gentle stream of Ar. Subsequently, the surfaces were exposed to an air plasma in a plasma cleaner (Diener electronic GmbH, Germany) for 5 min. The freshly activated surfaces were immediately immersed in a freshly prepared solution of 11-(trichlorosilyl)undecyl-2-bromo-2-methylpropanoate (1 $mg \cdot mL^{-1}$) in dry toluene at RT for 16 h. The substrates were subsequently rinsed with toluene, acetone, EtOH and Milli-Q water and blow dried with Ar.

Synthesis of visible-light-triggered poly(HPMA) brush. HPMA monomer (536 mg, 3.74 mmol) was dissolved in DMF (2 mL). The obtained solution was deoxygenated by bubbling Ar through for 30 min under stirring and kept in the dark by wrapping the flask in aluminum foil. Subsequently, $Ir(ppy)_3$ (3 mg, 4 µmol) was added to the solution under Ar protection. The polymerization solution was stirred for 15 min and transferred by syringe to individual deoxygenated crimped vials containing the initiator-coated SiN wafer substrates, which were closed immediately afterwards. Immediately after this, the polymerization was conducted by irradiating the vials with visible light from a halogen or LED light source for different periods of time. In these experiments, the light source was placed 3-4 cm from the substrates and an airflow was used to cool the vials. The polymerization was stopped by turning off the light. The samples were removed from the solution and subsequently rinsed with DMF, acetone, absolute ethanol, and water, and blown dry under a gentle stream of Ar (see for a picture of the set-up Figure S12, Supporting Information).

Formation of poly(CBMA-tBu)brushes grown on poly(HPMA)-coated surfaces. CBMA-tBu monomer (285 mg, 0.95 mmol) was dissolved in DMF (2 mL). The obtained solution was deoxygenated by bubbling through with Ar for 30 min under stirring and in the dark by wrapping the flask in aluminum foil. Afterwards, $Ir(ppy)_3$ (3 mg, 4 µmol) was added to the solution under argon flow. The polymerization solution was stirred for 15 min and transferred via syringe to individual deoxygenated crimped vials containing poly(HPMA) coated SiN substrates, which were closed immediately afterwards. Subsequently, the polymerization was conducted by irradiating the vials with visible light from a halogen or LED light source for different periods of time. The light source was placed 3 - 4 cm from the substrates and an airflow was used to cool the vials. The polymerization was stopped by turning off the light.

The samples were removed from the solution and subsequently rinsed with DMF, acetone, absolute ethanol, and water, and dried by blowing with Ar.

Micro-patterned poly(CBMA-tBu) on poly(HPMA)-coated surfaces. A specifically designed micro-patterned mask (see Supporting Information, Figure S13) was placed on top of a poly(HPMA)-coated silicon nitride surface and placed in a vial. The micro-patterned brushes of poly(CBMA-tBu) were grown on the of poly(HPMA) brush surface using the same procedure of chain extension of poly(HPMA) as described above.

Deprotection of poly(CBMA-tBu) moieties. The poly(CBMA-tBu)-poly(HPMA)-coated surfaces were immersed in trifluoroacetic acid for 1 h at RT to remove the tBu protective groups, and generate a poly(CBMA) block. Afterwards, the samples were washed with Milli-Q water and ethanol and dried by blowing with Ar.

Biofunctionalization of poly(CBMA)-poly(HPMA). The poly(CBMA)-poly(HPMA)-coated surfaces were incubated in freshly filtered Milli-Q water for 15 min at RT, followed by incubating in a mixture of NHS (5 mL, 0.1 M) and EDC (5 mL, 0.5 M) in 10 mM NaCl for 30 min. Afterwards, the activated surface was washed with Milli-Q water, and incubated for 30 min in a protein (BSA-FITC or AntiFbg, 0.1 mg·mL^{-1}) solution in phosphate-buffered saline (PBS; pH 7.4). The residual of non-covalently bound proteins was removed by rinsing with PBS and Milli-Q water. The surface was deactivated with glycine blocking solution (pH 6.0, 1 M) for 30 min, and afterwards rinsed with Milli-Q water.

Fluorescence microscopy. Fluorescence images of the patterned bioactive layers were taken with a widefield fluorescent microscope (Zeiss Axioskop 2+). A Leica TCS SP8 confocal laser scanning microscope (CLMS) (Leica Microsystems, Mannheim, Germany) was used to measure protein fouling and specific interactions of the coated surfaces. A Leica HyDTM hybrid detector was used in photon counting mode to measure the intensity of the fluorescence signal. A 10× objective was used and the samples were set in focus by maximizing the reflected light intensity from the laser. Fluorescence images were obtained by accumulating 10 consecutive images. Images were analyzed with the Leica LAS X Life Science software.

Protein adsorption and selective capture. The protein fouling and selective capture ability of the coated surfaces in complex biological media were investigated by incubating surfaces in BSA-FITC (0.1 mg·mL^{-1}), Fbg-Alexa647 (0.1 mg·mL^{-1}), Str-FITC (0.1 mg·mL^{-1}), 10% diluted

biotinylated bovine serum, and in 10% diluted biotinylated bovine serum containing Fbg-Alexa647 (0.1 mg·mL^{-1}) for 15 min at RT. The surfaces exposed to biotinylated bovine serum were then copiously washed with PBS (10 mL, pH 7.4), followed by exposure to Str-FITC (0.1 mg·mL^{-1}) for 15 min at RT. Afterwards the samples were rinsed with PBS (10 mL, pH 7.4) and Milli-Q water (10 mL), and subsequently dried by blowing with Ar. Further, the samples were mounted on glass slides and the intensity of fluorescence of adsorbed proteins was measured.

X-ray photoelectron spectroscopy (XPS). XPS measurements were performed using a JPS-9200 photoelectron spectrometer (JEOL Ltd., Japan). All the samples were analyzed using a focused monochromated Al K X-ray source (spot size of 300 µm) radiation at 12 kV and 20 mA with an analyzer energy pass of 10 eV. XPS wide-scan and narrow-scan spectra were obtained under UHV conditions (base pressure 3×10^{-7} Pa). All narrow-range spectra were corrected with a linear background before fitting. The spectra were fitted with symmetrical Gaussian/Lorentzian (GL(30)) line shapes using CasaXPS. All spectra were referenced to the C1s peak attributed to C–C and C–H atoms at 285.0 eV.

Attenuated total reflection Fourier-transform infrared spectroscopy (ATR-FTIR). IR spectra were recorded on a Bruker Tensor 27 FT-IR spectrometer (Massachusetts, United States) with an Auto Seagull Pro IR attachment and Ge hemispherical ATR crystal attachment. The spectrum of an unmodified plasma cleaned sample was measured as a background and was subtracted from the spectra of modified samples. In addition, a linear baseline correction was applied. Spectra were acquired with 256 scans at a resolution of 4 cm^{-1}. The starting angle was set at 68°, and with the p-polarization angle is 90° (horizontally polarized)

Atomic force microscopy (AFM). AFM surface topography images were acquired by an Asylum Research MFP-3D SA AFM (Oxford Instruments, United Kingdom). A sharp knife was used to scratch the surfaces. The scratched surfaces were sonicated in a mixture of Milli-Q water and absolute EtOH (1:1) to remove the residuals from scratching. The surfaces were subsequently dried with Ar, and the scratched surfaces were directly measured by AFM. The height differences between scratched and intact surface in AFM topography images were used to determine the thickness of polymer layers. Gwyddion software was used to process and analyze the AFM topography images.[54]

Scanning Auger electron spectroscopy (AES). Scanning AES measurements were performed at room temperature with a scanning Auger electron microscope (JEOL Ltd., Japan, JAMP-

9500F field emission scanning Auger microprobe) system. Elemental mapping was analyzed by AES. Elemental images were acquired with a primary beam of 10 keV and 8 nm probe diameter was used. The take-off angle of the instrument was 0°.

Electronic Core Level Calculations. All calculations were done with the GAUSSIAN 16 program.[55] The geometries of the different systems were optimized at the B3LYP/6-311G(d,p) level of theory. Natural bond orbital (NBO) analysis was employed to obtain the core orbital energies.[56]

Supporting information is available free of charge at the Wiley Online Library website:

Acknowledgements

This project has received funding from the European Union's Horizon 2020 research and innovation program under the MarieSklodowska-Curie grant agreement No 720325, FoodSmartphone. The authors thank Esther van Andel, Sidharam Pujari, Jan Willem Borst, Barend van Lagen, Ileana Micu and Cees van Rijn for insightful discussions and technical assistance.

References

1. Williams, D. F., On the Nature of Biomaterials. *Biomaterials* **2009,** *30* (30), 5897-5909.

2. Wischerhoff, E.; Badi, N.; Lutz, J.-F.; Laschewsky, A., Smart Bioactive Surfaces. *Soft Matter* **2010,** *6* (4), 705-713.

3. Nguyen, A. T.; van Doorn, R.; Baggerman, J.; Paulusse, J. M. J.; Klerks, M. M.; Zuilhof, H.; van Rijn, C. J. M., Flow-Through Microbial Capture by Antibody-Coated Microsieves. *Advanced Materials Interfaces* **2015,** *2* (3), 1400292.

4. Yu, Q.; Zhang, Y.; Wang, H.; Brash, J.; Chen, H., Anti-fouling Bioactive Surfaces. *Acta Biomaterialia* **2011,** *7* (4), 1550-1557.

5. Chapman, R. G.; Ostuni, E.; Takayama, S.; Holmlin, R. E.; Yan, L.; Whitesides, G. M., Surveying for Surfaces that Resist the Adsorption of Proteins. *Journal of the American Chemical Society* **2000,** *122* (34), 8303-8304.

6. Jeon, S. I.; Andrade, J. D., Protein—surface Interactions in the Presence of Polyethylene Oxide: II. Effect of Protein Size. *Journal of Colloid and Interface Science* **1991,** *142* (1), 159-166.

7. Andree, K. C.; Barradas, A. M. C.; Nguyen, A. T.; Mentink, A.; Stojanovic, I.; Baggerman, J.; van Dalum, J.; van Rijn, C. J. M.; Terstappen, L. W. M. M., Capture of Tumor Cells on Anti-EpCAM-Functionalized Poly(acrylic acid)-Coated Surfaces. *ACS Applied Materials & Interfaces* **2016,** *8* (23), 14349-14356.

8. Matsuda, T.; Ohya, S., Photoiniferter-Based Thermoresponsive Graft Architecture with Albumin Covalently Fixed at Growing Graft Chain End. *Langmuir* **2005,** *21* (21), 9660-9665.

9. Nguyen, A. T.; Baggerman, J.; Paulusse, J. M. J.; van Rijn, C. J. M.; Zuilhof, H., Stable Protein-Repellent Zwitterionic Polymer Brushes Grafted from Silicon Nitride. *Langmuir* **2011,** *27* (6), 2587-2594.

10. Rodriguez-Emmenegger, C.; Brynda, E.; Riedel, T.; Houska, M.; Šubr, V.; Alles, A. B.; Hasan, E.; Gautrot, J. E.; Huck, W. T. S., Polymer Brushes Showing Non-Fouling in Blood Plasma Challenge the Currently Accepted Design of Protein Resistant Surfaces. *Macromolecular Rapid Communications* **2011,** *32* (13), 952-957.

11. Zamfir, M.; Rodriguez-Emmenegger, C.; Bauer, S.; Barner, L.; Rosenhahn, A.; Barner-Kowollik, C., Controlled Growth of Protein Resistant PHEMA Brushes via S-RAFT Polymerization. *Journal of Materials Chemistry B* **2013,** *1* (44), 6027-6034.

12. Hong, D.; Hung, H.-C.; Wu, K.; Lin, X.; Sun, F.; Zhang, P.; Liu, S.; Cook, K. E.; Jiang, S., Achieving Ultralow Fouling under Ambient Conditions via Surface-Initiated ARGET ATRP of Carboxybetaine. *ACS Appl. Mater. & Interfaces* **2017,** *9* (11), 9255-9259.

13. Zoppe, J. O.; Ataman, N. C.; Mocny, P.; Wang, J.; Moraes, J.; Klok, H.-A., Surface-Initiated Controlled Radical Polymerization: State-of-the-Art, Opportunities, and Challenges in Surface and Interface Engineering with Polymer Brushes. *Chem. Rev.* **2017,** *117* (3), 1105-1318.

14. Rosso, M.; Nguyen, A. T.; de Jong, E.; Baggerman, J.; Paulusse, J. M. J.; Giesbers, M.; Fokkink, R. G.; Norde, W.; Schroën, K.; Rijn, C. J. M. v.; Zuilhof, H., Protein-Repellent Silicon Nitride Surfaces: UV-Induced Formation of Oligoethylene Oxide Monolayers. *ACS Appl. Mater. & Interfaces* **2011,** *3* (3), 697-704.

15. Chen, L.; Zeng, R.; Xiang, L.; Luo, Z.; Wang, Y., Polydopamine-graft-PEG antifouling coating for quantitative analysis of food proteins by CE. *Anal. Methods* **2012,** *4* (9), 2852-2859.

16. de los Santos Pereira, A.; Rodriguez-Emmenegger, C.; Surman, F.; Riedel, T.; Alles, A. B.; Brynda, E., Use of Pooled Blood Plasmas in the Assessment of Fouling Resistance. *RSC Advances* **2014,** *4* (5), 2318-2321.

17. Rodriguez Emmenegger, C.; Brynda, E.; Riedel, T.; Sedlakova, Z.; Houska, M.; Alles, A. B., Interaction of Blood Plasma with Antifouling Surfaces. *Langmuir* **2009,** *25* (11), 6328-6333.

18. Jiang, S.; Cao, Z., Ultralow-Fouling, Functionalizable, and Hydrolyzable Zwitterionic Materials and Their Derivatives for Biological Applications. *Advanced Materials* **2010,** *22* (9), 920-932.

19. Schlenoff, J. B., Zwitteration: Coating Surfaces with Zwitterionic Functionality to Reduce Nonspecific Adsorption. *Langmuir* **2014,** *30* (32), 9625-9636.

20. Krause, J. E.; Brault, N. D.; Li, Y.; Xue, H.; Zhou, Y.; Jiang, S., Photoiniferter-Mediated Polymerization of Zwitterionic Carboxybetaine Monomers for Low-Fouling and Functionalizable Surface Coatings. *Macromolecules* **2011,** *44* (23), 9213-9220.

21. Lange, S. C.; van Andel, E.; Smulders, M. M. J.; Zuilhof, H., Efficient and Tunable Three-Dimensional Functionalization of Fully Zwitterionic Antifouling Surface Coatings. *Langmuir* **2016,** *32* (40), 10199-10205.

22. Wang, Z.; van Andel, E.; Pujari, S. P.; Feng, H.; Dijksman, J. A.; Smulders, M. M. J.; Zuilhof, H., Water-repairable zwitterionic polymer coatings for anti-biofouling surfaces. *J. Mater. Chem. B* **2017,** *5* (33), 6728-6733.

23. Vorobii, M.; de los Santos Pereira, A.; Pop-Georgievski, O.; Kostina, N. Y.; Rodriguez-Emmenegger, C.; Percec, V., Synthesis of Non-fouling poly[N-(2-hydroxypropyl)methacrylamide] Brushes by Photoinduced SET-LRP. *Polymer Chemistry* **2015,** *6* (23), 4210-4220.

24. Kuzmyn, A. R.; de los Santos Pereira, A.; Pop-Georgievski, O.; Bruns, M.; Brynda, E.; Rodriguez-Emmenegger, C., Exploiting End Group Functionalization for the Design of Antifouling Bioactive Brushes. *Polymer Chemistry* **2014,** *5* (13), 4124-4131.

25. Matyjaszewski, K., Advanced Materials by Atom Transfer Radical Polymerization. *Advanced Materials* **2018,** *30* (23), 1706441.

26. Pan, X.; Fantin, M.; Yuan, F.; Matyjaszewski, K., Externally controlled atom transfer radical polymerization. *Chem. Soc. Rev.* **2018,** *47* (14), 5457-5490.

27. Song, Y.; Ye, G.; Lu, Y.; Chen, J.; Wang, J.; Matyjaszewski, K., Surface-Initiated ARGET ATRP of Poly(Glycidyl Methacrylate) from Carbon Nanotubes via Bioinspired Catechol Chemistry for Efficient Adsorption of Uranium Ions. *ACS Macro Lett.* **2016,** *5* (3), 382-386.

28. Konkolewicz, D.; Magenau, A. J. D.; Averick, S. E.; Simakova, A.; He, H.; Matyjaszewski, K., ICAR ATRP with ppm Cu Catalyst in Water. *Macromolecules* **2012,** *45* (11), 4461-4468.

29. Pan, X.; Tasdelen, M. A.; Laun, J.; Junkers, T.; Yagci, Y.; Matyjaszewski, K., Photomediated Controlled Radical Polymerization. *Progress in Polymer Science* **2016,** *62*, 73-125.

30. Lalevée, J.; Tehfe, M.-A.; Dumur, F.; Gigmes, D.; Blanchard, N.; Morlet-Savary, F.; Fouassier, J. P., Iridium Photocatalysts in Free Radical Photopolymerization under Visible Lights. *ACS Macro Lett.* **2012,** *1* (2), 286-290.

31. Poelma, J. E.; Fors, B. P.; Meyers, G. F.; Kramer, J. W.; Hawker, C. J., Fabrication of Complex Three-Dimensional Polymer Brush Nanostructures through Light-Mediated Living Radical Polymerization. *Angew. Chem. Int. Ed.* **2013,** *52* (27), 6844-6848.

32. Treat, N. J.; Fors, B. P.; Kramer, J. W.; Christianson, M.; Chiu, C.-Y.; Read de Alaniz, J.; Hawker, C. J., Controlled Radical Polymerization of Acrylates Regulated by Visible Light. *ACS Macro Lett.* **2014,** *3* (6), 580-584.

33. Zhang, G.; Song, I. Y.; Park, T.; Choi, W., Recyclable and stable ruthenium catalyst for free radical polymerization at ambient temperature initiated by visible light photocatalysis. *Green Chem.* **2012,** *14* (3), 618-621.

34. Wang, C.-G.; Chen, C.; Sakakibara, K.; Tsujii, Y.; Goto, A., Facile Fabrication of Concentrated Polymer Brushes with Complex Patterning by Photocontrolled Organocatalyzed Living Radical Polymerization. *Angew. Chem. Int. Ed.* **2018,** *57* (41), 13504-13508.

35. Baggerman, J.; Smulders, M. M. J.; Zuilhof, H., Romantic Surfaces: A Systematic Overview of Stable, Biospecific, and Antifouling Zwitterionic Surfaces. *Langmuir* **2019,** *35* (5), 1072-1084.

36. Vaisocherová-Lísalová, H.; Surman, F.; Víšová, I.; Vala, M.; Špringer, T.; Ermini, M. L.; Šípová, H.; Šedivák, P.; Houska, M.; Riedel, T.; Pop-Georgievski, O.; Brynda, E.; Homola, J., Copolymer Brush-Based Ultralow-Fouling Biorecognition Surface Platform for Food Safety. *Analytical Chemistry* **2016,** *88* (21), 10533-10539.

37. Lísalová, H.; Brynda, E.; Houska, M.; Víšová, I.; Mrkvová, K.; Song, X. C.; Gedeonová, E.; Surman, F.; Riedel, T.; Pop-Georgievski, O.; Homola, J., Ultralow-Fouling Behavior of Biorecognition Coatings Based on Carboxy-Functional Brushes of Zwitterionic Homo- and Copolymers in Blood Plasma: Functionalization Matters. *Analytical Chemistry* **2017,** *89* (6), 3524-3531.

38. Nguyen, A. T.; Baggerman, J.; Paulusse, J. M. J.; Zuilhof, H.; van Rijn, C. J. M., Bioconjugation of Protein-Repellent Zwitterionic Polymer Brushes Grafted from Silicon Nitride. *Langmuir* **2012,** *28* (1), 604-610.

39. Bog, U.; de los Santos Pereira, A.; Mueller, S. L.; Havenridge, S.; Parrillo, V.; Bruns, M.; Holmes, A. E.; Rodriguez-Emmenegger, C.; Fuchs, H.; Hirtz, M., Clickable Antifouling Polymer Brushes for Polymer Pen Lithography. *ACS Appl. Mater. & Interfaces* **2017,** *9* (13), 12109-12117.

40. Vaisocherová, H.; Ševců, V.; Adam, P.; Špačková, B.; Hegnerová, K.; de los Santos Pereira, A.; Rodriguez-Emmenegger, C.; Riedel, T.; Houska, M.; Brynda, E.; Homola, J., Functionalized Ultra-low Fouling Carboxy- and Hydroxy-functional Surface Platforms:

Functionalization Capacity, Biorecognition Capability and Resistance to Fouling from Undiluted Biological Media. *Biosensors and Bioelectronics* **2014,** *51*, 150-157.

41. Kitano, H.; Suzuki, H.; Matsuura, K.; Ohno, K., Molecular Recognition at the Exterior Surface of a Zwitterionic Telomer Brush. *Langmuir* **2010,** *26* (9), 6767-6774.

42. Tajima, N.; Takai, M.; Ishihara, K., Significance of Antibody Orientation Unraveled: Well-Oriented Antibodies Recorded High Binding Affinity. *Anal. Chem.* **2011,** *83* (6), 1969-1976.

43. van Andel, E.; Lange, S. C.; Pujari, S. P.; Tijhaar, E. J.; Smulders, M. M. J.; Savelkoul, H. F. J.; Zuilhof, H., Systematic Comparison of Zwitterionic and Non-Zwitterionic Antifouling Polymer Brushes on a Bead-Based Platform. *Langmuir* **2019,** *35* (5), 1181-1191.

44. Bisel, P.; Al-Momani, L.; Müller, M., The tert-butyl group in chemistry and biology. *Org. Biomol. Chem* **2008,** *6* (15), 2655-2665.

45. Tugulu, S.; Klok, H.-A., Stability and Nonfouling Properties of Poly(poly(ethylene glycol) methacrylate) Brushes under Cell Culture Conditions. *Biomacromolecules* **2008,** *9* (3), 906-912.

46. Paripovic, D.; Klok, H.-A., Improving the Stability in Aqueous Media of Polymer Brushes Grafted from Silicon Oxide Substrates by Surface-Initiated Atom Transfer Radical Polymerization. *Macromol. Chem. Phys.* **2011,** *212* (9), 950-958.

47. Giesbers, M.; Marcelis, A. T. M.; Zuilhof, H., Simulation of XPS C1s Spectra of Organic Monolayers by Quantum Chemical Methods. *Langmuir* **2013,** *29* (15), 4782-4788.

48. Zhao, J.; Gao, F.; Pujari, S. P.; Zuilhof, H.; Teplyakov, A. V., Universal Calibration of Computationally Predicted N 1s Binding Energies for Interpretation of XPS Experimental Measurements. *Langmuir* **2017,** *33* (41), 10792-10799.

49. Cao, Z.; Yu, Q.; Xue, H.; Cheng, G.; Jiang, S., Nanoparticles for Drug Delivery Prepared from Amphiphilic PLGA Zwitterionic Block Copolymers with Sharp Contrast in Polarity between Two Blocks. *Angew. Chem. Int. Ed.* **2010,** *49* (22), 3771-3776.

50. de los Santos Pereira, A.; Riedel, T.; Brynda, E.; Rodriguez-Emmenegger, C., Hierarchical Antifouling Brushes for Biosensing Applications. *Sensors and Actuators B: Chemical* **2014,** *202*, 1313-1321.

51. Laschewsky, A.; Rosenhahn, A., Molecular Design of Zwitterionic Polymer Interfaces: Searching for the Difference. *Langmuir* **2019,** *35* (5), 1056-1071.

52. Huang, C.-J.; Li, Y.; Jiang, S., Zwitterionic Polymer-Based Platform with Two-Layer Architecture for Ultra Low Fouling and High Protein Loading. *Analytical Chemistry* **2012,** *84* (7), 3440-3445.

53. Weisel, J. W.; Litvinov, R. I., Mechanisms of fibrin polymerization and clinical implications. *Blood* **2013,** *121* (10), 1712.

54. Nečas, D.; Klapetek, P., Gwyddion: an Open-source Software for SPM Data Analysis. *Open Physics* **2012,** *10* (1), 181-188.

55. Frisch, M. J.; Trucks, G. W.; Schlegel, H. B.; Scuseria, G. E.; Robb, M. A.; Cheeseman, J. R.; Scalmani, G.; Barone, V.; Petersson, G. A.; Nakatsuji, H.; Li, X.; Caricato, M.; Marenich, A. V.; Bloino, J.; Janesko, B. G.; Gomperts, R.; Mennucci, B.; Hratchian, H. P.; Ortiz, J. V.; Izmaylov, A. F.; Sonnenberg, J. L.; Williams; Ding, F.; Lipparini, F.; Egidi, F.; Goings, J.; Peng, B.; Petrone, A.; Henderson, T.; Ranasinghe, D.; Zakrzewski, V. G.; Gao, J.; Rega, N.; Zheng, G.; Liang, W.; Hada, M.; Ehara, M.; Toyota, K.; Fukuda, R.; Hasegawa, J.; Ishida, M.; Nakajima, T.; Honda, Y.; Kitao, O.; Nakai, H.; Vreven, T.; Throssell, K.; Montgomery Jr., J. A.; Peralta, J. E.; Ogliaro, F.; Bearpark, M. J.; Heyd, J. J.; Brothers, E. N.; Kudin, K. N.; Staroverov, V. N.; Keith, T. A.; Kobayashi, R.; Normand, J.; Raghavachari, K.; Rendell, A. P.; Burant, J. C.; Iyengar, S. S.; Tomasi, J.; Cossi, M.; Millam, J. M.; Klene, M.; Adamo, C.; Cammi, R.; Ochterski, J. W.; Martin, R. L.; Morokuma, K.; Farkas, O.; Foresman, J. B.; Fox, D. J. *Gaussian 16 Rev. B.01*, Rev. B.01; Gaussian Inc.: Wallingford, CT, 2016.

56. Glendening, E. D., Reed, A.E., Carpenter, J.E. and Weinhold, F., *NBO (version 3.1)*

Chapter 3

Antifouling Polymer Brushes via Oxygen-Tolerant Surface-Initiated PET-RAFT

Kuzmyn, A. R., Nguyen, A. T., Teunissen, L. W., Zuilhof, H., & Baggerman, J. (2020). Antifouling Polymer Brushes via Oxygen-Tolerant Surface-Initiated PET-RAFT. Langmuir, 36(16), 4439–4446. https://doi.org/10.1021/acs.langmuir.9b03536

Abstract

This work presents a new method for the synthesis of antifouling polymer brushes using surface-initiated photoinduced electron transfer–reversible addition–fragmentation chain transfer (SI-PET-RAFT) polymerization with Eosin Y and triethanolamine as catalysts. This method proceeds in an aqueous environment under atmospheric conditions without any prior degassing, and without use of heavy metal catalysts. The versatility of the method is shown by using three chemically different monomers: oligo(ethylene glycol) methacrylate, *N*-(2-hydroxypropyl)methacrylamide and carboxybetaine methacrylamide. In addition, the light-triggered nature of the polymerization allows the creation of complex three-dimensional structures. The composition and topological structuring of the brushes are confirmed by X-ray photoelectron spectroscopy (XPS) and atomic force microscopy (AFM). The kinetics of the polymerizations are followed by measuring the layer thickness with ellipsometry. The polymer brushes demonstrate excellent antifouling properties when exposed to single-protein solutions and complex biological matrices such as diluted bovine serum. This method thus presents a new simple approach for the manufacturing of antifouling coatings for biomedical and biotechnological applications.

Introduction

Non-specific interactions between engineering materials and complex biological fluids obstruct the performance of many biotechnological and biomedical devices.[1-2] In particular, non-specific adsorption of protein or fouling from biological media can cause issues such as blockage of flow-through separation columns and porous membranes,[3] non-specific response of label-free affinity-based biosensors,[1, 4] reduced circulation time of nanocarriers in the bloodstream,[5] and bacterial attachment on contact lenses.[6-7] The fouling can be curbed by introducing antifouling coatings on the surfaces of the materials that are in contact with a biological matrix.[1-2, 8-10] The creation of these coatings that can resist non-specific interactions with a biological medium still poses a challenge, in particular their formation in mass manufacturing processes.[1, 8, 11-12]

Numerous approaches to create antifouling coatings have been developed, for example, based on self-assembled monolayers[13] and “grafted to”[14-15] and “grafted from”[1-2, 8-9, 11-12, 16-22] polymer coatings. Although self-assembled monolayers and “grafted to”-polymer layers

can decrease adsorption from single-protein solutions, most of them fail when contacted with complex biological matrices, such as blood serum or cells.[13-15] The introduction of surface-initiated living radical polymerization (SI-LRP) provided a new efficient instrument to form antifouling layers based on "grafted from"-polymer brushes.[23] For instance, polymer brushes based on oligo(ethylene glycol) methacrylate,[2, 9, 18] *N*-(2-hydroxypropyl) methacrylamide,[20, 22, 24] carboxybetaine methacrylamide,[2, 9, 17, 20, 24-25] sulfobetaine methacrylamide[10, 21, 26] and their derivatives have shown remarkable resistance to nonspecific adsorption of proteins and also cells from complex biological fluids. Surface-initiated atom-transfer radical polymerization (SI-ATRP) is the most commonly applied SI-LRP method thus far.[1-2, 8, 19-20, 27] The well-controlled nature of SI-ATRP allows to tune the thickness and density of polymer brushes in order to achieve the best resistance to nonspecific protein adsorption.[23, 28] The versatility of SI-ATRP allowed to grow polymer brushes from almost any type of surfaces.[29] However, the SI-ATRP technique uses relatively high concentrations of metal-based catalysts to generate radicals from alkyl halides,[8, 10, 18, 20-21] provides limited means to structure the brush layer in either composition or thickness, and requires a rigorous control over an oxygen-free atmosphere to perform the reaction in. Therefore, new approaches have been developed that overcome these limitations.

An approach based on single-electron transfer living radical polymerization (SET-LRP) strongly reduced the amount of Cu^0 needed to conduct the polymerization.[22] Recently, our group introduced the use of light-triggered living radical polymerization (LT-LRP) using an iridium-based catalyst, which allowed to control the thickness and functionality of antifouling polymer brushes in a spatial manner (via patterning) and over time (via intensity and duration of the illumination). This thus opened up the possibility to create micro-patterned antifouling bioactive layers with a controlled thickness and functionality per pattern.[24] However, the third limitation still remains: despite the well-controlled and tunable nature of SI-ATRP, SET-LRP, and LT-LRP, they all require an oxygen-free environment during the polymerization.[8-9, 11-12, 18, 20, 22, 24] This also applies to novel surface-initiated approaches based on reversible addition–fragmentation chain transfer (SI-RAFT)[30] and photoiniferter-mediated polymerization (SI-PIMP):[31-33] no heavy metal catalysts are required, and a wide compatibility with a large number of monomers exists, but they still require oxygen-free conditions to sustain the controlled radical polymerization.

Recently, a new RAFT-based technique was introduced: photoinduced electron transfer–reversible addition–fragmentation chain transfer (PET-RAFT).[34-37] This method allowed to synthetize polymers in a controlled fashion in the presence of oxygen. The mechanism and living nature of PET-RAFT polymerizations were previously investigated by Jiangtao Xu *et al.*[38] They proposed that the reaction proceeds according to a reductive quenching cycle of EY in which TEOA acts as a sacrificing electron donor to reduce oxygen in the polymerization system. The reduction of oxygen allows the polymerization to proceed in an oxygen-containing environment. In addition, the mild conditions and water compatibility enabled the synthesis of polymers grafting of polymer chains from a DNA and living cells.[35-36] Moreover, it was recently shown that this method is also suitable for surface-initiated polymerization of polymer brushes.[37]

Herein, we show the synthesis of antifouling polymer brushes employing surface-initiated photoinduced electron transfer–reversible addition–fragmentation chain transfer polymerization (SI-PET-RAFT). We demonstrate that this method is suitable for growing brushes in water with an accessible and affordable organic photocatalyst, Eosin Y. The applied technique is thus free from heavy metal. We have synthesized polymer brushes based on three different types of antifouling monomers: oligo(ethylene glycol) methacrylate, *N*-(2-hydroxypropyl) methacrylamide and carboxybetaine methacrylamide (see Scheme 1), as these represent three main chemical approaches towards minimizing the nonspecific adsorption of proteins by polymer brushes. Moreover, we aimed for a truly robust method that should allow polymerization in two- and three-dimensional patterns of all three of those chemically different monomers in oxygen-tolerant conditions. The composition, thickness and pattern formation of the resulting brushes were characterized extensively by X-ray Photoelectron Spectroscopy (XPS), Atomic Force Microscopy (AFM) and imaging ellipsometry. The antibiofouling properties of the synthetized polymer brushes were analyzed using fluorescence confocal laser scanning microscopy (CLSM) of surfaces exposed to single-fluorescent protein solutions and bovine serum.

Experimental section

Materials. All chemical reagents were used without further purification, unless otherwise specified. 4-Cyano-4-(phenylcarbonothioylthio)pentanoic acid *N*-succinimidyl ester (RAFT-

NHS), (3-Aminopropyl)triethoxysilane (APTES), triethanolamine (TEOA), eosin Y (EY), triethylamine (TEA), poly(ethylene glycol) methyl ether methacrylate (average Mn 300) (MeOEGMA), ethanol (EtOH) (99.9%), acetone (99.5%), dry tetrahydrofuran (THF, 99.9%), and phosphate-buffered saline (PBS) were purchased from Sigma-Aldrich, *N*-(2-hydroxypropyl) methacrylamide (HPMA) was obtained from Polysciences, Inc., and streptavidin-Alexa488 conjugate (Str-Alexa488) and bovine serum albumin-Alexa488 conjugate (BSA-Alexa488) were purchased from Fisher Thermo Scientific. Silicon substrates were acquired from Siltronix. Deionized water was produced with a Milli-Q integral 3 system Millipore, Molscheim, France (Milli-Q water). (3-Acryloylamino-propyl)-(2-carboxy-ethyl)-dimethyl-ammonium (CBMA) was synthetized according to a previously described procedure.[11-12, 20] Bovine serum was obtained and biotinylated as previously described.[21]

Light Source. LEDs with a maximum intensity at 410 nm (Intelligent LED Solutions product number: ILH-XO01-S410-SC211-WIR200) were used, current was set at 700 mA, corresponding to a total radiometric power of 2.9 W, according to manufacturer specifications.

Formation of RAFT agent-functionalized monolayers. The substrates were rinsed with, acetone, absolute ethanol (EtOH) and Milli-Q water and blown dry under a gentle stream of Ar. Subsequently, the surfaces were exposed to an oxygen plasma for 5 min in a plasma cleaner (100 W; 5 mbar O_2; Diener electronic GmbH, Germany). The freshly activated surfaces were immediately immersed in a freshly prepared solution of (3-aminopropyl)triethoxysilane (APTES) (1 mg·mL^{-1}) in absolute ethanol at RT for 16 h. The substrates were subsequently rinsed with EtOH and Milli-Q water and blow dried with Ar. After immobilization of the APTES on surfaces the substrates were submerged in a solution of RAFT-NHS (20 mg, 53 µmol) and TEA (7 mg, 10 µL, 72 µmol) in 1 mL of dry THF at RT for 16 h. The substrates were subsequently rinsed with THF, acetone, EtOH and Milli-Q water and blow dried with Ar. The substrates were stored under Ar protection before use.

SI-PET-RAFT synthesis of polymer brushes. A stock solution with photocatalyst was prepared containing: EY (25 mg, 39 µmol), TEOA (160 mg, 1.6 mmol) in 10 ml of Milli-Q water. The monomer HPMA (178 mg, 1.3 mmol) or MeOEGMA (94 mg, 0.3 mmol) or CBMA (76 mg, 0.3 mmol) was dissolved in Milli-Q water (1 mL) and subsequently 10 µL of the stock solution was added. The mixture was vortexed and added to the vials containing surfaces with immobilized RAFT agent. Immediately after this, the polymerization was conducted by

irradiating the vials with visible light from a LED light source for different periods of time. The thickness of polymerization solution on top of the surfaces was 2 mm. In these experiments, the light source was placed 3 - 4 cm from the substrates (Figure S1, Supporting information), to prevent substantial heating of the samples with the light. The polymerization was stopped by turning off the light. The samples were removed from the solution and subsequently rinsed with Milli-Q water and ethanol, and blown dry under a stream of Ar.

X-ray photoelectron spectroscopy (XPS). XPS measurements were performed using a JPS-9200 photoelectron spectrometer (JEOL Ltd., Japan). All the samples were prepared and stored under ambient conditions, prior to analysis using a focused monochromated Al Kα X-ray source (spot size of 300 µm) radiation at 12 kV and 20 mA with an analyzer energy pass of 10 eV. XPS wide-scan and narrow-scan spectra were obtained under UHV conditions (base pressure $3 \cdot 10^{-7}$ Pa). All narrow-range spectra were corrected with a linear background before fitting. The spectra were fitted with symmetrical Gaussian/Lorentzian (GL(30)) line shapes using CasaXPS. All spectra were referenced to the C1s peak attributed to C–C and C–H atoms at 285.0 eV.

Static water contact angle measurements. The wettability of the modified surfaces was determined by automated static water contact angle measurements with the use of a Kruss DSA 100 goniometer. The volume of a drop of demineralized water is 3 µL. Contact angles from sessile drops measured by the tangent method was estimated using a standard error propagation technique involving partial derivatives.

Spectroscopic ellipsometry. The polymerization kinetics were followed by measuring the dry thickness of the brushes using an Accurion Nanofilm_ep4 Imaging Ellipsometer. The ellipsometric data were acquired in air at room temperature using light in the wavelength range of λ = 400.6 – 761.3 nm at an angle of incidence of 50°. The data were fitted with EP4 software using a multilayer model.

Atomic force microscopy (AFM). AFM surface topography images were acquired by an Asylum Research MFP-3D SA AFM (Oxford Instruments, United Kingdom). Gwyddion software was used to process and analyze the AFM topography images.[39]

Fluorescence microscopy. A Leica TCS SP8 confocal laser scanning microscope (CLMS) (Leica Microsystems, Mannheim, Germany) was used to measure protein fouling and specific

interactions of the coated surfaces. A Leica HyDTM hybrid detector was used in photon counting mode to measure the intensity of the fluorescence signal. A 10× objective was used and the samples were set in focus by maximizing the reflected light intensity from the laser. Fluorescence images were obtained by accumulating 10 consecutive images. Images were analyzed with the Leica LAS X Life Science software.

Protein fouling studies. Fouling of the coated surfaces by individual proteins or in complex biological media were investigated by incubating surfaces in single-protein solution of Str-Alexa488 (0.5 mg·mL^{-1}) or BSA-Alexa488 (0.5 mg·mL^{-1}), or in a 10%-dilution biotinylated bovine serum 15 min at RT. The surfaces were then washed with PBS (10 mL, pH 7.4). The samples exposed to biotinylated bovine serum were further labeled and followed by exposure to Str-Alexa (0.5 mg·mL^{-1}) for 15 min at RT. Afterwards the samples were again rinsed with PBS (10 mL, pH 7.4) and Milli-Q water (10 mL), and subsequently dried by blowing with Ar. Further, the samples were mounted on the glass slides and measured the intensity of fluorescence of adsorbed proteins.

The limit of detection was determined by placing 1 µL droplets containing known concentrations of BSA-Alexa488 on plasma-cleaned silicon oxide surfaces. The droplets were allowed to dry. The spot sizes of the dried drops were measured, allowing to calculate a surface density of the dried protein in ng·mm^{-2}. The fluorescence intensity of the spots was measured according to method described above.

Electronic core level calculations. All calculations were done with the GAUSSIAN 16 program.[40] The geometries of the different systems were optimized at the B3LYP/6-311G(d,p) level of theory. Natural bond orbital (NBO) analysis was employed to obtain the core orbital energies.[41]

Results and discussions

Synthesis of initiator-coated surfaces. The antifouling polymer brushes were created in four steps starting from bare silicon surfaces (Scheme 1). The surfaces were first coated with a RAFT agent-functionalized monolayer, which was then used for surface-initiated polymerization of the brushes. To this aim bare silicon surfaces were first oxidized using an air plasma for 5 min and subsequently coated with (3-aminopropyl)triethoxysilane (APTES). The amine-terminated surfaces were reacted with 4-cyano-4-(phenylcarbonothioylthio)pentanoic acid *N*-succinimidyl ester (RAFT-NHS) yielding a RAFT

agent-functionalized monolayer. From the RAFT agent-coated surfaces antifouling polymer brushes were grown using SI-PET-RAFT, in the presence of eosin Y (EY) and triethanolamine (TEOA) as catalysts, based on poly(ethylene glycol) methyl ether methacrylate (average Mn 300) (MeOEGMA), *N*-(2-hydroxypropyl) methacrylamide (HPMA) and carboxybetaine methacrylamide (CBMA). We will now discuss each step in detail.

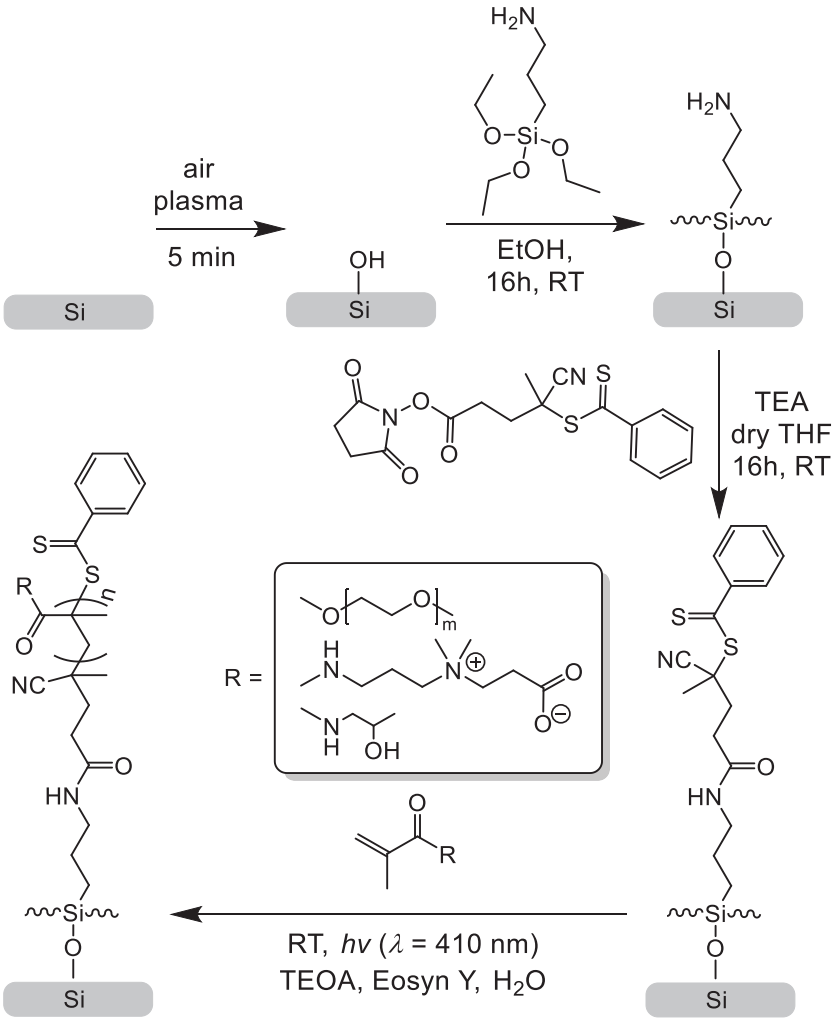

Scheme 1. Schematic depiction of the air-tolerant SI-PET-RAFT technique to make antifouling polymer brushes.

The silicon surfaces were functionalized with the initiator in two stages. First, the silicon surfaces were functionalized with APTES. The successful modification with APTES was

confirmed with XPS. The XPS wide-scan spectrum showed main peaks that correspond to O1s, C1s, N1s and Si2p atoms (Figure 1a). The experimental ratio between C : N was 4.3 : 1.0, i.e. slightly higher than the theoretical elemental ratio in the compound (3: 1), which is attributed to atmospheric contamination. The high content of oxygen in the XPS spectrum confirms the presence of a thin silicon oxide layer. The XPS narrow-scan spectrum of the C1s region (Figure 1b) can be deconvoluted with two peaks. The peak at 285.0 eV is attributed to the carbon atoms in the alkyl backbone of APTES, and the peaks at 286.5 eV is assigned to the carbon atoms adjacent to the amino group [**C**-N]. The observed ratio between the [**C**-C/H]: [**C**-N] peaks is 1.7 : 1.0, which is comparable to the theoretical ratio of 2 : 1 between [**C**-C/H]: [**C**-N]. The XPS spectrum of the C1s region of the APTES monolayer is also in agreement with the predicted XPS spectrum based on calculated core orbital energy levels as obtained by density functional theory (DFT) calculations (Figure S2).[42-43] The XPS wide-scan spectrum also allowed to estimate the thickness of the APTES monolayer based on the Si : C ratio.[44] This thickness was estimated to be 0.5 ± 0.1 nm, in line with expectations for an APTES monolayer.

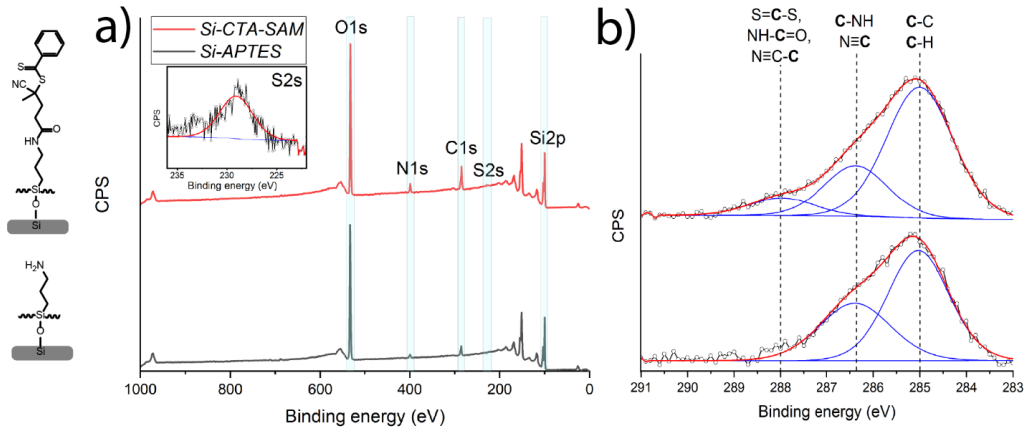

Figure 1. XPS characterization of the APTES and initiator-functionalized monolayers. (a) Wide-scan spectra of the APTES (grey line) and initiator-functionalized monolayers (red line), the inset shows the narrow-scan spectrum of the S2s region. (b) Corresponding narrow-scan C1s spectra.

The initiator-functionalized surfaces were created by exposing previously prepared APTES-modified surfaces to 4-cyano-4-(phenylcarbonothioylthio)pentanoic acid *N*-succinimidyl ester (RAFT-NHS) (Scheme 1). The reaction was conducted in dry THF in the presence of

triethylamine. The success of the reaction was confirmed by XPS. In the XPS wide-scan spectrum main peaks can be observed that correspond to O1s, C1s, N1s, S2s and Si2p atoms with a ratio of 5.2 : 1.0 : 0.4 for C : N : S. The theoretical ratio for these elements is 8.0 : 1.0 : 1.0 in case of a 100% conversion of the reaction between APTES and RAFT-NHS. Based on the C / N ratio obtained from eight samples 29 ± 4% of the surface-bound amines has reacted to hold an RAFT agent moiety (Equation S1). This was confirmed by the narrow-range C1s spectrum, which can be fitted with three major peaks attributed to [**C**-C/H] at 285.0 eV, [**C**-NH, N≡**C**] at 286.4 eV and [S=**C**-S, NH-**C**=O, N≡C-**C**] at 288.X eV. DFT-based simulations of the C 1s spectrum agree with this peak assignment (Figure S3).[42-43] In addition, the presence of sulfur was clearly shown in the XPS S2s narrow-scan spectrum (Figure 1a, inset) with peak maximum at 228 eV, indicating the presence of the RAFT-agent on the surface. This results are in accordance with previously published XPS spectra of RAFT-agent.[30] The thickness of the obtained layer has increased in comparison with the APTES monolayer and was calculated to be 1.1 ± 0.2 nm based on the C / Si ratio. Moreover, the static water contact angle of the coated surfaces before and after RAFT-NHS modification increased from 54° to 97°. All together, these characterizations confirm the successful immobilization of the RAFT agent on the silicon oxide surfaces.

Synthesis and characterization of poly(MeOEGMA), poly(CBMA) and poly(HPMA) brushes. Poly(HPMA), poly(MeOEGMA) and poly(CBMA) brushes with different thicknesses were grown from the RAFT-agent-coated surfaces by SI-PET-RAFT using Eosin Y, as a photocatalyst. Eosin Y was used because it has been shown to be oxygen-tolerant photocatalyst for polymerizations.[45] The polymerizations were conducted in Milli-Q water solution in presence of triethanolamine (TEOA). The AFM topography images of brush-coated surfaces through the range of the thicknesses from 4 nm to 45 nm revealed highly homogeneous layers with roughnesses of Rq = 0.36 ± 0.03 nm for poly(HPMA), Rq = 0.14 ± 0.04 nm for poly(MeOEGMA), and Rq = 0.50 ± 0.18 nm for poly(CBMA). The chemical composition of each synthetized polymer brush was confirmed by XPS (only layers > 20 nm thickness are discussed, so as to minimize the effects of the underlying Si surface and original APTES monolayer). The XPS wide-scan spectrum of a poly(MeOEGMA) layer with a thickness of 27 nm, as determined by ellipsometry, showed two main peaks for O1s and C1s in a ratio of 1.0 : 2.6 (Figure 2a). The XPS narrow-scan spectrum of C1s region shows three main peaks of carbon atoms: [C-C/H]: [C-O]: [O-C=O]

in a ratio of 2.8 : 9.4 : 1 (Figure 2b). In addition, this C1s narrow spectrum was simulated for two MeOEGMA monomers (Figure S3, Supporting information) with an average *Mw* of 300 (*Mw* = 278.35 and *Mw* = 322.40). The simulated spectrum gives a ratio between [**C**-C/H]: [**C**-O]: [O-**C**=O] of 3 : 10 : 1, which is in good agreement with the ratio found by fitting the experimental data.[42-43] The static water contact angle of poly(MeOEGMA)-coated surfaces was determined to be 49 ± 1°, indicating the formation of an hydrophilic layer. In summary, the XPS, AFM and contact angle data confirm the presence of well-defined poly(MeOEGMA) brushes.

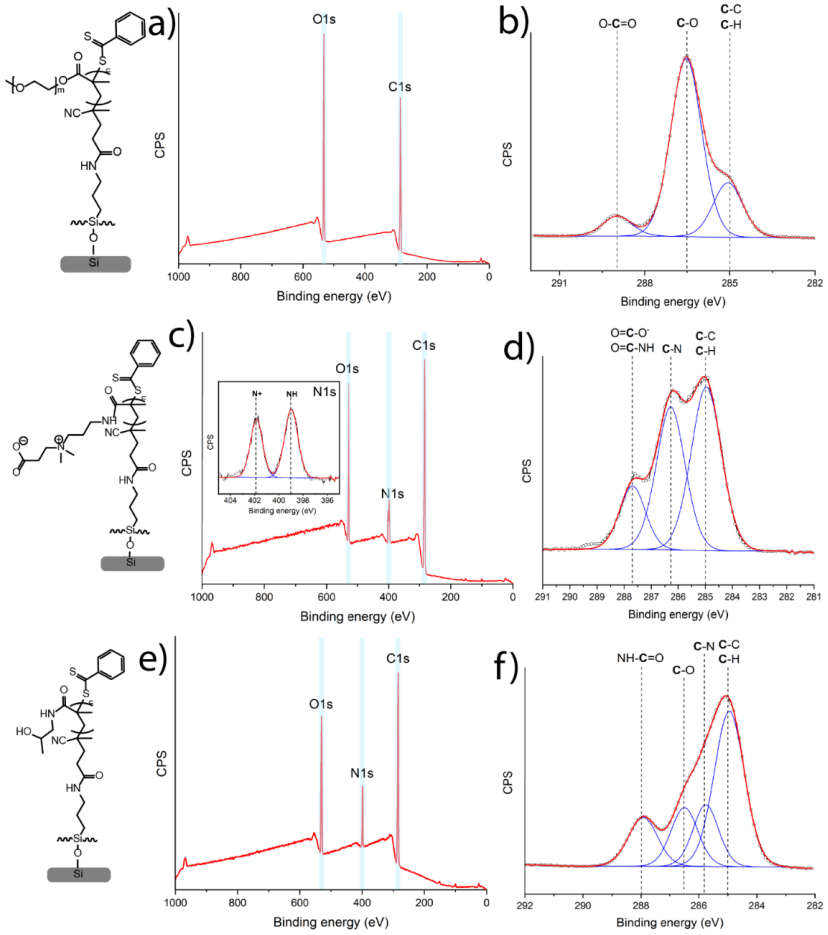

Figure 2. XPS characterization of: Poly(MeOEGMA) brushes: (a) wide-scan spectrum, and (b) narrow-scan C1s spectrum. Poly(CBMA) brushes: (c) wide-scan spectrum with inset narrow-scan spectrum of N1s region, and (d) narrow-scan C1s spectrum. Poly(HPMA) brushes: (e) wide-scan spectrum, and (f) narrow-scan C1s spectrum.

The XPS wide-scan spectrum of poly(CBMA) brushes with an ellipsometric thickness of 29 nm (Figure 3c) shows three main peaks related to O, N, and C atoms, in a ratio of 2.6 : 1.8 : 12.6. This indicates an enhanced carbon content compared to the expected ratio based on the elemental composition of the poly(CBMA) structure: 3 : 2 : 12, due to atmospheric contamination. The zwitterionic nature of poly(CBMA) brushes was confirmed also by XPS narrow-scan spectrum of N 1s region that displays two chemically different types of nitrogen atoms [N^+] and [NH] in a ratio 1 : 1.3. The deviation from 1 : 1 ratio seems to be an XPS-induced change, as noted by Van Andel et al.[21] The narrow-scan XPS C1s spectrum (Figure 2d) displays two broad peaks at 285.X eV and 286.3 eV assigned to [**C**-C/H] and [**C**-N] atoms, and a smaller peak at 287.7 eV attributed to the carbonyl and carboxyl atoms. The ratio between the [**C**-C/H]: [**C**-N]: [**C**=O] peaks is 5.5 : 4.6 : 1.8, which indicates a relatively high aliphatic carbon content compared to the theoretically expected composition of the poly(CBMA) structure (5 : 5 : 2). The poly(CBMA) layers also showed high hydrophilicity with a static water contact angle of 20 ± 1°. The overall physicochemical characterization for the poly(CBMA) layers is in good agreement with the properties found for poly(CBMA) layers synthetized using other polymerization methods such, as ATRP and PIMP.[2, 11-12, 20-21, 33]

The chemical composition of poly(HPMA) brushes was also confirmed by XPS. The XPS wide-scan spectrum of poly(HPMA) brushes with an ellipsometric thickness of 26 nm (Figure 2e) shows three main peaks related to O1s, N1s, and C1s electrons, in a 1.8 : 1 : 7.6 ratio, which is in agreement with the elemental composition of the poly(HPMA) structure (2 : 1 : 7). The narrow-scan XPS C1s spectrum (Figure 2c) displays a broad peak at 285.X eV, with a shoulder between 286-287 eV, attributed to overlapping signals from aliphatic, alcohol and amine carbon atoms, and a smaller peak at 288.2 eV attributed to the carbonyl atom. The spectrum was deconvoluted by fitting it with four peaks at: 285.0 eV assigned to aliphatic [C-H] and [C-C] atoms, at 285.7 eV from the [C-N] atoms, at 286.6 eV from the [C-O] atoms, and at 288.2 eV from the NH-C=O atoms. The fitted ratio between the [C-C/H]: [C-N]: [C-O]: [C=O] peaks is 3.6 : 1.2 : 1.2 : 1.1, which correlates with the theoretically expected composition of the poly(HPMA) structure (4 : 1 : 1 : 1). Accurate fitting is in this case difficult, due to the overlap between the [C-C/H], [C-N] and [C-O] peaks, in line with previously reported experimental and simulated C1s XPS spectra.[24] The poly(HPMA) brushes displayed a static water contact angle of 49 ± 1°, confirming the formation of a

hydrophilic brush. In summary, also well-defined poly(HPMA) brushes could be made by this SI-PET-RAFT method, and yield characteristics that correspond to that of analogous coatings made by other methods, such as SET-LRP,[22] ATRP[20] and LT-LRP.[24]

Kinetics of polymer brush growth. The kinetics of the polymer brush growth for all three monomers were followed by measuring the polymer brush layer thicknesses with scanning ellipsometry (Figure 3). The polymer brushes all demonstrated a linear growth in the first hour, which indicates the controlled nature of the polymerization. This allows tuning of the polymer brush thickness from 0 to 40 nm, and reaching thicknesses higher than 10 nm within the first 20 min of polymerization under ambient conditions, i.e. in an oxygen-containing environment. Thicknesses higher than 10-15 nm are required for significant resistance towards non-specific adsorption from complex biological matrices by polymer brushes based on antifouling monomers such MeOEGMA, HPMA and CBMA.[18, 20-21] The rate of polymerization during the first hour for poly(MeOEGMA), poly(HPMA) and poly(CBMA) were determined to be 0.44 ± 0.04, 0.51 ±0.05 and 0.21 ± 0.04 $nm \cdot min^{-1}$, respectively. [Note: The concentration of the HPMA monomer was increased four times in comparison with CBMA and MeOEGMA protocols. Lower monomer concentrations of HPMA did not allow to create brushes thicker than 14 nm.] After 2 h of the polymerization of kinetics all three monomers had slowed down, which is probably related to gradual oxidation of the photocatalyst.[37, 46] However, it is has been shown before that it is possible to grow thicker brushes by refreshing the polymerization solution or conducting the polymerization in presence of oxygen consuming agent.[34, 37] This indicates that the living nature of the polymers is not lost during PET-RAFT polymerization. Moreover, it has been reported that the rate of polymerization in an oxygen-containing environment in PET-RAFT polymerization conditions is slower and less controlled than that in an inert atmosphere,[47] although such factors do clearly not prevent the smooth growth of thick, homogeneous polymer brushes.

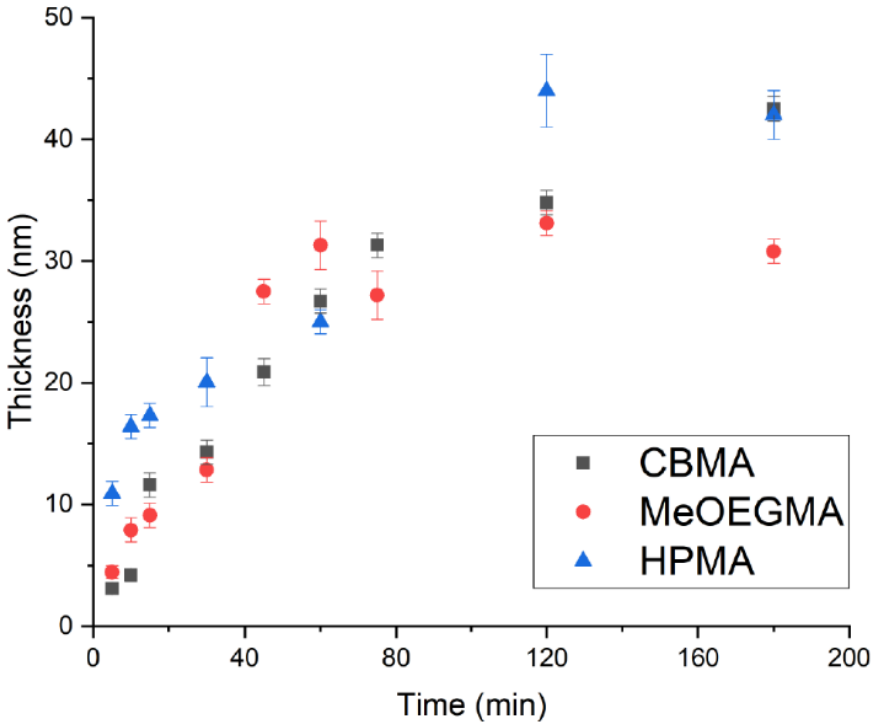

Figure 3. Dry thickness of poly(MeOEGMA), poly(CBMA) and poly(HPMA) brushes as function of the polymerization time, as determined by ellipsometry.

The relatively fast rate and oxygen-tolerant nature of the polymerization allow the SI-PET-RAFT technique to be easily scaled up and used in a wide range of biotechnological and biomedical applications. Moreover, we demonstrate that the SI-PET-RAFT technique can be used with relatively low concentrations of monomer (typically 0.3 – 1.3 M) and photocatalyst (~ 39 mM) that creates favorable conditions for its mass application.

Patterning. Another significant advantage of our SI-PET-RAFT approach is that it enables the formation of complex 3D-structured polymer brush layers by using a mask and tuning its thickness. This was demonstrated by the growth of poly(HPMA) from a RAFT agent-functionalized surface with a patterning mask. This resulted in a surface with a patterned polymer (Figure S5, Supporting information), with a brush thickness of 30 nm in the exposed regions. In addition, we conducted a control experiment in which a plasma-cleaned silicon substrate without immobilized RAFT-agent was submerged into the polymerization solution and exposed to the same polymerization conditions for 4 h. The sample showed a negligible

amount of absorbed monomer by XPS and an average thickness of 2.1 ± 0.3 nm. This confirms that the polymerization indeed proceeds via the RAFT agent linked to the surface.

Antifouling properties of polymer brushes synthetized by SI-PET-RAFT. To demonstrate the antifouling properties of the obtained polymer brushes, they were challenged with fluorescently labeled single-protein solutions of streptavidin-Alexa488 conjugate (Str-Alexa488, 0.5 mg·mL^{-1}) and of bovine serum albumin-Alexa488 conjugate (BSA-Alexa488, 0.5 mg·mL^{-1}), and by 10-fold diluted biotinylated bovine serum (BS), in each case for 15 min. The fouling by biotinylated BS was detected by subsequent exposure to the Str-Alexa488 solution, which binds to the biotin residues of any fouling serum proteins present on the surface. The bare silicon surface showed high fluorescence intensities from all three solutions (Figure 4), indicating significant fouling. The fluorescence intensity of all polymer brush-coated samples was low after exposure, and similar to the background level measured for unexposed surfaces (Figure 4). The limit of detection of this fluorescent label-based method was determined to be ~ 0.3 ng·mm^{-2} (corresponding to a fluorescent intensity of about 6 a.u.), by measuring the fluorescence intensity and size of spots of dried drops with known concentrations of fluorescence-labeled proteins (Figure S6, Supporting information). The fluorescence intensities of all polymer brush coated surfaces after exposure are below the detection limit. Overall, the synthetized polymer brushes showed good antifouling properties (< 0.3 ng·mm^{-2}) towards single-protein solution as well as complex biological liquids such as diluted bovine serum.

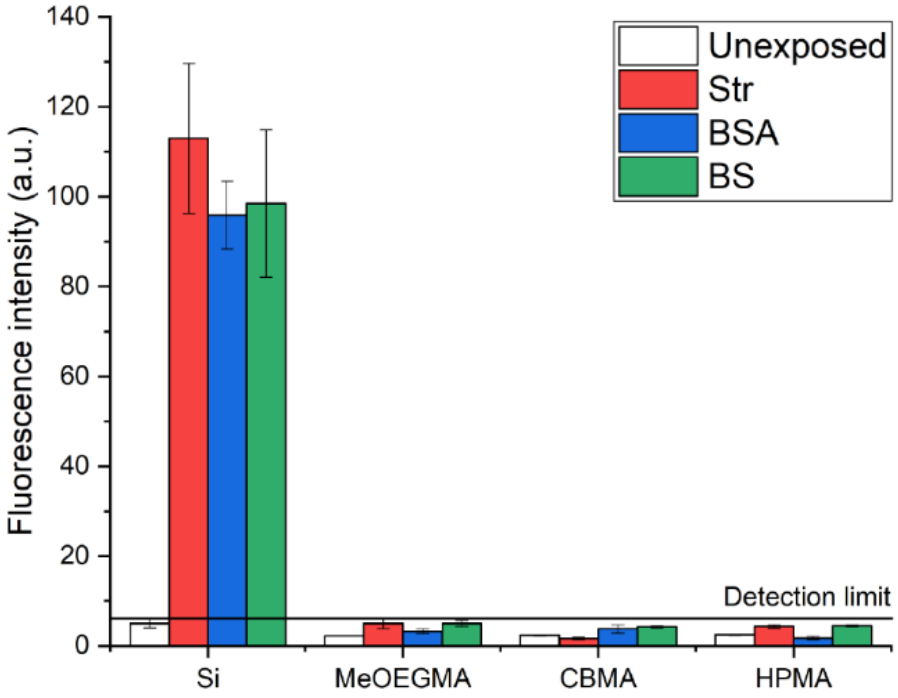

Figure 4. Fluorescence intensity at 500-550 nm of bare silicon, poly(MeOEGMA), thickness: 27 nm, poly(CBMA), thickness: 29 nm and poly(HPMA), thickness: 26 nm, before and after exposure to solutions of Str-Alexa488 (0.5 mg·mL^{-1}), BSA-Alexa488 (0.5 mg·mL^{-1}) and Str-Alexa488 labeled 10% diluted biotinylated bovine serum (BS).

Conclusions

We developed a simple light-induced and oxygen-tolerant way for creating antifouling polymer brushes. The brush growth involved a surface-initiated photoinduced electron transfer–reversible addition–fragmentation chain transfer (SI-PET-RAFT) polymerization. The polymerization was conducted using visible light in an aqueous environment in the presence of eosin Y and triethanolamine as catalysts. We demonstrated that this approach creates well-defined antifouling polymer brushes based on: oligo(ethylene glycol) methacrylate, *N*-(2-hydroxypropyl)methacrylamide and carboxybetaine methacrylamide. The designed polymer brush coatings showed good antifouling properties in single-protein solutions of bovine serum albumin, streptavidin, and also in diluted bovine serum medium. The absence of heavy metal catalysts, the tolerance towards the presence of oxygen, and the photo-triggered

nature of this polymerization method allow this technique to be used for the construction of patterned surfaces, and also to be readily scaled up. We envision that the simplicity of this technique will facilitate the introduction of antifouling coatings based on polymer brushes in mass manufacturing of biomedical and biotechnological devices.

Supporting information is available free of charge at the ACS Publications:

Acknowledgment

The authors thank Sidharam Pujari, Jan Willem Borst, Barend van Lagen, and Cees van Rijn for insightful discussions and technical assistance. Esther van Andel is acknowledged for providing biotinylated bovine serum. The first part of this work has received funding from the European Union's Horizon 2020 research and innovation program under the Marie Sklodowska-Curie grant agreement No 720325, FoodSmartphone. The second part of this work is part of the Science PPP Fund research program with project number 741.018.105, which is partly financed by the Dutch Research Council (NWO)

References

1. Baggerman, J.; Smulders, M. M. J.; Zuilhof, H., Romantic Surfaces: A Systematic Overview of Stable, Biospecific, and Antifouling Zwitterionic Surfaces. *Langmuir* **2019,** *35* (5), 1072-1084.

2. de los Santos Pereira, A.; Rodriguez-Emmenegger, C.; Surman, F.; Riedel, T.; Alles, A. B.; Brynda, E., Use of Pooled Blood Plasmas in the Assessment of Fouling Resistance. *RSC Advances* **2014,** *4* (5), 2318-2321.

3. Rana, D.; Matsuura, T., Surface Modifications for Antifouling Membranes. *Chemical Reviews* **2010,** *110* (4), 2448-2471.

4. Homola, J., Surface Plasmon Resonance Sensors for Detection of Chemical and Biological Species. *Chemical Reviews* **2008,** *108* (2), 462-493.

5. Yang, J.; Kopeček, J., Design of Smart HPMA Copolymer-Based Nanomedicines. *J Control Release* **2016,** *240*, 9-23.

6. Xiao, A.; Dhand, C.; Leung, C. M.; Beuerman, R. W.; Ramakrishna, S.; Lakshminarayanan, R., Strategies to Design Antimicrobial Contact Lenses and Contact Lens Cases. *Journal of Materials Chemistry B* **2018,** *6* (15), 2171-2186.

7. Thissen, H.; Gengenbach, T.; du Toit, R.; Sweeney, D. F.; Kingshott, P.; Griesser, H. J.; Meagher, L., Clinical Observations of Biofouling on PEO Coated Silicone Hydrogel Contact Lenses. *Biomaterials* **2010,** *31* (21), 5510-5519.

8. Rodriguez-Emmenegger, C.; Avramenko, O. A.; Brynda, E.; Skvor, J.; Alles, A. B., Poly(HEMA) Brushes Emerging as a New Platform for Direct Detection of Food Pathogen in Milk Samples. *Biosensors and Bioelectronics* **2011,** *26* (11), 4545-4551.

9. Rodriguez Emmenegger, C.; Brynda, E.; Riedel, T.; Sedlakova, Z.; Houska, M.; Alles, A. B., Interaction of Blood Plasma with Antifouling Surfaces. *Langmuir* **2009,** *25* (11), 6328-6333.

10. Nguyen, A. T.; Baggerman, J.; Paulusse, J. M. J.; van Rijn, C. J. M.; Zuilhof, H., Stable Protein-Repellent Zwitterionic Polymer Brushes Grafted from Silicon Nitride. *Langmuir* **2011,** *27* (6), 2587-2594.

11. Vaisocherová-Lísalová, H.; Surman, F.; Víšová, I.; Vala, M.; Špringer, T.; Ermini, M. L.; Šípová, H.; Šedivák, P.; Houska, M.; Riedel, T.; Pop-Georgievski, O.; Brynda, E.; Homola, J., Copolymer Brush-Based Ultralow-Fouling Biorecognition Surface Platform for Food Safety. *Analytical Chemistry* **2016,** *88* (21), 10533-10539.

12. Vaisocherová, H.; Ševců, V.; Adam, P.; Špačková, B.; Hegnerová, K.; de los Santos Pereira, A.; Rodriguez-Emmenegger, C.; Riedel, T.; Houska, M.; Brynda, E.; Homola, J., Functionalized Ultra-low Fouling Carboxy- and Hydroxy-functional Surface Platforms: Functionalization Capacity, Biorecognition Capability and Resistance to Fouling from Undiluted Biological Media. *Biosensors and Bioelectronics* **2014,** *51*, 150-157.

13. Chapman, R. G.; Ostuni, E.; Takayama, S.; Holmlin, R. E.; Yan, L.; Whitesides, G. M., Surveying for Surfaces that Resist the Adsorption of Proteins. *Journal of the American Chemical Society* **2000,** *122* (34), 8303-8304.

14. Andree, K. C.; Barradas, A. M. C.; Nguyen, A. T.; Mentink, A.; Stojanovic, I.; Baggerman, J.; van Dalum, J.; van Rijn, C. J. M.; Terstappen, L. W. M. M., Capture of Tumor Cells on Anti-EpCAM-Functionalized Poly(acrylic acid)-Coated Surfaces. *ACS Applied Materials & Interfaces* **2016,** *8* (23), 14349-14356.

15. Jeon, S. I.; Andrade, J. D., Protein—surface Interactions in the Presence of Polyethylene Oxide: II. Effect of Protein Size. *Journal of Colloid and Interface Science* **1991,** *142* (1), 159-166.

16. Gahtory, D.; Sen, R.; Kuzmyn, A. R.; Escorihuela, J.; Zuilhof, H., Strain-Promoted Cycloaddition of Cyclopropenes with o-Quinones: A Rapid Click Reaction. *Angewandte Chemie* **2018,** *130* (32), 10275-10279.

17. de los Santos Pereira, A.; Riedel, T.; Brynda, E.; Rodriguez-Emmenegger, C., Hierarchical Antifouling Brushes for Biosensing Applications. *Sensors and Actuators B: Chemical* **2014,** *202*, 1313-1321.

18. Kuzmyn, A. R.; de los Santos Pereira, A.; Pop-Georgievski, O.; Bruns, M.; Brynda, E.; Rodriguez-Emmenegger, C., Exploiting End Group Functionalization for the Design of Antifouling Bioactive Brushes. *Polymer Chemistry* **2014,** *5* (13), 4124-4131.

19. Lísalová, H.; Brynda, E.; Houska, M.; Víšová, I.; Mrkvová, K.; Song, X. C.; Gedeonová, E.; Surman, F.; Riedel, T.; Pop-Georgievski, O.; Homola, J., Ultralow-Fouling Behavior of Biorecognition Coatings Based on Carboxy-Functional Brushes of Zwitterionic Homo- and Copolymers in Blood Plasma: Functionalization Matters. *Analytical Chemistry* **2017,** *89* (6), 3524-3531.

20. Rodriguez-Emmenegger, C.; Brynda, E.; Riedel, T.; Houska, M.; Šubr, V.; Alles, A. B.; Hasan, E.; Gautrot, J. E.; Huck, W. T. S., Polymer Brushes Showing Non-Fouling in Blood Plasma

Challenge the Currently Accepted Design of Protein Resistant Surfaces. *Macromolecular Rapid Communications* **2011,** *32* (13), 952-957.

21. van Andel, E.; Lange, S. C.; Pujari, S. P.; Tijhaar, E. J.; Smulders, M. M. J.; Savelkoul, H. F. J.; Zuilhof, H., Systematic Comparison of Zwitterionic and Non-Zwitterionic Antifouling Polymer Brushes on a Bead-Based Platform. *Langmuir* **2019,** *35* (5), 1181-1191.

22. Vorobii, M.; de los Santos Pereira, A.; Pop-Georgievski, O.; Kostina, N. Y.; Rodriguez-Emmenegger, C.; Percec, V., Synthesis of Non-fouling poly[N-(2-hydroxypropyl)methacrylamide] Brushes by Photoinduced SET-LRP. *Polymer Chemistry* **2015,** *6* (23), 4210-4220.

23. Zoppe, J. O.; Ataman, N. C.; Mocny, P.; Wang, J.; Moraes, J.; Klok, H.-A., Surface-Initiated Controlled Radical Polymerization: State-of-the-Art, Opportunities, and Challenges in Surface and Interface Engineering with Polymer Brushes. *Chemical Reviews* **2017,** *117* (3), 1105-1318.

24. Kuzmyn, A. R.; Nguyen, A. T.; Zuilhof, H.; Baggerman, J., Bioactive Antifouling Surfaces by Visible-Light-Triggered Polymerization. *Advanced Materials Interfaces* **2019,** *6* (12), 1900351.

25. Laschewsky, A.; Rosenhahn, A., Molecular Design of Zwitterionic Polymer Interfaces: Searching for the Difference. *Langmuir* **2019,** *35* (5), 1056-1071.

26. Nguyen, A. T.; Baggerman, J.; Paulusse, J. M. J.; Zuilhof, H.; van Rijn, C. J. M., Bioconjugation of Protein-Repellent Zwitterionic Polymer Brushes Grafted from Silicon Nitride. *Langmuir* **2012,** *28* (1), 604-610.

27. Jiang, S.; Cao, Z., Ultralow-Fouling, Functionalizable, and Hydrolyzable Zwitterionic Materials and Their Derivatives for Biological Applications. *Advanced Materials* **2010,** *22* (9), 920-932.

28. Matyjaszewski, K., Advanced Materials by Atom Transfer Radical Polymerization. *Advanced Materials* **2018,** *30* (23), 1706441.

29. Pop-Georgievski, O.; Rodriguez-Emmenegger, C.; Pereira, A. d. l. S.; Proks, V.; Brynda, E.; Rypáček, F., Biomimetic Non-fouling Surfaces: Extending the Concepts. *Journal of Materials Chemistry B* **2013,** *1* (22), 2859-2867.

30. Zamfir, M.; Rodriguez-Emmenegger, C.; Bauer, S.; Barner, L.; Rosenhahn, A.; Barner-Kowollik, C., Controlled Growth of Protein Resistant PHEMA Brushes via S-RAFT Polymerization. *Journal of Materials Chemistry B* **2013,** *1* (44), 6027-6034.

31. Rahane, S. B.; Kilbey, S. M.; Metters, A. T., Kinetics of Surface-Initiated Photoiniferter-Mediated Photopolymerization. *Macromolecules* **2005,** *38* (20), 8202-8210.

32. Matsuda, T.; Ohya, S., Photoiniferter-Based Thermoresponsive Graft Architecture with Albumin Covalently Fixed at Growing Graft Chain End. *Langmuir* **2005,** *21* (21), 9660-9665.

33. Krause, J. E.; Brault, N. D.; Li, Y.; Xue, H.; Zhou, Y.; Jiang, S., Photoiniferter-Mediated Polymerization of Zwitterionic Carboxybetaine Monomers for Low-Fouling and Functionalizable Surface Coatings. *Macromolecules* **2011,** *44* (23), 9213-9220.

34. Niu, J.; Page, Z. A.; Dolinski, N. D.; Anastasaki, A.; Hsueh, A. T.; Soh, H. T.; Hawker, C. J., Rapid Visible Light-Mediated Controlled Aqueous Polymerization with In Situ Monitoring. *ACS Macro Letters* **2017,** *6* (10), 1109-1113.

35. Lueckerath, T.; Strauch, T.; Koynov, K.; Barner-Kowollik, C.; Ng, D. Y. W.; Weil, T., DNA–Polymer Conjugates by Photoinduced RAFT Polymerization. *Biomacromolecules* **2019,** *20* (1), 212-221.

36. Niu, J.; Lunn, D. J.; Pusuluri, A.; Yoo, J. I.; O'Malley, M. A.; Mitragotri, S.; Soh, H. T.; Hawker, C. J., Engineering Live Cell Surfaces with Functional Polymers via Cytocompatible Controlled Radical Polymerization. *Nature Chemistry* **2017,** *9*, 537.

37. Li, M.; Fromel, M.; Ranaweera, D.; Rocha, S.; Boyer, C.; Pester, C. W., SI-PET-RAFT: Surface-Initiated Photoinduced Electron Transfer-Reversible Addition–Fragmentation Chain Transfer Polymerization. *ACS Macro Letters* **2019,** *8* (4), 374-380.

38. Xu, J.; Shanmugam, S.; Duong, H. T.; Boyer, C., Organo-photocatalysts for Photoinduced Electron Transfer-Reversible Addition–Fragmentation Chain Transfer (PET-RAFT) Polymerization. *Polymer Chemistry* **2015,** *6* (31), 5615-5624.

39. Nečas, D.; Klapetek, P., Gwyddion: an Open-source Software for SPM Data Analysis. *Open Physics* **2012,** *10* (1), 181-188.

40. Frisch, M. J.; Trucks, G. W.; Schlegel, H. B.; Scuseria, G. E.; Robb, M. A.; Cheeseman, J. R.; Scalmani, G.; Barone, V.; Petersson, G. A.; Nakatsuji, H.; Li, X.; Caricato, M.; Marenich, A. V.; Bloino, J.; Janesko, B. G.; Gomperts, R.; Mennucci, B.; Hratchian, H. P.; Ortiz, J. V.; Izmaylov, A. F.; Sonnenberg, J. L.; Williams; Ding, F.; Lipparini, F.; Egidi, F.; Goings, J.; Peng, B.; Petrone,

A.; Henderson, T.; Ranasinghe, D.; Zakrzewski, V. G.; Gao, J.; Rega, N.; Zheng, G.; Liang, W.; Hada, M.; Ehara, M.; Toyota, K.; Fukuda, R.; Hasegawa, J.; Ishida, M.; Nakajima, T.; Honda, Y.; Kitao, O.; Nakai, H.; Vreven, T.; Throssell, K.; Montgomery Jr., J. A.; Peralta, J. E.; Ogliaro, F.; Bearpark, M. J.; Heyd, J. J.; Brothers, E. N.; Kudin, K. N.; Staroverov, V. N.; Keith, T. A.; Kobayashi, R.; Normand, J.; Raghavachari, K.; Rendell, A. P.; Burant, J. C.; Iyengar, S. S.; Tomasi, J.; Cossi, M.; Millam, J. M.; Klene, M.; Adamo, C.; Cammi, R.; Ochterski, J. W.; Martin, R. L.; Morokuma, K.; Farkas, O.; Foresman, J. B.; Fox, D. J. *Gaussian 16 Rev. B.01*, Rev. B.01; Gaussian Inc.: Wallingford, CT, 2016.

41. Glendening, E. D., Reed, A.E., Carpenter, J.E. and Weinhold, F., *NBO (version 3.1)*

42. Giesbers, M.; Marcelis, A. T. M.; Zuilhof, H., Simulation of XPS C1s Spectra of Organic Monolayers by Quantum Chemical Methods. *Langmuir* **2013,** *29* (15), 4782-4788.

43. Zhao, J.; Gao, F.; Pujari, S. P.; Zuilhof, H.; Teplyakov, A. V., Universal Calibration of Computationally Predicted N 1s Binding Energies for Interpretation of XPS Experimental Measurements. *Langmuir* **2017,** *33* (41), 10792-10799.

44. Scheres, L.; Giesbers, M.; Zuilhof, H., Organic Monolayers onto Oxide-Free Silicon with Improved Surface Coverage: Alkynes versus Alkenes. *Langmuir* **2010,** *26* (7), 4790-4795.

45. Zhang, Y.; Ye, C.; Li, S.; Ding, A.; Gu, G.; Guo, H., Eosin Y-Catalyzed Photooxidation of Triarylphosphines Under Visible Light Irradiation and Aerobic Conditions. *RSC Advances* **2017,** *7* (22), 13240-13243.

46. Alvarez-Martin, A.; Trashin, S.; Cuykx, M.; Covaci, A.; De Wael, K.; Janssens, K., Photodegradation Mechanisms and Kinetics of Eosin-Y in Oxic and Anoxic Conditions. *Dyes and Pigments* **2017,** *145*, 376-384.

47. Zhou, J.; Ye, L.; Lin, Y.; Wang, L.; Zhou, L.; Hu, H.; Zhang, Q.; Yang, H.; Luo, Z., Surface Modification PVA Hydrogel with Zwitterionic via PET-RAFT to Improve the Antifouling Property. *Journal of Applied Polymer Science* **2019,** *136* (24), 47653.

Chapter 4

PLL-poly(HPMA) Bottlebrush-Based Antifouling Coatings: Three Grafting Routes

Roeven, E., Kuzmyn, A. R*, Scheres, L., Baggerman, J., Smulders, M. M. J., & Zuilhof, H. (2020). PLL–Poly(HPMA) Bottlebrush-Based Antifouling Coatings: Three Grafting Routes. Langmuir, 36(34), 10187–10199. https://doi.org/10.1021/acs.langmuir.0c01675*

**Contributed equally*

Abstract

In this work, we compare three routes to prepare antifouling coatings that consist of PLL-HPMA bottlebrushes. The poly(L-lysine) (PLL) backbone is self-assembled onto the surface by charged-based interactions between the lysine groups and the negatively charged silicon oxide surface, whereas the poly(*N*-(2-hydroxypropyl)methacrylamide) (HPMA) side chains, grown by RAFT polymerization, provide antifouling properties to the surface. First, the PLL-HPMA coatings are synthesized in a bottom-up fashion through a *grafting-from* approach. In this route, the PLL is self-assembled onto a surface, after which a polymerization agent is immobilized and finally HPMA is polymerized from the surface. In the second explored route the PLL is modified in solution by a RAFT agent to create a macroinitiator. After self-assembly of this macroinitiator onto the surface, the HPMA is polymerized from the surface by RAFT. In the third and last route, the whole PLL-HPMA bottlebrush is initially synthesized in solution. To this end, HPMA is polymerized from the macroinitiator in solution and the PLL-HPMA bottlebrush is then self-assembled onto the surface in just one step (*grafting-to*). Additionally, in this third route, we also design and synthesize a bottlebrush polymer with a PLL backbone and HPMA side chains, with the latter containing 5% carboxybetaine (CB) monomers that eventually allow for additional (bio)functionalization in solution or after surface immobilization. These three routes are evaluated in terms of: ease of synthesis, scalability, ease of characterization and a preliminary investigation of their antifouling performance. All three coating procedures result in coatings that show antifouling properties in single-protein antifouling tests. This method thus presents a new, simple, versatile and highly scalable approach for the manufacturing of PLL-based bottlebrush coatings that can be synthesized partly or completely on the surface or in solution, depending on the desired production process and/or application.

Introduction

The non-specific adsorption of proteins on a surface, *i.e.* fouling, is an initial step in the process of accumulation of unwanted biomaterial on that surface. The adsorption of such biomolecules and biomaterials impairs the functions of biotechnological and biomedical devices, whose correct functioning is crucially dependent on the availability of a non-fouled surface.[1] Surface modification by means of the application of antifouling coatings is

advantageous for, *e.g.*, manufacturing biosensors,[2] implants,[3,4] bioactive surfaces,[5] and even big objects like the hull of a ship.[6]

Especially for sensing low concentrations of a target analyte in complex media, there is a demand for facile surface modifications to impart biosensors with antifouling properties in order to prevent non-specific interactions and thereby enhance the signal-to-noise ratio.[7] Antifouling coatings frequently consist of polyethyleneglycol (PEG)[8,9] or zwitterionic polymers.[10–15] More recently, however, also poly(*N*-(2-hydroxypropyl)methacrylamide) (polyHPMA) brushes grown by controlled radical polymerizations have been reported to result in stable and highly antifouling coatings, on a par with –and in some cases outperforming– zwitterionic coatings.[7,13,16–19] Although the antifouling properties of poly(HPMA) brushes are not entirely understood, the reported fouling levels are extremely low, even despite being a hydrogen bond donor and displaying a moderate wettability. Mechanisms that are proposed are related to the ability to bind water.[16,18]

These polymeric coatings can be created via a *grafting-from* approach, in which a polymer is grown from the surface.[20,10,11] This is currently considered a highly promising route towards antifouling coatings in terms of long-term antifouling properties, as it leads to a high-density brush structure on the surface with tunable thickness.[21–23] However, despite these advantageous properties of polymer brushes grown via the *grafting-from* method, there is a major hurdle to be overcome if these antifouling coatings are to be applied reproducibly on large, industrially relevant scales.[24] Namely, these *grafting-from* polymer brushes are typically fabricated by surface-initiated, controlled living polymerization in the presence of a metal catalyst and in an oxygen-free environment.[11,13,18,25,26] Since this is typically a rather critical technique, it is difficult to scale up and implement in, *e.g.*, industrial production lines in a reproducible manner.[20,23] For this reason, there is a need to investigate other macromolecular coatings that can potentially match the antifouling properties of these coatings, but at the same time allow easy and reproducible fabrication.[11,13,20,25] To this aim, one-step coatings using zwitterionic antifouling polymer brushes with a catechol end group were developed for *grafting-to* surface anchoring.[27,28] In addition, Honda *et al.* created randomly composed block copolymers of zwitterionic antifouling groups, combined with triethoxy silanes for surface binding, to create antifouling coatings on glass.[23]

Another well-known example of combining antifouling groups with polydentate surface anchoring moieties are poly(L-lysine)-*graft*-poly(ethylene glycol) (PLL-*g*-PEG) polymers, which are known to assemble onto silicon oxide, metal oxide and polymeric surfaces.[29–34] PLL-*g*-PEG self-assembles on silicon oxide at pH > 2 through multiple electrostatic attractions between the negatively charged surface (SiO_2 isoelectric point (IEP) ~ 2.2)[35] and the positively charged pendant amine groups present in PLL (IEP ~9.5),[36] leaving the PEG chains oriented away from the surface.[34] Despite the ease of application and good antifouling properties of such PLL-*g*-PEG coatings, their use under certain circumstances can be limited due to properties inherent to PEG chains: PEG is known to undergo oxidative degradation, which may yield toxic compounds and leads to degradation of the coating, and has been shown to elicit antibody expression *in vivo*.[37–41]

In response to these limitations, Morgese *et al.* published in 2018 a study on polymers with PLL backbones that were grafted with other types of antifouling polymer brushes, such as poly(2-oxazines) and poly(2-oxazolines) to create bio-interfaces that resist protein adsorption.[31] However, the promising HPMA polymer was not included as a candidate in this study, and the authors only considered the *grafting to* approach. Therefore, we aimed to develop and investigate a bottlebrush macromolecule with poly(HPMA) grafted side chains for antifouling properties, together with a PLL backbone for multivalent surface interactions to achieve strong surface anchoring to silicon oxide surfaces.[28] Previously, PLL and HPMA-based polymers have been combined in hybrid macromolecules for the synthesis of gene delivery agents,[42] or as transfection reagents with minimized toxicity.[43] However, to the best of our knowledge, PLL-HPMA bottlebrushes have not yet been used for the creation of antifouling coatings. The overall goal of this project is to construct PLL bottlebrush coatings in an easy and highly scalable manner without loss of antifouling performance, and the current paper is the first step in this approach for PLL-HMPA bottlebrushes as antifouling coatings.

In this study, silicon oxide was used as a model substrate because of its relevance in, *e.g.*, biosensors[44] and microfluidic devices.[45] We explored three different routes towards such a coating with varying degrees of *grafting-to* and *grafting-from* components (Figure 1).

- *Route A*: a coating was completely *grafted-from* the surface. First, PLL was self-assembled on the surface. The RAFT agent that allows for polymerization was subsequently reacted to the PLL coating, after which HPMA side chains were RAFT-polymerized from the PLL backbone.
- *Route B*: a coating that was partly *grafted-from* the surface. The RAFT agent (RA) was coupled to PLL in a solution to synthesize a PLL-RA macroinitiator. The PLL-RA was self-assembled on the surface and HPMA was finally RAFT-polymerized from the RA-modified PLL coating.
- *Route C*: a completely pre-synthesized, *grafted-to* coating. HPMA was RAFT-polymerized from the PLL-RA macroinitiator in solution to create PLL-HPMA bottlebrushes. These bottlebrushes were then self-assembled on the surface in one single step.

For the growth of the poly(HPMA) brushes, photoinduced electron transfer–reversible addition-fragmentation chain transfer (PET-RAFT) technique was applied. This polymerization technique is oxygen tolerant, metal-free and can be applied to polymerizations in water,[46,47] works with an accessible and affordable organic photocatalyst (EosinY),[46,45] and has been shown to be also applicable to the surface-initiated polymerization of different monomers.[48] Especially this final feature makes PET-RAFT very suitable for our purpose, as it works well both in solution as well as from a surface. Subsequently, we determined and evaluated the various properties of the thus formed coatings in detail, including ease of synthesis, scalability, reproducibility, modularity, and ease of characterization. Finally, we performed a preliminary investigation of the antifouling performance obtained for these three coating approaches, and provide a perspective on the use of such PLL-HPMA bottlebrush coatings for antifouling purposes.

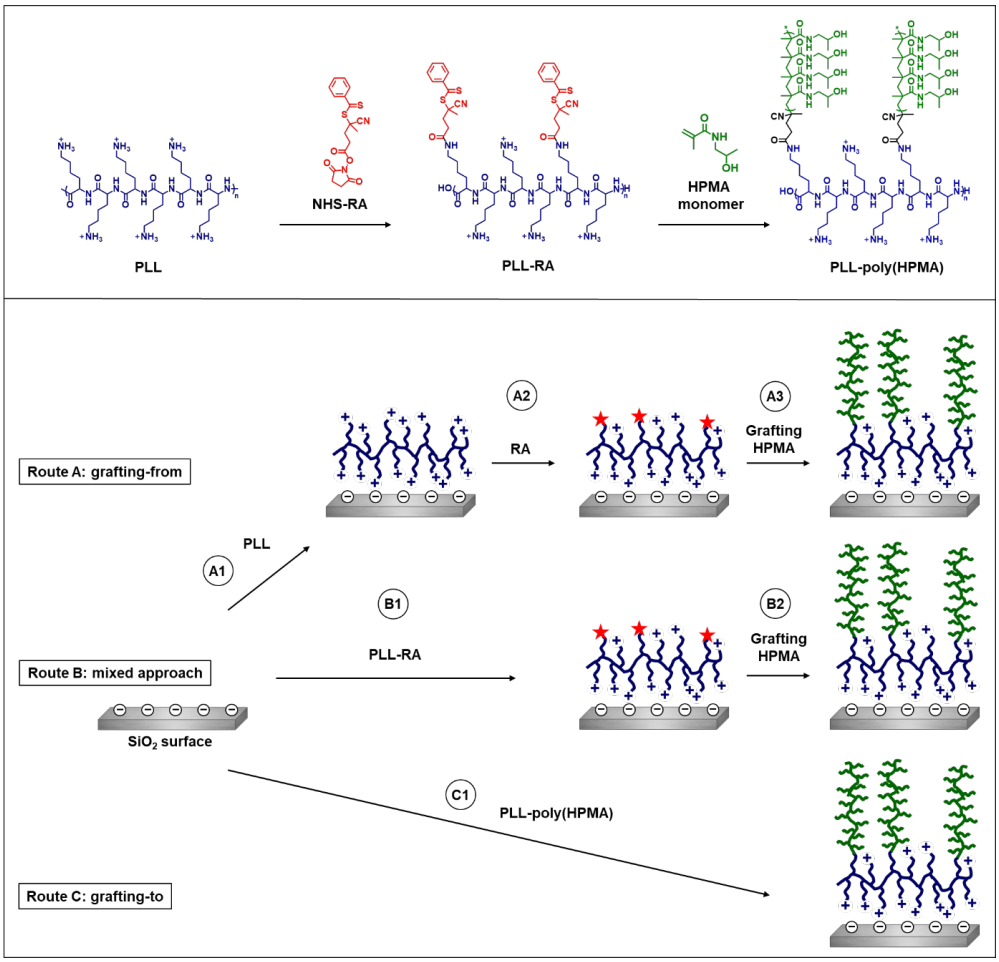

Figure 1. Schematic overview of the solution-based synthesis of the macroinitiator (PLL-RA) and PLL-HPMA bottlebrush structure (top). The three investigated routes A–C towards surface-immobilized PLL-HPMA bottlebrushes (bottom). PLL is poly(L-lysine), RA is RAFT agent, HPMA is 2-hydroxypropyl methacrylamide.

Results and discussion

We will first discuss the synthesis of the PLL-HPMA bottlebrush-based coatings on silicon oxide surfaces, as obtained via the three different routes presented in

Figure **1**. Afterwards, the results of antifouling studies on the coatings prepared by these different routes will be discussed and evaluated.

Route A: PLL-poly(HPMA) coating via the *grafting-from* procedure

In route A, the poly(HPMA)-based coating was completely *grafted-from* the surface. First, PLL was self-assembled on the surface, followed by coupling of the surface-bound PLL to the RAFT agent (RA), and finally, the polymerization of the poly(HPMA) side chains from the PLL backbone (Figure 2).

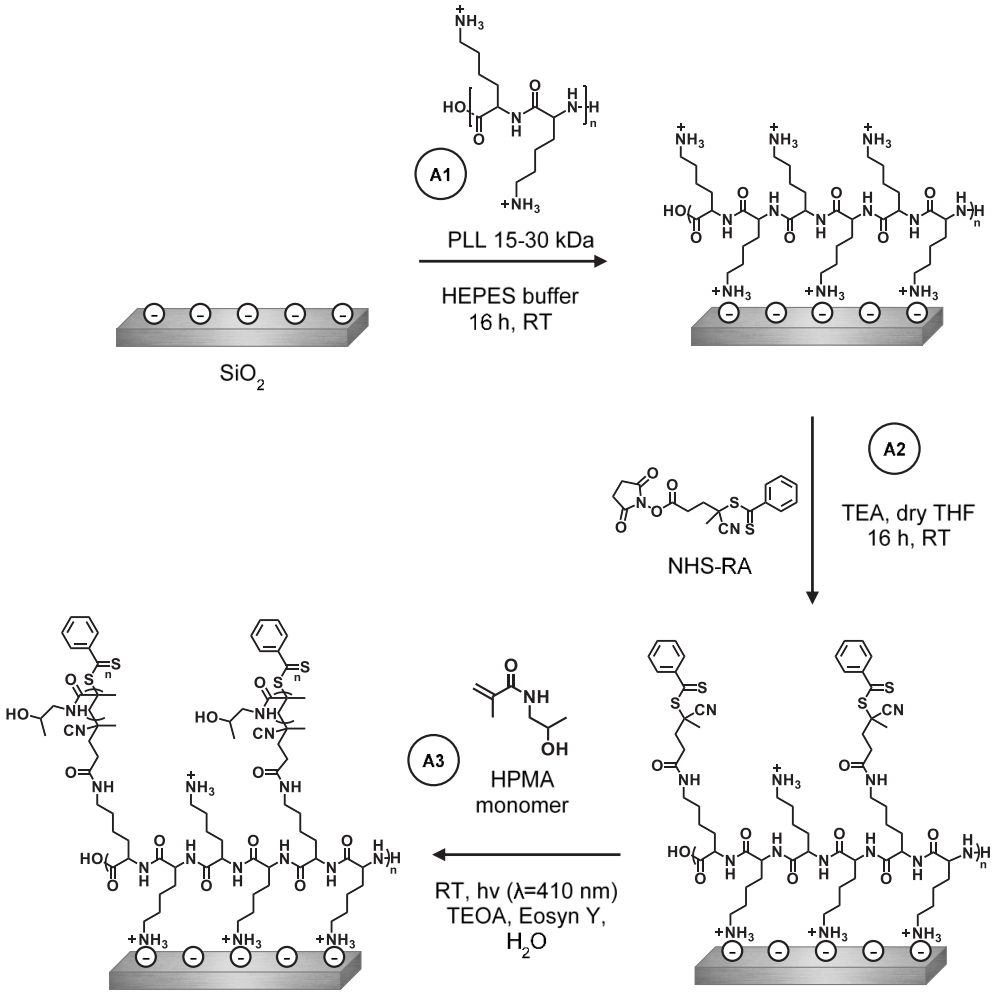

Figure 2. Schematic depiction of the construction of the PLL-RA coating via a *grafting-from* approach, followed by SI-PET-RAFT to grow poly(HPMA) brushes.

A1: Self-assembly of Poly(L-lysine) on SiO_2

PLL-HPMA bottlebrush-coated surfaces were prepared in this first route by building the layer from the surface upwards. To this end, PLL (M_w = 15-30 kDa) was self-assembled to form a monolayer by overnight immersion of freshly cleaned, negatively charged silicon oxide surfaces in a 0.1 mg/ml solution of PLL in HEPES buffer (following the procedure reported by Morgese *et al.*[31]). Upon modification of the silicon oxide surfaces with PLL, the presence of a thin layer of polymers on the surfaces was confirmed by analytical techniques. Firstly, by

X-ray photoelectron spectroscopy (XPS) we found signals corresponding to the presence of nitrogen (at 400 eV) and carbon (285 eV) on the surface (Figure 3, top). Furthermore, the C_{1s} narrow scan measurements showed the characteristic signals for the amide carbonyls (C=O, 288.4 eV), and for the *C*–N and *C*–C=O carbon atoms (both at 286.4 eV). Since these monolayers were too thin to be measured by ellipsometry (*vide infra*), we used the Si/C ratio in the XPS wide scan to calculate the average thickness of the layer,[49,50] which was approximately 0.5 nm, which is in good agreement with values reported in the literature.[51,52] The static water contact angle (SWCA) of the PLL-coated surfaces was < 20°, displaying the very hydrophilic character of the coating due to the charges on the protonated terminal amines. These combined data suggest that PLL was deposited as a monolayer on the SiO_2 surfaces.

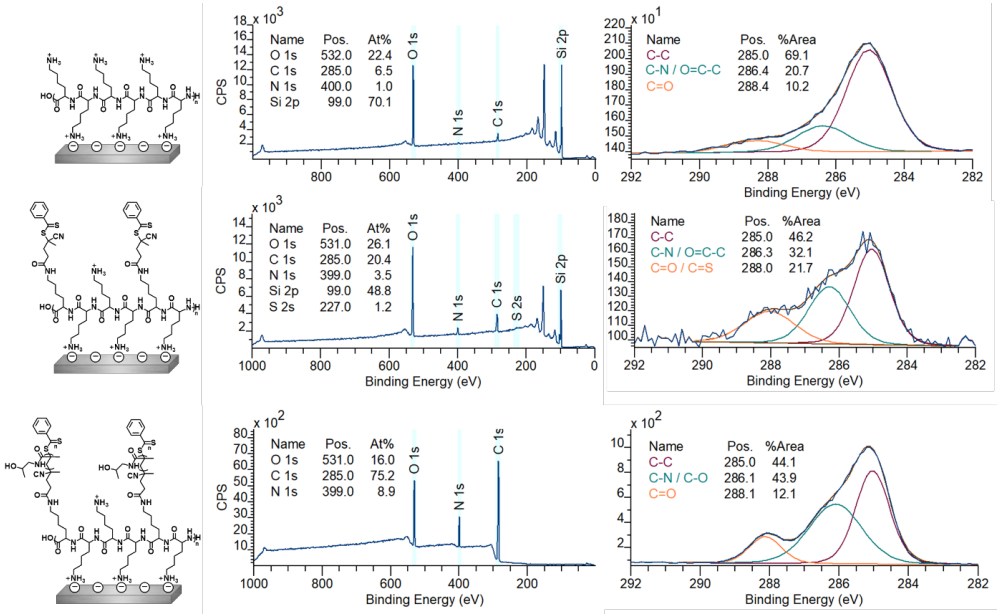

Figure 3. XPS wide scan spectrum and C_{1s} narrow scan spectrum of self-assembled PLL on silicon oxide (top), surface-bound PLL, functionalized with RAFT agent (middle) and poly(HPMA) grafted from RAFT agent-modified silicon oxide (after 80 min polymerization) (bottom). On the left, the chemical structure of the analyzed surface is depicted.

A2: Surface immobilization of RAFT agent on PLL-modified SiO_2

While a fraction of the pendant amine groups of PLL was involved in surface binding, the remaining free primary amines of the PLL coating can be used to immobilize a RAFT agent to allow in the following step the polymerization from the surface. To this end, an NHS-activated RAFT agent was reacted with the surface-bound PLL overnight in dry THF (see Figure 2, step A2). In the XPS spectrum of the thus prepared surface (Figure 3, middle), we found an expected increase in both the C_{1s} (285 eV) and N_{1s} (399 eV) signals in the wide scan, since these elements are predominantly present in the RAFT agent. Moreover, indicatively, we detected sulfur (S_{2s}, 227 eV), which confirms the presence of the RAFT agent. Based on the N/S ratio obtained from XPS wide spectra, roughly 40% of all PLL primary amines have reacted to hold a RAFT agent moiety (Figure S8). Taking into account that also a portion of the primary amines is involved in surface binding by electrostatic interactions, this conversion can be considered relatively high, compared to what would be maximally feasible for still strongly surface-bound PLL. The conversion was also confirmed in the C_{1s} narrow scan, which showed that the carbonyl signal at 288 eV became more dominant, which can be attributed to the introduced carbonyl and thiocarbonyls. As expected, the thickness of the coating increased upon the addition of the RAFT agent to approximately 1.3 nm. The SWCA of the RAFT-modified surfaces increased to 42°, in line with the more hydrophobic nature of the RAFT agent.

A3: PET-RAFT polymerization of HPMA on RAFT agent modified SiO_2

Poly(HPMA) side chains were grown from the RAFT-modified, PLL-covered silicon oxide surfaces by surface-initiated PET-RAFT in water using visible light and Eosin Y as an oxygen tolerant photocatalyst, which allowed polymerization in air.[46,48] Triethanolamine (TEOA) was used as a co-catalyst,[46] and also acted as a sacrificing electron donor to reduce oxygen in the polymerization system.[48] The study of the polymer growth kinetics showed a linear growth for the first 40 min (Figure 4), which indicates the controlled nature of this surface-initiated polymerization. The leveling off after 40 min might indicate a reduced availability of the RAFT groups by either increased steric hindrance or chemical degradation.

The chemical composition of the grown poly(HPMA) brushes was studied using XPS, while ellipsometry was used to determine the layer thickness of the polymer brushes. After 80 min

of polymerization, the coating reached a total thickness of 32.0 ± 0.2 nm. Similar growth rates have been reported for this HPMA monomer using PET-RAFT on silane anchoring layers.[48] This implies that from a self-assembled polymeric PLL starting layer, the polymerization works equally well compared to well-defined silane monolayers. Figure **3** shows the XPS spectra for the polymer brushes that were grown for 80 min. In the wide scan, only three main peaks are observed, namely O_{1s} (531 eV), N_{1s} (388 eV), and C_{1s} (285 eV) in a 1.8 : 1 : 8.3 ratio. This is in reasonable agreement with the elemental composition of the poly(HMPA) structure (2 : 1 : 7) and previously published papers on HPMA brushes, which report a ratio of 1.8 : 1 : 7.6,[48] given the possibility of atmospheric contamination

In the C_{1s} narrow scan, a clear, more intense signal around 286 eV could be discerned, compared to the RAFT agent-terminated surfaces from before the polymerization. This indicates the increase of C–heteroatom species, which is in agreement with the structure of the HPMA polymer. The SWCA of the polymer layers reached a stable SWCA of ~50° after 40 min of polymerization. Additionally, after 80 min of polymerization, the layers showed a low roughness (see Figure S12) as could been expressed by a root mean square roughness: *Rq* = 2.44 ± 0.44 nm as measured by AFM (see supporting information). Overall, these data suggest a surface structure that is similar to that previously reported for HPMA polymer brushes grown by different surface-initiated controlled polymerization methods.[13,18,48]

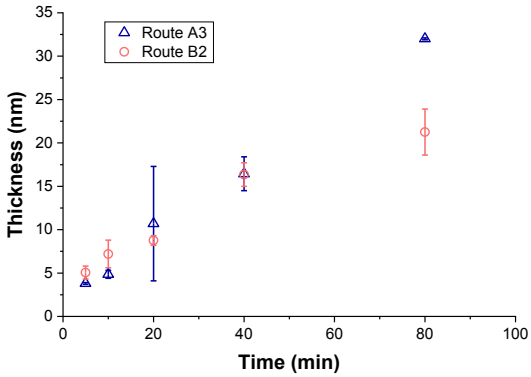

Figure 4. Polymerization kinetics of both on-surface PET-RAFT polymerizations of HPMA: Route A3: polymerization on RAFT agent-modified surfaces that were obtained by reacting NHS-RAFT with surface-immobilized PLL (orange). Route B2: polymerization on RAFT agent-modified surfaces that were obtained by the self-assembly of a PLL-RA macroinitiator (blue). Thicknesses were measured in duplicate by ellipsometry.

Route B: Synthesis and self-assembly of a PLL-RA macroinitiator and HPMA polymerization from PLL-RA-modified surfaces.

In route B the coating was only partly *grafted-from* the surface. The RA was first coupled to PLL in a solution to synthesize a PLL-RA macroinitiator. This PLL-RA macroinitiator was then self-assembled on the surface, after which HPMA was polymerized from the RA-modified PLL side chains (Figure 5).

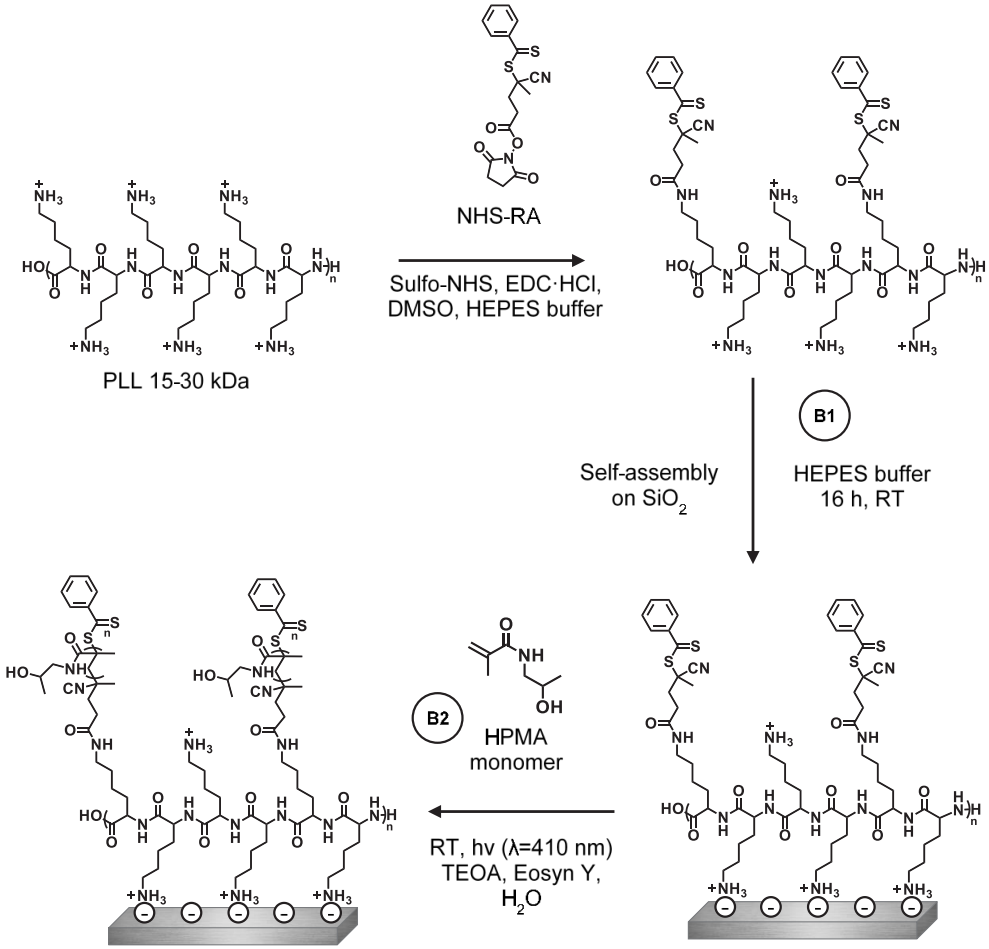

Figure 5. Schematic depiction of the build-up of the PLL-RA coating in a partly *grafting-to* approach, followed by SI-PET-RAFT to grow polyHPMA brushes.

B1: Synthesis and self-assembly of PLL-RA macroinitiator on SiO_2

Route B started with the synthesis of a RAFT agent-functionalized PLL polymer macroinitiator that could afterward be immobilized on the surface (Figure 5). By reacting a part of the amine end groups with an NHS-activated RA, we envisioned that enough lysine moieties would be left unreacted to achieve efficient binding of PLL to the silicon oxide surface in the subsequent self-assembly process. Therefore, we chose a 1 : 3 ratio of NHS-RA : lysine monomer in the synthesis of PLL-RA. The synthesized PLL-RA macroinitiator was first of all characterized by ^{1}H NMR spectroscopy, also allowing for the determination of the actual achieved RA : lysine ratio, which was found to be 1 : 9.8 (Figure S1, Supporting information). This ratio was also supported by the elemental composition of the PLL-RA after immobilization on a silicon oxide surface: by comparing the ratios between the N_{1s} and S_{2s} signals in XPS we found the RAFT : lysine ratio to be 1 : 8.5, which is comparable to the ratio found by ^{1}H NMR (Figure S9, Supporting information).

Several reasons could account for the lower observed degree of RAFT agent incorporation. First of all, the reaction was stopped after 16 h, which might be before full conversion had been reached. The lower degree might have also been affected by the relatively low solubility of PLL and NHS-activated RAFT agent in a common solvent (HEPES buffer with 10 v/v% DMSO), or by partial hydrolysis of the NHS ester. Finally, partial protonation of the amine end groups might have lowered the conversion of the reaction.

Nevertheless, having approximately 9 out of 10 lysines available for surface anchoring likely leads to a more stable coating, while still having enough initiation points for the growth of relatively long polymer brushes. This was demonstrated by the successful growth of poly(HPMA) brushes from silicon oxide surfaces that were coated by the PLL-RA macroinitiator, as discussed below. The PLL-RA macroinitiator formed a monolayer by self-assembly on a freshly cleaned silicon oxide surface using the same protocol as in route A1 (Figure 5). XPS analysis of this coating revealed signals for the elements N (at 400 eV), C (285 eV) and S (231 eV) on the surface. In addition, the C_{1s} narrow scan showed the characteristic signals for the amide carbonyls (N–*C*=O, 288.2 eV), and the nitrogen- and carbonyls-bound carbon atoms (*C*–N and *C*–C=O), both at 286.2 eV (Figure 6).

The layer thickness of the PLL-RAFT macroinitiator coating was calculated using the Si_{2p} : C_{1s} ratio from the XPS wide scan, and was found to be approximately 2.2 nm, which thicker than the value obtained in route A (1.3 nm), in which an analogous coating was created by reacting the NHS-RA moiety on pre-assembled PLL. The assembled PLL-RA coating (in route B) had a SWCA of 36°, which is slightly less hydrophobic than the PLL-RA coating from route A (SWCA of 42°). This could be ascribed to the fact that the coupling of the RAFT agent to PLL in solution (step B1) occurs randomly on the entire polymer, while the coupling on the surface (step A2) predominantly occurs on the top (solution-exposed) part of the PLL coating. Therefore, in route B a smaller fraction of the RAFT moieties could have an upward orientation compared to the PLL-functionalized polymer discussed in route A, which would explain the reduced increase in the hydrophobic character of the overall coating for route B.

B2: PET-RAFT polymerization of HPMA on PLL-RA macroinitiator-modified SiO_2

Once the PLL-RA macroinitiator was immobilized on the surface, poly(HPMA) brushes were grown using PET-RAFT conditions, as described in the previous paragraph (Figure 5). The layer thicknesses of the polymer coatings that were grown for different time intervals were measured using ellipsometry, allowing the comparison of the kinetics of the polymerization for routes A and B (Figure 4). The rate of polymerization is similar for the first 40 min, which implies that the amount of RAFT agent and hydrophilicity of the surface are not rate-determining. After 40 min, the polymerization in route A seems to continue, while the route B polymerization seems to level off. This might be due to the different availability of RA at the surface as discussed in step B1.

Figure 6 shows the XPS data of a polymer brush that was grown for 80 min, and which had a thickness of 21 nm, as determined from ellipsometry. In the wide scan, we see three main peaks, namely for the elements O_{1s} (532 eV), N_{1s} (400 eV) and C_{1s} (285 eV) in a 2.3 : 1 : 9.1 ratio, which is in reasonable agreement with the ratios found in the full *grafting-from* procedure in route A (1.8 : 1 : 8.3). In this case, also a very small signal is visible from the silicon oxide surface (Si_{2p}, 102 eV), which confirms the slightly thinner coating as already measured by ellipsometry. Also, the C_{1s} narrow scan gave a very similar spectrum as previously observed for the poly(HPMA) coating in route A. The SWCA stabilized after 30 min polymerization of HPMA to ~50°. AFM topology measurements of the surfaces after 80 min

of polymerization revealed a somewhat higher roughness *Rq* = 5.47 ± 0.75 nm compared to surface A3 (2.44 ± 0.44 nm). This is probably due to the more hydrophobic, hence less soluble, character of the initial PLL-RA. Overall, it can be concluded that the polymerization by PET-RAFT from the PLL-RA macroinitiator-modified surfaces was possible in only two surface modification steps. The coupling of the RAFT agent to the PLL polymer in solution did not significantly affect the final polymerization step, which implies that the surface modification procedure can be shortened by one step.

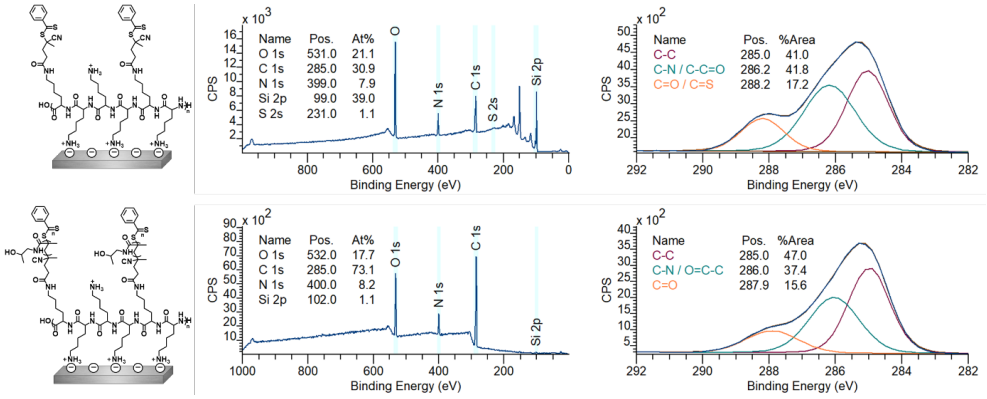

Figure 6. XPS wide scan spectrum and C_{1s} narrow scan spectrum of self-assembled macroinitiator PLL-RA (top) and poly(HPMA) grafted from these surfaces (80 min polymerization) (bottom). On the left, the chemical structure of the analyzed surface is depicted.

Route C: PLL-HPMA coating via the *grafting-to* procedure

Route C comprises a completely pre-synthesized, *grafted-to* coating. HPMA was first polymerized from the PLL-macroinitiator in solution to create PLL-HPMA bottlebrushes. These bottlebrushes were then self-assembled on the surface in one single step (Figure 7). Furthermore, bottlebrushes with carboxybetaine groups that offer the possibility for later biofunctionalization (PLL-HPMA/CBMA) were also synthesized and immobilized on a surface using the method presented in route C.

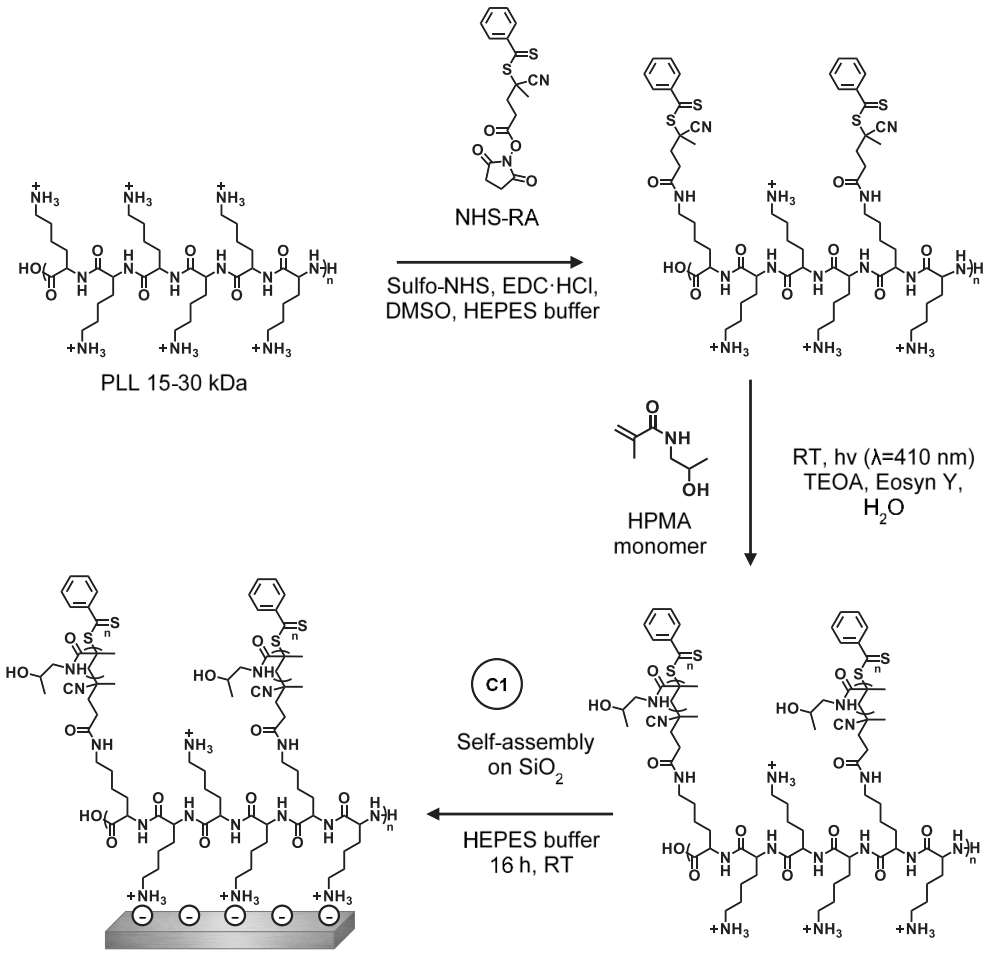

Figure 7. Schematic depiction of the build-up of the PLL-HPMA coating in a completely *grafting-to* approach.

C1: Solution synthesis and surface immobilization of PLL-HPMA by PET-RAFT polymerization of HPMA from PLL-RA macroinitiator

The previously discussed routes (A and B) required two or three consecutive surface modification steps to create a PLL-HPMA coating on silicon oxide. While route B is thus certainly attractive in terms of scalability, we considered it to be of even more interest to further decrease the number of surface modifications steps, so as to have a one-step procedure for the coating of silicon oxide surfaces by PLL-HPMA bottlebrush polymers. In such a route, the full polymer, a backbone polymer (PLL) with polymeric poly(HPMA) side chains is

pre-synthesized in solution, and only subsequently applied to the surface. To this aim, poly(HPMA) side chains were grown from the PLL-RA macroinitiator, which was already synthesized for route B, in solution (Figure 7). From the RAFT agent side groups of this macroinitiator, poly(HPMA) chains were grown by PET-RAFT polymerization in water using visible light, Eosin Y as an oxygen tolerant photocatalyst and triethanolamine (TEOA) as a co-catalyst, in line with the conditions used in route B to grow the poly(HPMA).[48] Extensive dialysis allowed the isolation of the PLL-HPMA bottlebrush that could then be characterized by ^{1}H NMR spectroscopy (Figure 8). In the ^{1}H NMR spectrum, peaks at δ 3.08 ppm and δ 3.84 ppm confirm the presence of the poly(HPMA) side chains of the bottlebrush. From the ratio between the ^{1}H signal at δ 4.15 ppm from the PLL backbone and the ^{1}H signal at δ 3.84 ppm from HPMA, the ratio between HPMA monomer : lysine monomer was found to be 1.4 : 1. Combining this ratio, with the previously determined RA : lysine ratio of the PLL-RA macroinitiator, the average chain length of the each HPMA side chain could be calculated to be roughly 14 repeating monomers, corresponding to approximately 2 kDa. The total weight of the PLL-HPMA bottlebrush was calculated to be 41 kDa (see calculations in Supporting Information).

The polymer molecular weight and polydispersity index (PDI) were determined by gel permeation chromatography (GPC) in water. Based on calibration by a set of poly(ethylene glycol) standards and a poly(HPMA) standard, a molecular weight of approximately 43 kDa was found, *i.e.* close to the NMR-derived value. Furthermore, from GPC a polydispersity index (PDI) of 1.4 was determined. Further characterization by dynamic light scattering (DLS) revealed a narrow size distribution with an intensity peak maximum at a hydrodynamic radius of 77 nm in water (Figure S11, Supporting information).

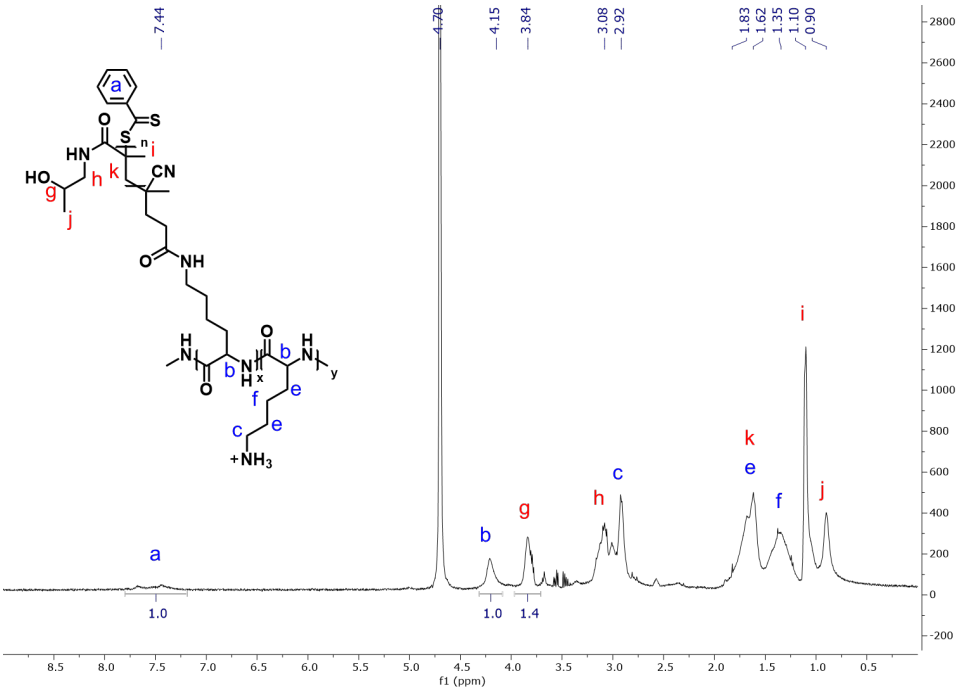

Figure 8. ^{1}H NMR spectrum of the PLL-HPMA bottlebrush synthesis in solution (in D_2O, 400 MHz, 298 K).

The synthesized PLL-HPMA bottlebrushes were allowed to self-assemble on silicon oxide surfaces by overnight immersion of in a 0.1 mg·mL^{-1} solution of PLL-HPMA in HEPES buffer. XPS analysis of this coating (Figure 9) showed signals for N (at 399 eV) and C (285 eV) on the silicon oxide surfaces, which is in agreement with the presence of a monolayer of PLL-HPMA. The C_{1s} narrow scan measurements showed the expected signals for the amide carbonyls (*C*=O, 288.2 eV), and carbon-nitrogen and carbon-carbonyls (*C*–N and *C*–C=O), both at 286.2 eV). The layer thickness of the PLL-HPMA coating was calculated using the Si_{2p} : C_{1s} ratio from the XPS wide scan and was found to be approximately 0.9 nm. While this is a rather low layer thickness for a surface-immobilized bottlebrush polymer, it should be pointed out that the XPS thickness measurements were taken under ultra-high vacuum conditions, creating a collapsed polymer layer (which will expand upon immersion). Furthermore, the found dry thickness is in agreement with other types of surface-immobilized PLL-based bottlebrushes reported in literature.[29–31] The self-assembly of PLL-HPMA lead to the formation of a smooth layer (see Figure S12), as the reported roughness by AFM was *Rq* = 2.37 ± 0.05.

The SWCA of this PLL-HPMA coating was approximately 20°. This hydrophilic character might be due to the polar (partially charged) amine groups of the PLL within the coating that are close to the solvent interface due to relatively low layer thickness of the overall coating. However, the SWCA of the PLL-HPMA self-assembled coating is higher than for the PLL monolayer with comparable thickness observed for step A1 (which has a reported SWCA below 20° for a 0.5 nm surface-immobilized brush) due to the presence of poly(HPMA).

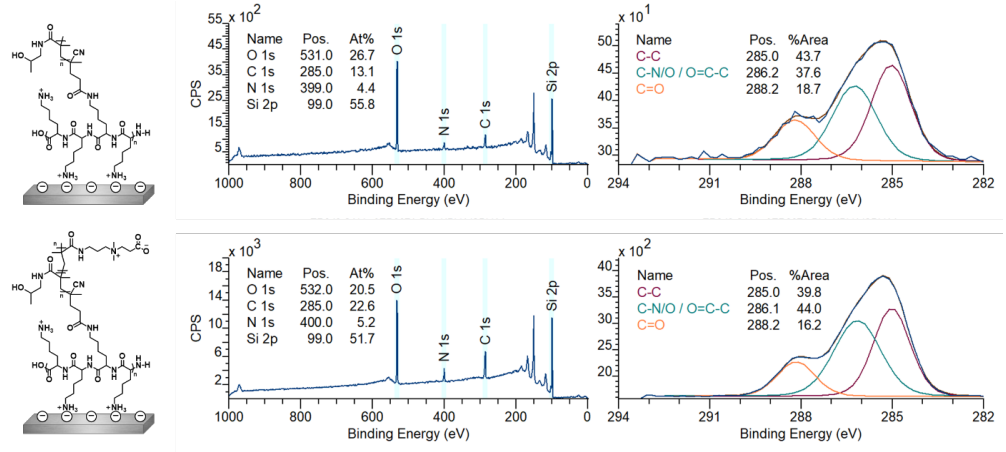

Figure 9. XPS wide scan spectrum and C_{1S} narrow scan spectrum of self-assembled PLL-HPMA (top) and PLL-HPMA/CBMA (bottom). On the left, the chemical structure of the analyzed surface is depicted.

Carboxybetaine-doped HPMA brushes for biofunctionalization purposes. We have further improved the concept of PLL-HPMA one-step antifouling coatings by incorporating the possibility for biomolecule immobilization, which is highly desirable for selective binding in, *e.g.*, biosensors and tissue engineering.[7,53,54] The polymerization of HPMA from the PLL-RA macroinitiator was also performed in the presence of a second antifouling monomer that contains a carboxylate group to allow for easy activation by conventional coupling strategies, *e.g.* NHS/EDC, to couple bioactive moieties. To this end, we selected a zwitterionic carboxybetaine (CBMA) monomer that was also used previously for surface functionalization.[7,10,13,55] To this aim, 5% of CBMA monomer was used for this polymerization, keeping the conditions the same as described for the PET-RAFT solution polymerization. The

obtained PLL-HPMA/CBMA polymer was analyzed by ^{1}H NMR spectroscopy (Figure S5, Supporting information). We observed the expected additional signals coming from the CBMA monomers, when comparing to the PLL-HPMA bottlebrush spectrum. Based on ^{1}H NMR integration, the content of CBMA was calculated to be 7.7% (see Figure S5). The somewhat higher incorporation of CBMA monomer likely stems from the previously reported difference in reactivity between the monomers.[48] The polymer molecular weight and PDI were approximated using GPC and gave an MW of approximately 53 kDa and a PDI of 1.6. In addition, DLS gave a narrow size distribution in water with a maximum at a hydrodynamic radius of 111 nm (see Figure S11).

The synthesized PLL-HPMA/CBMA bottlebrushes were allowed to self-assemble on silicon oxide surfaces under similar conditions as described above. XPS analysis of this coating (Figure 9), revealed signals for the elements N (at 400 eV) and C (285 eV) on the silicon oxide surfaces. The layer thickness of the PLL-HPMA/CBMA coating was calculated using the Si_{2p} : C_{1s} ratio from the XPS wide scan and was found to be approximately 1.3 nm, which is in accordance with the formation of a monolayer of PLL-HPMA/CBMA. The C_{1s} narrow scan measurements showed the expected signals for the amide carbonyls (*C*=O, 288.2 eV), carbon-nitrogen and carbon-carbonyls (*C*–N and *C*–C=O, both at 286.1 eV). The higher amount of carbon-nitrogen and carbon-carbonyl signals compared to the PLL-HPMA layer (44% vs. 38%) could be explained by the presence of the CBMA monomer that contains an additional carbonyl group. The layer thickness of the PLL-HPMA/CBMA coating was calculated using the Si_{2p} : C_{1s} ratio from the XPS wide scan, and was found to be approximately 1.3 nm. This layer was thus slightly thicker than the PLL-HPMA monolayer, which might be explained by the longer side chains. The SWCA of the PLL-HPMA/CBMA coating was approximately 22°, which is very similar to the PLL-HPMA analog. The self-assembly of the PLL-HPMA/CMBA lead to the formation of a smooth layer (Figure S12, Supporting information), as the reported roughness by AFM was Rq = 1.16 ± 0.05.

Having successfully incorporated CBMA in the PLL-HPMA bottlebrushes, a broad and versatile platform for (bio)functionalization was created. For both poly(HPMA) and poly(CBMA), the antifouling properties are most probably related to the strong binding of water molecules.[56] The combination of these polymers was previously utilized in polymer brush systems which showed good antifouling properties.[14,57] By activation of the carboxylate

groups – either in solution or on the surface – antibodies or other bioactive molecules can be installed for monitoring specific interactions in, *e.g.*, biosensor platforms.[7,14,58–60]

Antifouling properties of PLL-HPMA coatings. Having successfully immobilized the three different PLL-HPMA bottlebrush coatings on the silicon oxide surface, a preliminary investigation of their antifouling properties was performed. We quantified the amount of protein adsorption by fluorescence microscopy, by exposing the PLL-HPMA bottlebrush coatings to fluorescently labeled protein solutions.[13,23,28] This method allows for a limit of fluorescent protein detection of 300 pg·mm^{-1} and thus suffices for initial testing.[48] For this study, lysozyme (LYS) and bovine serum albumin (BSA) were used as model proteins at concentrations of 0.1 mg·mL^{-1} in PBS and contacted with the surfaces for 15 min before washing with PBS. BSA was chosen since it is one of the most common proteins in blood plasma with an overall negative charge at pH 7.4 (PBS buffer).[61] LYS is a relatively small, hydrophilic protein and was used because of its overall positive charge at pH 7.4 (PBS buffer).[62] As controls for the protein adsorption experiments, we used bare silicon oxide surfaces, PLL-modified surfaces, and surfaces modified with commercially available PLL-PEG, which is known to have good antifouling properties.[30]

The unmodified silicon oxide surface showed high fluorescence intensities from both solutions (Figure 10), indicating significant fouling. PLL-coated silicon oxide was used as a control and already showed less fouling compared to the bare silicon oxide surface, probably due to the hydrophilic and charged nature of the sample, which contributes to the antifouling properties.[20] However, there still is a significant amount of fouling by BSA visible on the PLL-coated silicon oxide, likely due to the oppositely charged nature of BSA and PLL. The PLL-PEG-coated silicon oxide control sample, showed the expected low fluorescence intensities, which confirms the functioning of the procedure and antifouling behavior. The fluorescent intensities for PLL-HPMA-based antifouling coatings were observed on the background level. These data show that PLL-HPMA coatings that were synthesized in different ways (route A, B, or C) show antifouling properties close to the limit of detection.

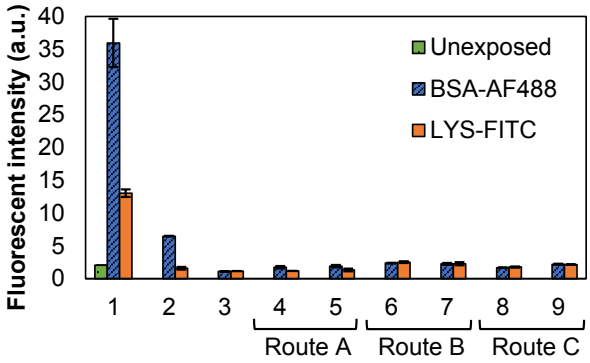

#	Route / Step	Surface – polymerization time
1	-	Bare silicon oxide
2	A1	PLL
3	-	PLL-PEG
4	A3	PLL-RAFT - 40 min HPMA
5	A3	PLL-RAFT - 80 min HPMA
6	B2	PLL-RAFT - 40 min HPMA
7	B2	PLL-RAFT - 80 min HPMA
8	C1	PLL-HPMA
9	C1	PLL-HPMA/CBMAA

Figure 10. Fluorescence intensities of different uncoated and coated silicon oxide surfaces (see table) after exposure to solution containing BSA-AF488 and LYS-FITC.

Comparing the different routes towards PLL-HPMA bottlebrush coatings

Coatings made by routes A, B and C showed very similar antifouling properties in single-protein solutions, irrespectively of any possible difference in their built-up, thickness, surface topology and/or brush density. However, depending on the to-be-coated surface and application, one can foresee that a certain route might be preferred over the other two.

Both routes A and B lead to relatively thick and dense coatings since the HPMA was *grafted-from* an initiator-modified surface. This could be beneficial for stability and long term use since the underlying anchoring layer is better shielded from the environment.

Route A showed the straightforward application of PLL as a multivalent, amine-terminated anchoring layer, on which a polymerization agent can be attached (step A1). PLL could, therefore, be an alternative to the often used silanes.[63–65] The follow-up steps are versatile with regard to the polymerization agent, technique, and monomer of choice.

In route B, the number of on-surface reactions is reduced to one. In solution, a macroinitiator is synthesized by a one-step coupling method. After that, the macroinitiator can be easily self-assembled on the surface, after which polymers can be grafted on the surface. This approach has also been used by Jain *et al.,*[66] who modified a polymer with polymerization initiator groups and embedded this new polymer in a layer-by-layer assay on porous membranes, to eventually grow polymer brushes from these membranes in a *grafting-from* approach. The pre-synthesis of the macroinitiator in solution, allows for precise

control over the amount of embedded polymerization agent, and could be specifically beneficial in cases were the anchoring layer (PLL) and the to be polymerized monomer are impossible to synthesize in solution because of opposite polarities (or other properties that are challenging to combine in synthesis).

Both route B and C might result in less long-term stable coatings compared to route A since the electrostatic interactions, that assure surface binding, are partly sacrificed by attaching the RAFT agent (route B) or poly(HPMA) side chains (route C) prior to surface binding.

Route C is easiest to apply on a surface and by far the easiest to scale-up, because of the one-step self-assembly and lack of on-surface reactions. The complete synthesis in solution allows control and knowledge of the composition, weight and dimensions of the formed polymer. Also, this approach allows precise and quantifiable immobilization of (bio)molecules in solution, which typically requires smaller quantities of the (bio)molecule of interest in the overall coating process or on the surface. The synthesis procedure in solution takes time and requires purification. However, once synthesized, only very small amounts of PLL-HPMA (as little as 0.1 $mg \cdot mL^{-1}$) are needed to coat a surface, which makes it very desirable and cost-effective when a coating needs be applied to multiple or large surfaces.

Conclusion

In this work, we developed three different routes (A–C) to prepare effective antifouling coatings that consist of PLL-HPMA bottlebrushes. In these coatings, the poly(L-lysine) (PLL) backbone self-assembles onto a silicon oxide surface by charge-based interactions between the lysine groups and the negatively charged surface, whereas the poly(*N*-(2-hydroxypropyl)methacrylamide) (HPMA) side chains contribute to the antifouling properties.

The PLL-HPMA bottlebrush polymer coatings were produced using *grafting-from* techniques by polymerizing HPMA from the surface (route A and B) and *grafting-to* of a pre-synthesized PLL-HMA bottlebrush (route C); the latter case – taking place fully under ambient conditions with only water as solvent – is both very easy for repeated and/or large-scale use, and allows detailed characterization of the finally polymer in solution, while methods A and B have to rely on surface-sensitive analytical methods for characterization. Additionally, in route C, a bottlebrush was synthesized that contains 5% carboxybetaine (CB) in its side chains, which offers the possibility for further functionalization after an ester activation step.

Overall, all surface modification routes (A–C) yield coatings that show single-protein antifouling properties and are worthy of further, more detailed antifouling studies.

Supporting Information

The Supporting information contains a description of the used materials and methods, supporting NMR, XPS, IR, DLS, and GPC data and calculations.

Supporting information is available free of charge at the ACS Publications:

Acknowledgments

This project was supported by Netherlands Organization for Scientific Research (NWO; LIFT program, grant 731.015.042) with Surfix BV as a partner and the Science PPP Fund research program with project number 741.018.105, which is partly financed by NWO.

The authors thank Hans Beijleveld, Remko Fokkink and Lucas Teunissen for helpful discussions and instrumental support.

References

1. Wisniewski, N.; Reichert, M. Methods for Reducing Biosensor Membrane Biofouling. *Colloids Surfaces B Biointerfaces* **2000**, *18* (3–4), 197–219.

2. Rodriguez-Emmenegger, C.; Avramenko, O. A.; Brynda, E.; Skvor, J.; Alles, A. B. Poly(HEMA) Brushes Emerging as a New Platform for Direct Detection of Food Pathogen in Milk Samples. *Biosens. Bioelectron.* **2011**, *26* (11), 4545–4551.

3. Huang, N.; Michel, R.; Voros, J.; Textor, M.; Hofer, R.; Rossi, A.; Elbert, D. L.; Hubbell, J. a; Spencer, N. D. Poly (l-Lysine)-g-Poly (Ethylene Glycol) Layers on Metal Oxide Surfaces : Surface-Analytical Characterization and Resistance to Serum and Fibrinogen Adsorption Poly (L-Lysine)-g-Poly (Ethylene Glycol) Layers on Metal Oxide Surfaces : Surface-An. *Langmuir* **2001**, No. 6, 489–498.

4 Yu, Y.; Cirelli, M.; Li, P.; Ding, Z.; Yin, Y.; Yuan, Y.; de Beer, S.; Vancso, G. J.; Zhang, S. Enhanced Stability of Poly(3-Sulfopropyl Methacrylate Potassium) Brushes Coated on Artificial Implants in Combatting Bacterial Infections. *Ind. Eng. Chem. Res.* **2019**, *58* (47), 21459–21465.

5. Thissen, H.; Gengenbach, T.; du Toit, R.; Sweeney, D. F.; Kingshott, P.; Griesser, H. J.; Meagher, L. Clinical Observations of Biofouling on PEO Coated Silicone Hydrogel Contact Lenses. *Biomaterials* **2010**, *31* (21), 5510–5519.

6. Rosenhahn, A.; Schilp, S.; Kreuzer, H. J.; Grunze, M. The Role of '"Inert"' Surface Chemistry in Marine Biofouling Prevention. *Phys. Chem. Chem. Phys.* **2010**, *12* (17), 4273–4274. https://doi.org/10.1039/c004746p.

7. Baggerman, J.; Smulders, M. M. J.; Zuilhof, H. Romantic Surfaces: A Systematic Overview of Stable, Biospecific, and Antifouling Zwitterionic Surfaces. *Langmuir* **2019**, *35* (5), 1072–1084.

8. Joshi, S.; Pellacani, P.; van Beek, T. a.; Zuilhof, H.; Nielen, M. W. F. Surface Characterization and Antifouling Properties of Nanostructured Gold Chips for Imaging Surface Plasmon Resonance Biosensing. *Sensors Actuators B Chem.* **2015**, *209*, 505–514.

9. Kuzmyn, A. R.; De Los Santos Pereira, A.; Pop-Georgievski, O.; Bruns, M.; Brynda, E.; Rodriguez-Emmenegger, C. Exploiting End Group Functionalization for the Design of Antifouling Bioactive Brushes. *Polym. Chem.* **2014**, *5* (13), 4124–4131.

10. van Andel, E.; de Bus, I.; Tijhaar, E. J.; Smulders, M. M. J.; Savelkoul, H. F. J.; Zuilhof, H.

Highly Specific Binding on Antifouling Zwitterionic Polymer-Coated Microbeads as Measured by Flow Cytometry. *ACS Appl. Mater. Interfaces* **2017**, *9* (44), 38211–38221.

11. Nguyen, A. T.; Baggerman, J.; Paulusse, J. M. J.; Rijn, C. J. M. Van; Zuilhof, H. Stable Protein-Repellent Zwitterionic Polymer Brushes Grafted from Silicon Nitride. *Langmuir* **2011**, *27* (6), 2587–2594.

12. Yang, W.; Chen, S.; Cheng, G.; Vaisocherová, H.; Xue, H.; Li, W.; Zhang, J.; Jiang, S. Film Thickness Dependence of Protein Adsorption from Blood Serum and Plasma onto Poly(Sulfobetaine)-Grafted Surfaces. *Langmuir* **2008**, *24* (17), 9211–9214.

13. Kuzmyn, A. R.; Nguyen, A. T.; Zuilhof, H.; Baggerman, J. Bioactive Antifouling Surfaces by Visible-Light-Triggered Polymerization. *Adv. Mater. Interfaces* **2019**, *6* (12).

14. Lísalová, H.; Brynda, E.; Houska, M.; Víšová, I.; Mrkvová, K.; Song, X. C.; Gedeonová, E.; Surman, F.; Riedel, T.; Pop-Georgievski, O.; Homola, J. Ultralow-Fouling Behavior of Biorecognition Coatings Based on Carboxy-Functional Brushes of Zwitterionic Homo- and Copolymers in Blood Plasma: Functionalization Matters. *Anal. Chem.* **2017**, *89* (6), 3524–3531.

15. Schönemann, E.; Laschewsky, A.; Wischerhoff, E.; Koc, J.; Rosenhahn, A. Surface Modification by Polyzwitterions of the Sulfabetaine-Type, and Their Resistance to Biofouling. *Polymers (Basel).* **2019**, *11* (6).

16. Van Andel, E.; Lange, S. C.; Pujari, S. P.; Tijhaar, E. J.; Smulders, M. M. J.; Savelkoul, H. F. J.; Zuilhof, H. Systematic Comparison of Zwitterionic and Non-Zwitterionic Antifouling Polymer Brushes on a Bead-Based Platform. *Langmuir* **2019**, *35* (5), 1181–1191.

17. Vorobii, M.; de los Santos Pereira, A.; Pop-Georgievski, O.; Kostina, N. Y.; Rodriguez-Emmenegger, C.; Percec, V. Synthesis of Non-Fouling Poly[N-(2-Hydroxypropyl)Methacrylamide] Brushes by Photoinduced SET-LRP. *Polym. Chem.* **2015**, *6* (23), 4210–4220.

18. Rodriguez-Emmenegger, C.; Brynda, E.; Riedel, T.; Houska, M.; Šubr, V.; Alles, A. B.; Hasan, E.; Gautrot, J. E.; Huck, W. T. S. Polymer Brushes Showing Non-Fouling in Blood Plasma Challenge the Currently Accepted Design of Protein Resistant Surfaces. *Macromol. Rapid Commun.* **2011**, *32* (13), 952–957.

19. Surman, F.; Riedel, T.; Bruns, M.; Kostina, N. Y.; Sedláková, Z.; Rodriguez-Emmenegger, C. Polymer Brushes Interfacing Blood as a Route toward High Performance Blood Contacting Devices. *Macromol. Biosci.* **2015**, *15* (5), 636–646.

20. Jiang, S.; Cao, Z. Ultralow-Fouling, Functionalizable, and Hydrolyzable Zwitterionic Materials and Their Derivatives for Biological Applications. *Adv. Mater.* **2010**, *22* (9), 920–932.

21. Yang, W.; Xue, H.; Li, W.; And, J. Z.; Jiang, S. Pursuing "Zero" Protein Adsorption of Poly(Carboxybetaine) from Undiluted Blood Serum and Plasma. *Langmuir* **2009**, *25* (19), 11911–11916.

22. Blaszykowski, C.; Sheikh, S.; Thompson, M. A Survey of State-of-the-Art Surface Chemistries to Minimize Fouling from Human and Animal Biofluids. *Biomater. Sci.* **2015**, *3* (10), 1335–1370.

23. Honda, T.; Nakao, A.; Ishihara, K.; Higaki, Y.; Higaki, K.; Takahara, A.; Iwasaki, Y.; Yusa, S. I. Polymer Coating Glass to Improve the Protein Antifouling Effect. *Polym. J.* **2018**, *50* (5), 381–388.

24. Michalek, L.; Barner, L.; Barner-Kowollik, C. Polymer on Top: Current Limits and Future Perspectives of Quantitatively Evaluating Surface Grafting. *Adv. Mater.* **2018**, *30* (21), 1–18.

25. Lange, S. C.; Van Andel, E.; Smulders, M. M. J.; Zuilhof, H. Efficient and Tunable Three-Dimensional Functionalization of Fully Zwitterionic Antifouling Surface Coatings. *Langmuir* **2016**, *32* (40), 10199–10205.

26. Vorobii, M.; De Los Santos Pereira, A.; Pop-Georgievski, O.; Kostina, N. Y.; Rodriguez-Emmenegger, C.; Percec, V. Synthesis of Non-Fouling Poly[N-(2-Hydroxypropyl)Methacrylamide] Brushes by Photoinduced SET-LRP. *Polym. Chem.* **2015**, *6* (23), 4210–4220.

27. Sundaram, H. S.; Han, X.; Nowinski, A. K.; Ella-Menye, J. R.; Wimbish, C.; Marek, P.; Senecal, K.; Jiang, S. One-Step Dip Coating of Zwitterionic Sulfobetaine Polymers on Hydrophobic and Hydrophilic Surfaces. *ACS Appl. Mater. Interfaces* **2014**, *6* (9), 6664–6671.

28. Xu, L. Q.; Pranantyo, D.; Neoh, K. G.; Kang, E. T.; Teo, S. L. M.; Fu, G. D. Synthesis of Catechol and Zwitterion-Bifunctionalized Poly(Ethylene Glycol) for the Construction of Antifouling Surfaces. *Polym. Chem.* **2016**, *7* (2), 493–501.

29. Kenausis, G. L.; Vo, J.; Elbert, D. L.; Huang, N.; Hofer, R.; Ruiz-taylor, L.; Textor, M.; Hubbell, J. A.; Spencer, N. D. Poly (L-Lysine)-g-Poly (Ethylene Glycol) Layers on Metal Oxide Surfaces : Attachment Mechanism and Effects of Polymer Architecture on Resistance to Protein Adsorption †. *J. Phys. Chem. B* **2000**, *104*, 3298–3309.

30. Paul, S. M. De; Vo, J.; Spencer, N. D.; Textor, M. Poly(L-Lysine)-Graft-Poly (Ethylene

Glycol) Assembled Monolayers on Niobium Oxide Surfaces : A Quantitative Study of the Influence of Polymer Interfacial Architecture on Resistance to Protein Adsorption by ToF-SIMS and in Situ OWLS. *Langmuir* **2003**, *19* (20), 9216–9225.

31. Morgese, G.; Verbraeken, B.; Ramakrishna, S. N.; Gombert, Y.; Cavalli, E.; Rosenboom, J. G.; Zenobi-Wong, M.; Spencer, N. D.; Hoogenboom, R.; Benetti, E. M. Chemical Design of Non-Ionic Polymer Brushes as Biointerfaces: Poly(2-Oxazine)s Outperform Both Poly(2-Oxazoline)s and PEG. *Angew. Chem. Int. Ed.* **2018**, *57* (36), 11667–11672.

32. Perry, S. S.; Yan, X.; Limpoco, F. T.; Lee, S.; Müller, M.; Spencer, N. D. Tribological Properties of Poly(l -Lysine)- Graft -Poly(Ethylene Glycol) Films: Influence of Polymer Architecture and Adsorbed Conformation. *ACS Appl. Mater. Interfaces* **2009**, *1* (6), 1224–1230.

33. Huang, W. M.; Gibson, S. J.; Facer, P.; Gu, J.; Polak, J. M. Improved Section Adhesion for Immunocytochemistry Using High Molecular Weight Polymers of L-Lysine as a Slide Coating. *Histochemistry* **1983**, *77* (2), 275–279.

34. Yan, X.; Perry, S. S.; Spencer, N. D.; Pasche, S.; De Paul, S. M.; Textor, M.; Lim, M. S. Reduction of Friction at Oxide Interfaces upon Polymer Adsorption from Aqueous Solutions. *Langmuir* **2004**, *20* (2), 423–428.

35. Parks, G. A. The Isoelectric Points of Solid Oxides, Solid Hydroxides, and Aqueous Hydroxo Complex Systems. *Chem. Rev.* **1965**, *65* (2), 177–198.

36. Weber, D.; Torger, B.; Richter, K.; Nessling, M.; Momburg, F.; Woltmann, B.; Müller, M.; Schwartz-Albiez, R. Interaction of Poly(L-Lysine)/Polysaccharide Complex Nanoparticles with Human Vascular Endothelial Cells. *Nanomaterials* **2018**, *8* (6).

37. Herold, D. A.; Keil, K.; Bruns, D. E. Oxidation of Polyethylene Glycols by Alcohol Dehydrogenase. *Biochem. Pharmacol.* **1989**, *38* (1), 73–76.

38. Lubich, C.; Allacher, P.; de la Rosa, M.; Bauer, A.; Prenninger, T.; Horling, F. M.; Siekmann, J.; Oldenburg, J.; Scheiflinger, F.; Reipert, B. M. The Mystery of Antibodies Against Polyethylene Glycol (PEG) - What Do We Know? *Pharm. Res.* **2016**, *33* (9), 2239–2249.

39. Garay, R. P.; El-Gewely, R.; Armstrong, J. K.; Garratty, G.; Richette, P. Antibodies against Polyethylene Glycol in Healthy Subjects and in Patients Treated with PEG-Conjugated Agents. *Expert Opin. Drug Deliv.* **2012**, *9* (11), 1319–1323.

40. Armstrong, J. K.; Hempel, G.; Koling, S.; Chan, L. S.; Fisher, T.; Meiselman, H. J.; Garratty,

G. Antibody against Poly(Ethylene Glycol) Adversely Affects PEG-Asparaginase Therapy in Acute Lymphoblastic Leukemia Patients. *Cancer* **2007**, *110* (1), 103–111.

41. Branden, R.; Matthew, G.; Anirudha, S.; Janis, T.; Cecilia, F.; Melissa, M.; Jennifer, E. PEG Hydrogel Degradation and the Role of the Surrounding Tissue Environment. *J. Tissue Eng. Regen. Med.* **2015**, *9*, 315–318.

42. Johnson, R. N.; Chu, D. S. H.; Shi, J.; SChellinger, J. G.; Carlson, P. M.; Pun, S. H. HPMA-Oligolysine Copolymers for Gene Delivery: Optimization of Peptide Length and Polymer Molecular Weight Russell. *J Control Release* **2011**, *155* (2), 303–311.

43. Tappertzhofen, K.; Weiser, F.; Montermann, E.; Reske-Kunz, A.; Bros, M.; Zentel, R. Poly- l -Lysine-Poly[HPMA] Block Copolymers Obtained by RAFT Polymerization as Polyplex-Transfection Reagents with Minimal Toxicity. *Macromol. Biosci.* **2015**, *15* (8), 1159–1173.

44. Thomson, D.; Zilkie, A.; Bowers, J. E.; Komljenovic, T.; Reed, G. T.; Vivien, L.; Marris-Morini, D.; Cassan, E.; Virot, L.; Fédéli, J. M.; Hartmann, J. M.; Schmid, J. H.; Xu, D. X.; Boeuf, F.; O'Brien, P.; Mashanovich, G. Z.; Nedeljkovic, M. Roadmap on Silicon Photonics. *J. Opt. (United Kingdom)* **2016**, *18* (7), 1–20.

45. Qi, Z. B.; Xu, L.; Xu, Y.; Zhong, J.; Abedini, A.; Cheng, X.; Sinton, D. Disposable Silicon-Glass Microfluidic Devices: Precise, Robust and Cheap. *Lab Chip* **2018**, *18* (24), 3872–3880.

46. Niu, J.; Lunn, D. J.; Pusuluri, A.; Yoo, J. I.; O'Malley, M. A.; Mitragotri, S.; Soh, H. T.; Hawker, C. J. Engineering Live Cell Surfaces with Functional Polymers via Cytocompatible Controlled Radical Polymerization. *Nat. Chem.* **2017**, *9* (6), 537–545.

47. Lueckerath, T.; Strauch, T.; Koynov, K.; Barner-Kowollik, C.; Ng, D. Y. W.; Weil, T. DNA-Polymer Conjugates by Photoinduced RAFT Polymerization. *Biomacromolecules* **2019**, *20* (1), 212–221.

48. Kuzmyn, A. R.; Nguyen, A. T.; Teunissen, L. W.; Zuilhof, H.; Baggerman, J. Antifouling Polymer Brushes via Oxygen-Tolerant Surface-Initiated PET-RAFT. *Langmuir* **2020**, *36* (16), 4439–4446.

49. Wallart, X.; Henry de Villeneuve, C.; Allongue, P. Truly Quantitative XPS Characterization of Organic Monolayers on Silicon: Study of Alkyl and Alkoxy Monolayers on H-Si(111). *J. Am. Chem. Soc.* **2005**, *127* (21), 7871–7878.

50. Scheres, L.; Giesbers, M.; Zuilhof, H. Organic Monolayers onto Oxide-Free Silicon with Improved Surface Coverage: Alkynes versus Alkenes. *Langmuir* **2010**, *26* (7), 4790–4795.

51. Morga, M.; Adamczyk, Z.; Gödrich, S.; Oćwieja, M.; Papastavrou, G. Monolayers of Poly-l-Lysine on Mica - Electrokinetic Characteristics. *J. Colloid Interface Sci.* **2015**, *456*, 116–124.

52. Elbert, D. L.; Herbert, C. B.; Hubbell, J. A. Thin Polymer Layers Formed by Polyelectrolyte Multilayer Techniques on Biological Surfaces. *Langmuir* **1999**, *15* (16), 5355–5362.

53. Xiao, A.; Dhand, C.; Leung, C. M.; Beuerman, R. W.; Ramakrishna, S.; Lakshminarayanan, R. Strategies to Design Antimicrobial Contact Lenses and Contact Lens Cases. *J. Mater. Chem. B* **2018**, *6* (15), 2171–2186.

54. Poręba, R.; de los Santos Pereira, A.; Pola, R.; Jiang, S.; Pop-Georgievski, O.; Sedláková, Z.; Schönherr, H. "Clickable" and Antifouling Block Copolymer Brushes as a Versatile Platform for Peptide-Specific Cell Attachment. *Macromol. Biosci.* **2020**, *20* (4), 1–10.

55. Krishnamoorthy, M.; Hakobyan, S.; Ramstedt, M.; Gautrot, J. E. Surface-Initiated Polymer Brushes in the Biomedical Field : Applications in Membrane Science , Biosensing , Cell Culture , Regenerative Medicine and Antibacterial Coatings. *Chem. Rev.* **2014**, *114*, 10976–11026

56. Yang, W.; Xue, H.; Li, W.; And, J. Z.; Jiang, S. Pursuing "Zero" Protein Adsorption of Poly(Carboxybetaine) from Undiluted Blood Serum and Plasma. *Langmuir* **2009**, *25* (19), 11911–11916.

57. Vaisocherova-Lisalova, H.; Surman, F.; Víšová, I.; Vala, M.; Špringer, T.; Ermini, M. L.; Šípová, H.; Šedivák, P.; Houska, M.; Riedel, T.; Pop-Georgievski, O.; Brynda, E.; Homola, J. Copolymer Brush-Based Ultralow-Fouling Biorecognition Surface Platform for Food Safety. *Anal. Chem.* **2016**, *88* (21), 10533–10539.

58. Carr, L. R.; Xue, H.; Jiang, S. Functionalizable and Nonfouling Zwitterionic Carboxybetaine Hydrogels with a Carboxybetaine Dimethacrylate Crosslinker. *Biomaterials* **2011**, *32* (4), 961–968.

59. Wang, Y. S.; Yau, S.; Chau, L. K.; Mohamed, A.; Huang, C. J. Functional Biointerfaces Based on Mixed Zwitterionic Self-Assembled Monolayers for Biosensing Applications. *Langmuir* **2019**, *35* (5), 1652–1661.

60. Lin, X.; Jain, P.; Wu, K.; Hong, D.; Hung, H. C.; O'Kelly, M. B.; Li, B.; Zhang, P.; Yuan, Z.; Jiang, S. Ultralow Fouling and Functionalizable Surface Chemistry Based on Zwitterionic Carboxybetaine Random Copolymers. *Langmuir* **2019**, *35* (5), 1544–1551.

61. Kowalczyńska, H. M.; Nowak-Wyrzykowska, M.; Szczepankiewicz, A. a.; Dobkowski, J.;

Dyda, M.; Kamiński, J.; Kołos, R. Albumin Adsorption on Unmodified and Sulfonated Polystyrene Surfaces, in Relation to Cell-Substratum Adhesion. *Colloids Surfaces B Biointerfaces* **2011**, *84* (2), 536–544.

62. Price, W. S.; Tsuchiya, F.; Arata, Y. Lysozyme Aggregation and Solution Properties Studied Using PGSE NMR Diffusion Measurements. *J. Am. Chem. Soc.* **1999**, *121* (49), 11503–11512.

63. Zhu, L. J.; Zhu, L. P.; Jiang, J. H.; Yi, Z.; Zhao, Y. F.; Zhu, B. K.; Xu, Y. Y. Hydrophilic and Anti-Fouling Polyethersulfone Ultrafiltration Membranes with Poly(2-Hydroxyethyl Methacrylate) Grafted Silica Nanoparticles as Additive. *J. Memb. Sci.* **2014**, *451*, 157–168.

64. Alswieleh, A. M.; Cheng, N.; Canton, I.; Ustbas, B.; Xue, X.; Ladmiral, V.; Xia, S.; Ducker, R. E.; Zubir, O. El; Cartron, M. L.; Hunter, C. N.; Leggett, G. J.; Armes, S. P. Zwitterionic Poly(Amino Acid Methacrylate) Brushes. *J. Am. Chem. Soc.* **2014**.

65. Chai, C.; Lee, J.; Park, J.; Takhistov, P. Antibody Immobilization on a Nanoporous Aluminum Surface for Immunosensor Development. *Appl. Surf. Sci.* **2012**, *263*, 195–201.

66. Jain, P.; Dai, J.; Grajales, S.; Saha, S.; Baker, G. L.; Bruening, M. L. Completely Aqueous Procedure for the Growth of Polymer Brushes on Polymeric Substrates. *Langmuir* **2007**, *23* (23), 11360–11365.

Chapter 5

Diblock and Random Antifouling Poly(HPMA)-poly(CBMA) Brushes on Gold Surfaces by Light-induced Controlled Polymerization (SI-PET-RAFT) in Water

Andriy R. Kuzmyn, Lucas W. Teunissen, Pina Fritz, Barend van Lagen, Maarten M. J. Smulders, Han Zuilhof. Diblock and Random Antifouling Poly(HPMA)-poly(CBMA) Brushes on Gold Surfaces by Light-induced Controlled Polymerization (SI-PET-RAFT) in water. (2021) Manuscript in preparation

Abstract

Surface-initiated photoinduced electron transfer–reversible addition-fragmentation chain transfer (SI-PET-RAFT) is for the first time used for the creation of antifouling polymer brushes on gold surfaces. The living nature of this method allows for the creation of random and diblock copolymer brushes based on *N*-(2-hydroxypropyl) methacrylamide (HPMA) and carboxybetaine methacrylamide (CBMA). The incorporation of poly(HPMA) in the polymer brush structure provides good antifouling properties. The introduction of the CBMA into the polymer brushes opens the route for further brush functionalization by versatile activated ester chemistry. The chemical composition of the brushes is confirmed by X-ray photoelectron spectroscopy (XPS), and the polymer brush thickness is determined by spectroscopic ellipsometry. The polymer brushes demonstrate good antifouling properties against undiluted human serum, as monitored by quartz crystal microbalance with dissipation (QCM-D) and surface plasmon resonance (SPR) spectroscopy in real-time. This approach represents a route towards building antifouling and functional copolymer brushes in a scalable, robust, oxygen-tolerant, and heavy metal-free way that opens up applications in biosensing and tissue engineering.

Introduction

Biologically active surfaces play a crucial role in biosensors, tissue engineering, and other biomedical devices.[1-2] Those surfaces are functionalized with biologically active moieties that perform certain biological functions, such as specific cell adsorption or interaction with a specific protein or analyte.[3] Bioactive surfaces usually need to perform in complex biological media such as blood, saliva, or urine.[1, 4-6] Those fluids typically contain numerous types of proteins and cells that may interfere with the performance of the bioactive surface. Such non-specific adsorption by proteins and cells from biological media on the surfaces is called fouling.[7-8] Thus, the practical application of bioactive surfaces requires antifouling layers capable of preventing protein and cell fouling from complex biological media.[9-10]

Antifouling coatings can be generated by immobilizing self-assembled monolayers (SAMs) or “grafted-to” or “grafted-from” polymer coatings on a surface.[6, 11-14] The SAMs are broadly applied to introduce different functionalities. Notably, oligo(ethyleneglycol)-terminated and zwitterionic SAMs can resist or decrease fouling from single-protein solutions and cell cultures.[4] The “grafted-to” polymers based on ethyleneglycol oxide, polyoxazoline, poly(*N*-(2-

hydroxypropyl) methacrylamide) and zwitterionic moieties have shown good resistance towards single-protein solutions and moderate to good resistance towards more complex biological media.[12, 15] The "grafted-from" approach allows the synthesis of high-density, covalently bound polymer brush systems.[16] Polymer brushes based on zwitterionic methacrylates and methacrylamides,[14, 17] *N*-(2-hydroxypropyl) methacrylamide[12, 18] and oligo(ethyleneglycol) methacrylates[11] have demonstrated excellent antifouling properties in contact with different complex biological media such as blood, blood plasma, serum, and cell cultures.[1, 6]

Polymer brushes are commonly synthesized via surface-initiated atom-transfer radical polymerization (SI-ATRP).[5, 14, 17, 19-21] The well-controlled nature of this polymerization technique allows accurate tailoring of the brush height. Generally, ATRP requires relatively high concentrations of copper halide salts to generate radicals from alkyl halides and an oxygen-free environment. Single-electron transfer living radical polymerization (SET-LRP)[22] and iridium-catalyzed light-triggered living radical polymerization (LT-LRP) allow a significant decrease in the amount of heavy metal catalyst and provide the option to tune the thickness and/or create patterned structures on surfaces using light.[18] However, those polymerization techniques still require an oxygen-free environment. In response to this, new approaches, based on reversible addition–fragmentation chain transfer (RAFT), have been introduced.[23] In particular, photoinduced electron transfer-RAFT (PET-RAFT) polymerizations have been developed, through which polymer brushes can be synthesized in the presence of oxygen and, additionally, do not require heavy metal catalysts.[12, 24] Also, the light-triggered nature of this technique facilitates the production of hierarchical, patterned structures.[24-25] The mild conditions of PET-RAFT techniques, utilizing Eosin Y and triethanolamine (TEOA) as a catalyst in an aqueous environment, were also applied to synthesize polymers from both cells and DNA.[26-27] Nevertheless, RAFT and RAFT-derived techniques have not yet been employed to create antifouling polymer brushes on gold surfaces, the substrate of choice for surface plasmon resonance (SPR) and quartz crystal microbalance (QCM) based label-free biosensors.

Polymer brush-based coatings have previously been demonstrated to provide good antifouling properties when brought in contact with human and bovine serum, cell cultures, and other complex biological matrixes.[6, 11, 14, 17-18, 21-22] However, incorporating bioactive moieties in polymer brushes structure without affecting antifouling properties still poses a

challenge.[28] Overall, there are two main post-polymerization methods for the biofunctionalization of antifouling polymer brushes: chain end modification and side chain modification. Chain end biofunctionalization of polymer brushes preserves the polymer brushes' antifouling properties, although with a necessarily limited number of immobilized biorecognition elements (per polymer chain).[6, 11, 29] Side chain functionalization, on the other hand, does provide a high amount of immobilized biomolecules per polymer chain.[5, 28] However, this typically strongly impairs the fouling resistance of such polymer brushes. Therefore, copolymer brushes have been developed for the creation of bioactive antifouling coating.[14, 17, 30] The combination of highly antifouling moieties and biofunctionalizable antifouling moieties has been shown to provide large amounts of immobilized bioreceptor while preserving the antifouling properties of the original brush.[17, 30-31]

Herein we apply surface-initiated PET-RAFT (SI-PET-RAFT) for the synthesis of antifouling polymer brushes based on *N*-(2-hydroxypropyl) methacrylamide (HPMA), oligo(ethyleneglycol) methacrylate (MeOEGMA), and carboxybetaine methacrylamide (CBMA). Furthermore, we explore the living character of this technique for the creation of random and diblock copolymer brushes based on HPMA and CBMA. The incorporation of CBMA in polymer brushes would allow subsequent biofunctionalization and application of the coatings in tissue engineering and biosensing. The antifouling properties of all created coatings were tested by subjecting them to undiluted human serum and monitoring of protein adhesion in real-time by both SPR and QCM-D techniques.

Experimental section

Materials. All chemical reagents were used without further purification unless otherwise specified. 4-Cyano-4-(phenylcarbonothioylthio)pentanoic acid *N*-succinimidyl ester (RAFT-NHS), cysteamine, triethanolamine (TEOA), eosin Y (EY), triethylamine (TEA), poly(ethylene glycol) methyl ether methacrylate (average M_n 300) (MeOEGMA), ethanol (EtOH) (99.9%), acetone (99.5%), dry tetrahydrofuran (THF, 99.9%), phosphate-buffered saline (PBS) (pH = 7.4), and human serum type AB male (HS) were purchased from Sigma-Aldrich. *N*-(2-Hydroxypropyl) methacrylamide (HPMA) was obtained from Polysciences. Inc. Gold-coated silicon wafers and surface plasmon resonance (SPR) chips were acquired from Ssense. Quartz crystal microbalance chips were acquired from Quantum Design GmbH. Deionized water was

produced with a Milli-Q integral 3 system Millipore, Molsheim, France (Milli-Q water). (3-Acryloylamino-propyl)-(2-carboxy-ethyl)-dimethyl-ammonium (CBMA) was synthesized according to a previously described procedure.[17, 24]

Light Source. LEDs with a maximum intensity at 410 nm (Intelligent LED Solutions product number: ILH-XO01-S410-SC211-WIR200) were used, and the current was set at 700 mA, corresponding to a total radiometric power of 2.9 W, according to manufacturer specifications.

Formation of RAFT agent-functionalized monolayers. The RAFT-agent immobilization was conducted accordingly to previously published procedures.[12, 24]

SI-PET-RAFT synthesis of polymer brushes. The polymerization was conducted according to a modification of a previously reported procedure.[4, 18] A dye stock solution with photocatalyst was prepared to contain: EY (25 mg, 39 µmol) and TEOA (160 mg, 1.6 mmol) in 10 mL of Milli-Q water. The monomer [HPMA (178 mg, 1.3 mmol), or MeOEGMA (94 mg, 0.3 mmol), or CBMA (76 mg, 0.3 mmol), or for random copolymer HPMA (190 mg, 1.3 mmol) and CBMA (34 mg, 0.14 mmol)] was dissolved in Milli-Q water (1 mL) and subsequently 10 µL of the stock solution was added. The mixture was vortexed and added to vials containing surfaces with immobilized RAFT agent so that the liquid formed a thin layer (ca 2 mm) on top of the surfaces. Immediately after this, polymerization was conducted by irradiating the vials with visible light from a LED light source for 1 h. In these experiments, the light source was placed 3–4 cm from the substrates. The polymerization was stopped by switching off the light source. The samples were then removed from the solution and subsequently rinsed with Milli-Q water, ethanol, and blown dry under a stream of argon.

The diblock copolymer was synthesized using solutions for the first block solutions [HPMA (178 mg, 1.3 mmol) dissolved in Milli-Q water (1 mL)] and subsequently 10 µL of the dye stock solution. The polymerization was conducted for 1 h. The surfaces were removed from the solution and subsequently rinsed with Milli-Q water, ethanol, and blown dry under a stream of argon. Subsequently, the thus modified surfaces were submerged in a new solution for the synthesis of the second block [CBMA (76 mg, 0.3 mmol) with 10 µL of the dye stock solution in a total of 1 mL of Milli-Q water]. This solution was also irradiated for 1 h. Then the surfaces were removed and washed with Milli-Q water, ethanol, and blown dry under a stream of argon.

X-ray photoelectron spectroscopy (XPS). XPS measurements were performed using a JPS-9200 photoelectron spectrometer (JEOL Ltd., Japan). All samples were analyzed using a focused monochromated Al Kα X-ray source (spot size of 300 µm) at a constant dwelling time for wide-scan 50 ms and narrow-scan of 100 ms and pass energy: wide-scan 50 eV narrow-scan: 10 eV. The power of the X-ray source was 240 W (20 mA and 12 kV). Charge compensation was applied during the XPS scans with an accelerating voltage of 2.8 eV and a filament current of 4.8 A. XPS wide-scan and narrow-scan spectra were obtained under ultra-high vacuum conditions (base pressure $3 \cdot 10^{-7}$ Pa). All narrow-range spectra were corrected with a linear background before fitting. The spectra were fitted with symmetrical Gaussian/Lorentzian (GL(30)) line shapes using CasaXPS. All spectra were referenced to the C1s peak attributed to C–C and C–H atoms at 285.0 eV.

The XPS depth profiling was performed utilizing an Argon source operating in small cluster ion mode at 500 eV. Each sputtering cycle lasted 10 s, and XPS spectra were acquired in between sputtering steps. The twin anode X-ray source was used at 15 kV and 10 mA.

Static water contact angle measurements. The wettability of the modified surfaces was determined by automated static water contact angle measurements using a Krüss DSA 100 goniometer. The volume of a drop of demineralized water is 3 µL. Contact angles from sessile drops measured by the tangent method were estimated using a standard error propagation technique involving partial derivatives.

Spectroscopic ellipsometry. The polymerization kinetics were followed by measuring the dry thickness of the brushes using an Accurion Nanofilm_ep4 Imaging Ellipsometer. The ellipsometric data were acquired in air at room temperature using light in the wavelength range of λ = 400.6 – 761.3 nm at an angle of incidence of 50°. The data were fitted with EP4 software using a multilayer model.

Quartz crystal microbalance with dissipation monitoring (QCM-D). QCM-D was used to measure mass changes as well as viscoelastic and structural properties of the various films.[32-33] The measurements were performed by using gold-coated quartz resonators (AT-cut, Biolin Scientific, Sweden) with a fundamental frequency (f_0) of 5 MHz in a QCM-D set-up (Q-Sense E4, Biolin Scientific, Sweden) at 18 °C. The QCM-D sensors were cleaned with a multistep cleaning procedure. The sensors were cleaned with UV-ozone treatment (Procleaner UV.PC.220, Bioforce Nanosciences,) for 10 min, dipped in 2% sodium dodecyl sulfate solution

for 30 min, and rinsed with demineralized water. After the sensors were dried with a gentle flow of argon, they were treated with UV-ozone cleaning for another 10 min as stated in the literature.[34-35] All solutions were bubbled with argon before the experiments to eliminate dissolved oxygen that may cause problems with the baseline. Before each experiment, the PBS buffer solution was pumped via a peristaltic pump (Ismatec high precision multichannel dispenser) with a flow rate of 50 µL/min for at least 15 min to have a stable baseline. QSoft (version 2.8.0.913 Analyzer) and DFind (version 1.2.7) software was used to record and process the data, respectively.

Frequency (Δf) and dissipation shifts (ΔD) were acquired real-time at the 3rd (15 MHz), 5th (25 MHz), 7th (35 MHz), 9th (45 MHz), and 11th (55 MHz) harmonic overtones. The 3rd (15 MHz) overtones were reported for comparison of different polymer coatings. The change in frequency of the quartz crystal can be associated with a change in mass (wet) after implementation of a film, resulting in the Sauerbrey equation (1)[36] where Δm = areal mass density of the film, Δf_n = frequency shift, n = harmonic number, and C (17.7 ng·cm^{-2}·Hz^{-1}) = mass sensitivity constant:

$$\Delta m = \frac{C}{n} \Delta f_n \qquad (1)$$

Surface plasmon resonance (SPR). SPR spectra were obtained on an SPR device from Kinetic Evaluation Instruments (The Netherlands). The baseline was acquired by running PBS buffer for at least 15 min. Subsequently, the undiluted human serum was introduced to the cuvette for 15 min. The solution was washed afterward with PBS buffer. The mass of the adsorbed protein was calculated accordingly to equation (2):

$$\Delta m\ (pg \cdot mm^2) = \Delta Response\ /\ (m° \text{Conversion factor } (m° \cdot (mm^2\ /ng)) \cdot 1000 \qquad (2)$$

In this equation, the conversion factor is equal to 122 m°·(mm^2 ·ng^{-1})

Results and discusions

The method applied to produce antifouling polymer brushes by Surface-Initiated Photoinduced Electron Transfer-Reversible Addition–Fragmentation Chain Transfer Polymerization (SI-PET-RAFT) consists of three consecutive steps (Scheme 1). The first step was immobilization of a cysteamine self-assembled monolayer on the gold surface. This was followed by incorporation of RAFT agent by reacting an active ester of the RAFT agent [4-cyano-4-(phenylcarbonothioylthio)pentanoic acid *N*-succinimidyl ester (RAFT-NHS)] with the primary amine of cysteamine monolayer. In the third step, PET-RAFT polymerization was conducted under visible-light irradiation in the presence of Eosin Y (EY) and triethanolamine (TEOA) (Scheme 1). Each step is now discussed in detail.

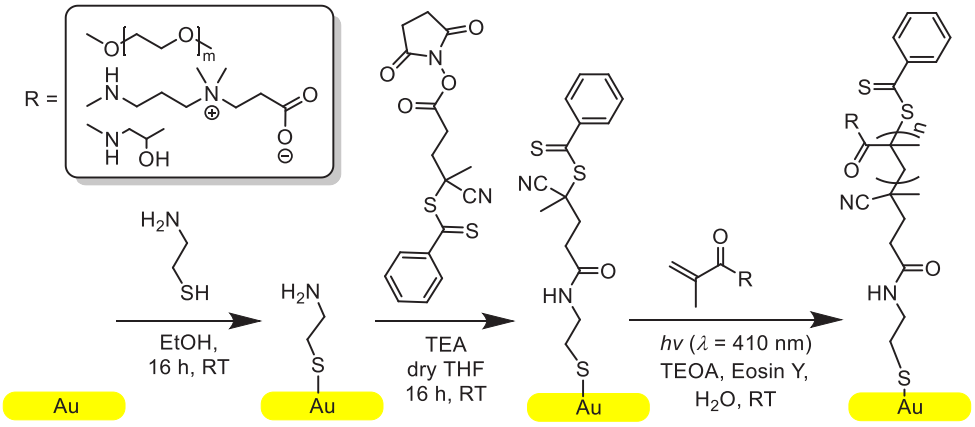

Scheme 1. Schematic depiction of the formation of antifouling coatings on Au by SI-PET-RAFT.

Immobilization of RAFT agent on the gold surface. Gold surfaces were functionalized with the RAFT agent in two steps. Initially, the self-assembled monolayer of cysteamine was immobilized on the gold surface. Formation of the cysteamine monolayer was confirmed with XPS. The XPS wide-scan spectrum showed four main peaks that correspond to O1s, C1s, N1s, and Au4d atoms (Figure 1a (2)). The experimental ratio between C : N : S was 4.5 : 1.0 : 1.0, i.e., the carbon content was significantly higher than the theoretical elemental ratio in the compound (2 : 1 : 1). This is attributed to atmospheric contamination and the initial presence of a significant amount of carbon in the bare gold layer (also present after extensive plasma cleaning of the sample). The ratio between N and S species correspond to theoretically

expected value. The XPS narrow-scan spectrum of the S2p region (Figure 1b (2)) can be deconvoluted into two peaks that can be assigned to $S2p_{1/2}$ (163.3 eV) and $S2p_{3/2}$ (162.0 eV) in the [C–S–Au] species.

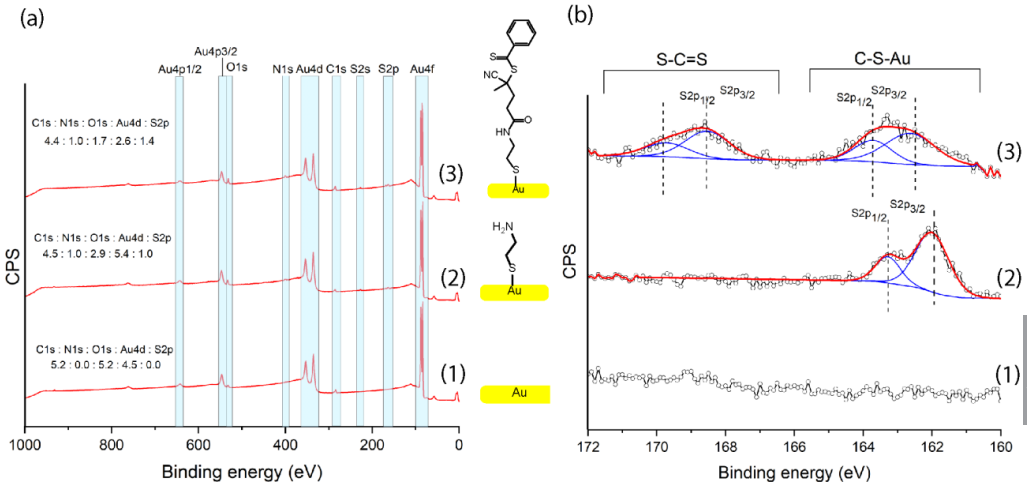

Figure 1. (a) XPS characterization of the cysteamine and RAFT-functionalized monolayers: (1) wide-scan bare gold surface, (2) cystamine monolayer; (3) RAFT agent functionalized monolayer. (b) Narrow-scan XPS data of the S2p region of the corresponding surfaces.

The RAFT agent functionalized surfaces were created according to a previously published procedure[12, 24] by exposing the surface to 4-cyano-4-(phenylcarbonothioylthio)pentanoic acid *N*-succinimidyl ester (RAFT-NHS) in the presence of triethylamine (TEA) (Scheme 1). The success of the reaction was confirmed by XPS characterization. In the XPS wide-scan spectrum an increase of the S2s peak intensity was observed as well as the appearance of two new peaks at 168.6 eV ($S2p_{3/2}$) and 169.8 eV ($S2p_{1/2}$) in the narrow-scan of the S2p region, which correspond to the thiocarbonylthiol [**S**–C=**S**] species. The ratio between [**S**–C=**S**] and [C–**S**–Au] species in S2p and S2s XPS narrow-scans was obtained from five samples and indicated that on average 32 ± 4% of the surface-bound amines had reacted with RAFT-NHS. This degree of conversion is similar to values previously reported for (3-aminopropyl)triethoxysilane on silicon oxide surfaces.[12, 24] Also, the surface gained a more hydrophobic character after modification with RAFT-NHS as the static water contact angle increased from 34 ± 1° to 92 ± 1°.

Synthesis and characterization of poly(MeOEGMA), poly(CBMA), and poly(HPMA) brushes. Polymer brushes based on MeOEGMA, CBMA, and HPMA have shown unparalleled resistance to non-specific adsorption of proteins.[11-12, 18, 21, 24] Thus, employing a robust, oxygen-tolerant, and heavy metal-free polymer brush route such as the SI-PET-RAFT technique for the synthesis of these brushes on gold surfaces has the potential to allow easier access to such surfaces. Poly(HPMA), poly(MeOEGMA), and poly(CBMA) brushes were therefore grafted from the RAFT agent-coated surfaces by SI-PET-RAFT using Eosin Y as a photocatalyst in water according to a previously published procedure.[12, 24] The chemical composition of the coatings was characterized by XPS, and the polymer brush thickness was determined by spectroscopic ellipsometry. The polymerization of MeOEGMA on gold was conducted for 1 h, reaching an average thickness of 29 ± 1 nm. The XPS wide-scan spectrum of a poly(MeOEGMA) layer with a thickness of 29 nm showed two main peaks for O1s and C1s in a ratio of 1.0 : 2.7 (Figure 2a). The C1s XPS narrow-scan spectrum shows three main peaks of carbon atoms: [**C**–C/H] (285.0 eV) : [**C**–O] (286.5 eV) : [O–**C**=O] (289.0 eV) in a ratio of 8.7 : 3.9 : 1 (Figure 2b). The static water contact angle of poly(MeOEGMA)-coated surfaces was determined to be 52 ± 1°. The overall characteristics of this brush correspond to brushes made by different techniques such as ATRP[11] or on different surfaces.[24]

The XPS wide-scan spectrum of poly(CBMA) brushes, with an ellipsometric thickness of 11 ± 1 nm after 1 hour of SI-PET-RAFT polymerization, (Figure 3c) showed four main peaks related to C, O, N, and Au atoms, in a ratio of 6.6 : 1.0 : 1.0 : 0.2. The lower content of oxygen in the XPS wide-range spectra may be related to degradation of the CBMA polymer during exposure to X-rays. The narrow-scan XPS C1s spectrum (Figure 2d) displayed three peaks: [**C**–C/H] (285.0 eV) : [**C**–N] (286.3 eV) : [**C**=O] (287.8 eV) in a ratio of 2.7 : 2.5 : 1 that correlates well with the theoretically expected composition of the poly(CBMA) structure (2.5 : 2.5 : 1). The poly(CBMA) layers also showed high hydrophilicity with a static water contact angle of 18 ± 1°.

Poly(HPMA) brushes achieved an average thickness of 41 ± 1 nm after 60 min of irradiation. The XPS wide-scan spectrum of the poly(HPMA) brushes (Figure 2e) showed three main peaks related to O1s, N1s, and C1s, in a 1.6 : 1.0 : 7.7 ratio. This is in reasonable agreement with the expected elemental composition of the poly(HPMA) structure (2 : 1 : 7), given the presence of some atmospheric contamination. The fitted ratio in the XPS C1s spectrum between the

[**C**–C/H] (285.0 eV) : [**C**–N] (285.8 eV) : [C–O] (286.5 eV) : [NH–**C**=O] (288.0 eV) peaks is 3.7 : 1.2 : 1.2 : 1, which closely corresponds to the theoretically expected composition of the poly(HPMA) structure (4 : 1 : 1 : 1). The poly(HPMA) brushes displayed a static water contact angle of 40 ± 1°, and all these physicochemical characteristics are highly similar to those of poly(HPMA) brushes synthesized by other techniques and on other types of surfaces or initiator layers.[12, 14, 22, 24]

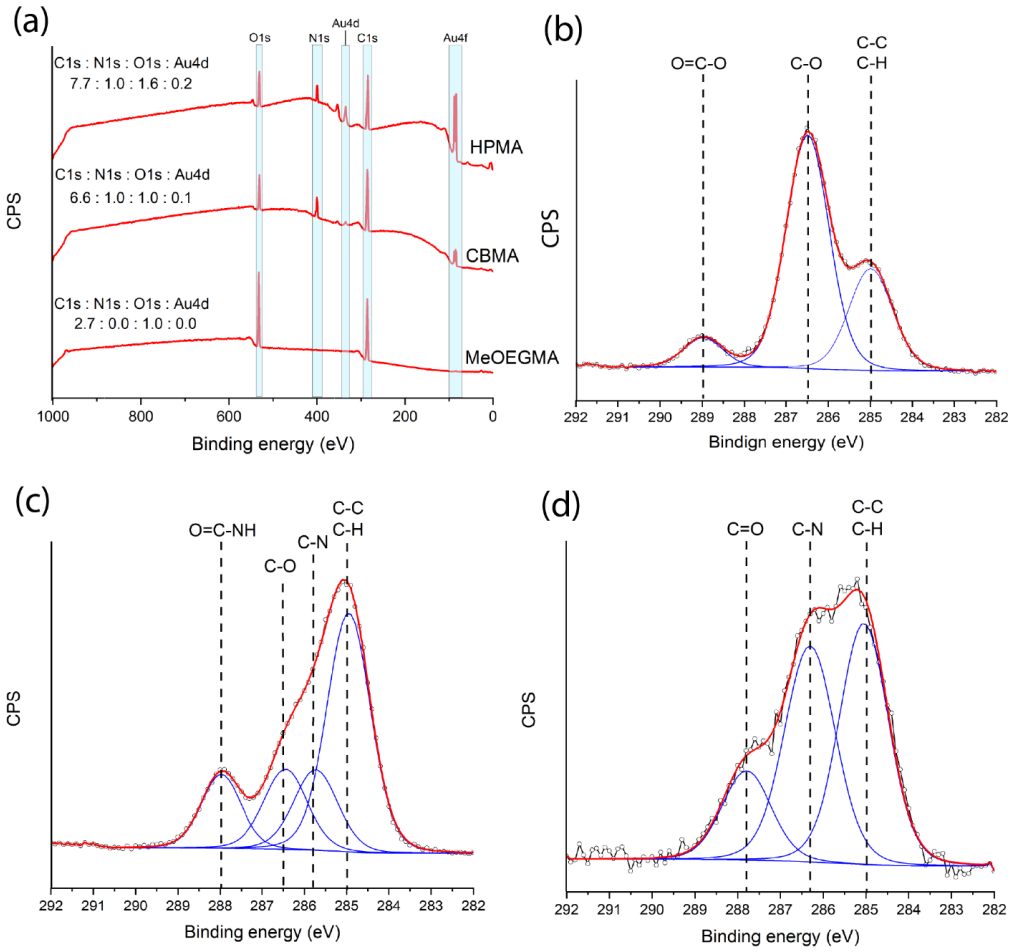

Figure 2. (a) XPS wide-range scans of the three polymer brush layers under study. (b-d) Narrow-scan XPS C1s spectrum of (b) poly(MeOEGMA) brushes [41 nm], (c) poly(HPMA) brushes [29 nm], and (d) poly(CBMA) brushes [11 nm].

Synthesis of poly(HPMA)-poly(CBMA) random and diblock copolymer brushes. To overcome the challenges of the biofunctionalization of antifouling polymer brushes without impairing their antifouling properties, the combination of HPMA and CBMA and combination in hydroxy-terminated and methoxy-terminated oligo(ethyleneglycol) methacrylate using ATRP and other methods has been used in both random copolymer brushes.[17, 31] Analogously, we have applied the SI-PET-RAFT technique for the synthesis of random copolymer brushes of HPMA and CBMA (Scheme 2 "Random brush path"). Furthermore, we exploited the living nature of PET-RAFT polymerizations for the production of a diblock copolymer brush of HPMA and CBMA (Scheme 2 "Diblock brush path"). Here we strove for a bottom layer of HPMA, as this displays an overall superior antifouling behavior, while the CBMA block combines still very good antifouling properties with functionalizability.

The random copolymer brushes were synthesized according to the SI-PET-RAFT procedure, adding a monomer mixture of CBMA and HPMA in the molar ratio 1 : 10. The polymerizations were conducted for by submerging gold surfaces that were covalently functionalized with RAFT-agent in the polymerization solutions containing EY and TEOA, and subsequent irradiation for 60 min. The ratio of the two monomers was chosen based on previous studies of this type of random copolymer brush from the perspective of antifouling and bioreceptor immobilization properties.[17, 30] The diblock copolymer brush was analogously synthesized in two steps: First, the bottom block of poly(HPMA) was grown for 60 min. After which surfaces were washed and placed in new polymerization solution contanining CBMA. The top block of poly(CBMA) was added by another 60 min polymerization.

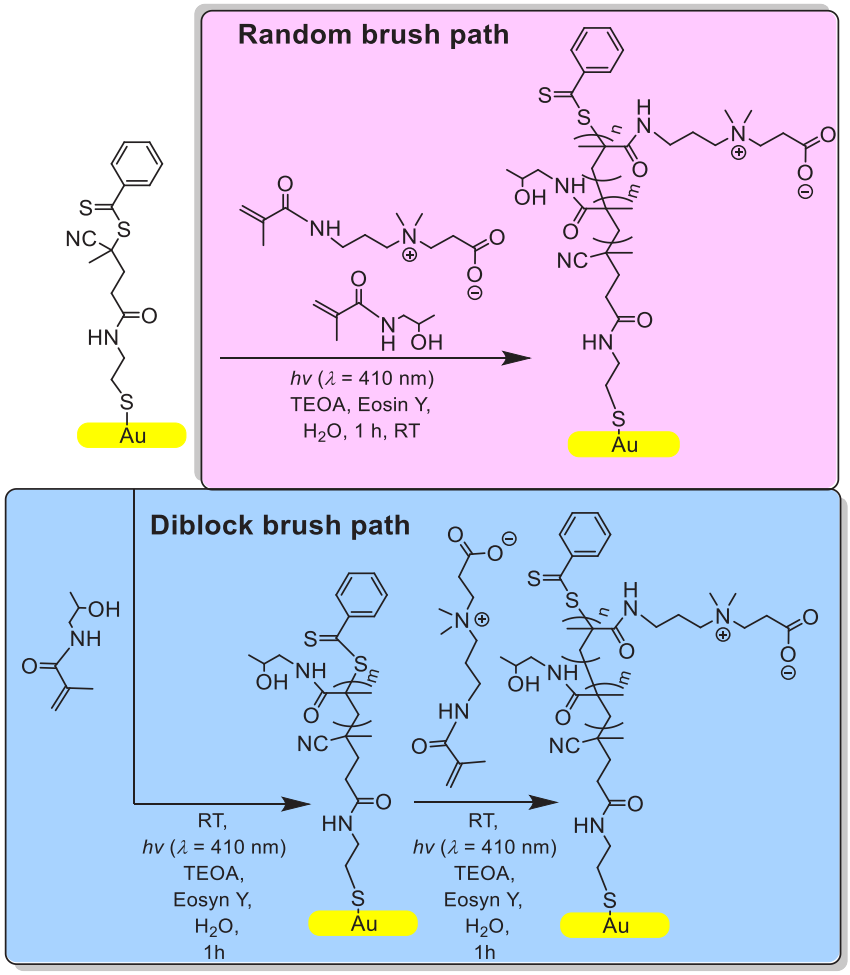

Scheme 2. Schematic depiction of the synthetic pathways to create diblock and random poly(HPMA)-poly(CBMA) brushes by SI-PET-RAFT.

The diblock and random copolymer brushes were characterized by XPS and ellipsometry. The XPS wide-scan spectrum of random poly(HPMA)-poly(CBMA) brushes, with an ellipsometric thickness of 26 nm, showed four main peaks related to C1s, O1s, N1s, and Au4d atoms, in a ratio of 8.1 : 1.0 : 1.7 : 0.1. The increase of C1s, and O1s peaks with respect to poly(HPMA) brushes (XPS ratios poly(HPMA) 41 nm O1s : N1s : C1s correspond 1.6 : 1.0 : 7.7) is related to contribution of CBMA moieties to the copolymer structure (Figure 3a). Further confirmation of the incorporation of CBMA in the brush structure was provided by the XPS N1s narrow-scan, (Figure 3b) due to the appearance of a signal related to the quaternary

ammonium species [N^+] at 403.4 eV. The ratio between [N^+] (403.4 eV) : [NH] (400.2 eV) in XPS N1s narrow-scan was determined to be 1.0 : 8.7, which indicates a HPMA / CBMA ratio of 1 : 9 in close agreement with the ratio used in the solution that contained both monomers. The random copolymer brushes displayed a more hydrophilic static water contact angle of 32 ± 1° than poly(HPMA) brushes (41 ± 1°) due to the CBMA moieties.

The XPS wide-range spectrum of the diblock poly(HPMA)-poly(CBMA) brushes, with an average total ellipsometric thickness of 54 ± 2 nm (41 ± 1 nm first block poly(HPMA) and 13 ± 2 nm second block poly(CBMA)), showed four main peaks related to C1s, O1s, N1s, and Au4d atoms, in a ratio of 7.3 : 1.0 : 1.4 : 0.0 (Figure 3c). The ratio between [N^+] (403.2 eV) : [NH] (400 eV)) in the XPS N1s narrow-scan was determined at 1.0 : 5.2. (Figure 3d). Here the relatively low ratio of N^+ species to NH is related to the low grafting density of the second block, the limited presence of available reinitiations sides, and degradation of N^+ under XPS conditions. The diblock brushes displayed a static water contact angle of 29 ± 1°. The higher affinity to water in this copolymer brush is related to CBMA species' presence on top of the poly(HPMA) brush.

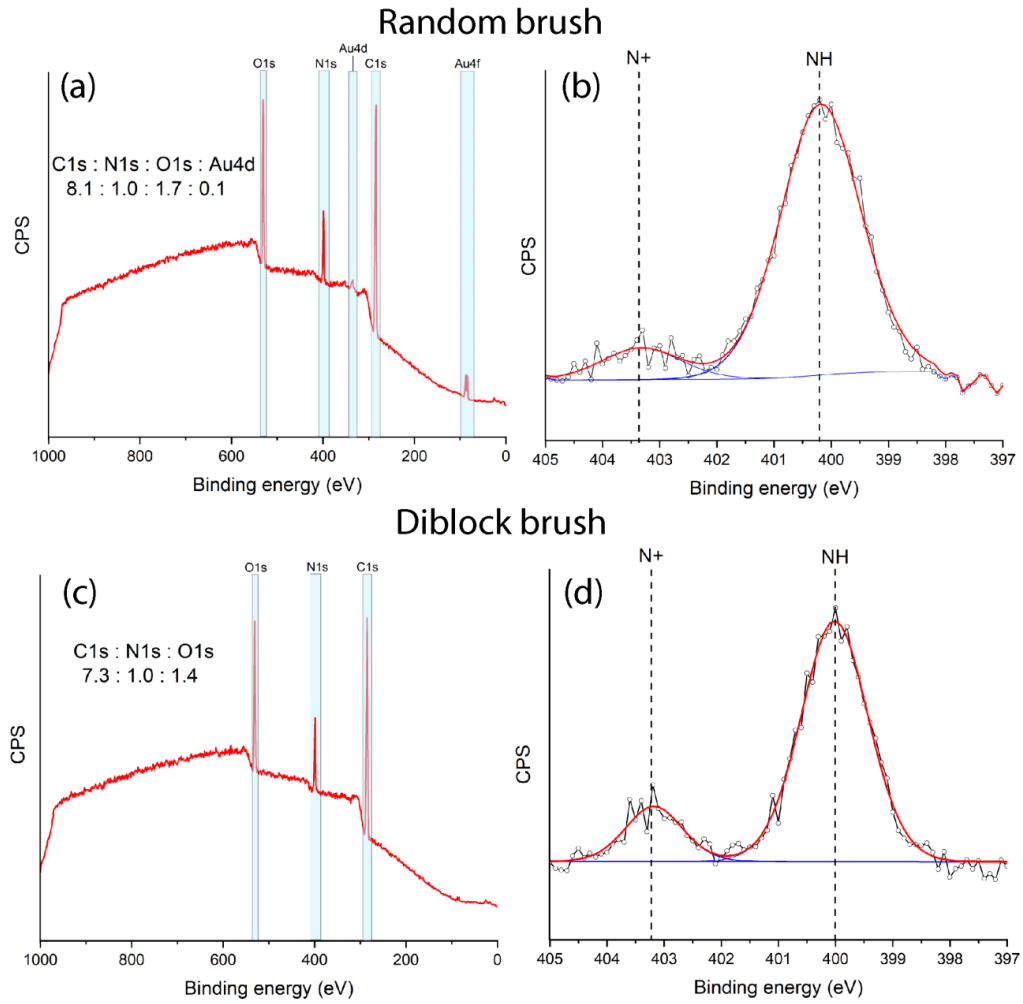

Figure 3. Random versus diblock polymer brushes. (a-b) Poly(HPMA)-poly(CBMA) random brushes: (a) XPS wide-range characterization. (b) N1s XPS narrow-scan. (c-d) Poly(HPMA)-poly(CBMA) diblock polymer brushes: (c) XPS wide-range characterization. (d) N1s XPS narrow-scan.

The diblock polymer brush structure was further confirmed by XPS depth profiling (Figure 4). The XPS N1s narrow-scan was monitored after equal intervals of exposure to the Ar^+ beam. The disappearance of [N^+] signal in the spectrum with the progression of sputtering indicates the presence of CBMA species on the top of the first poly(HPMA) block of the brush.

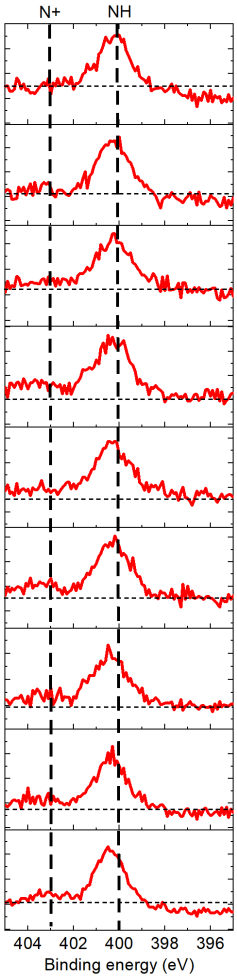

Figure 4. XPS depth profile of diblock poly(HPMA)-poly(CBMA). The spectra were recorded at 10 seconds interval while exposing the coating to the Ar^+ beam.

Antifouling properties. The design of antifouling biointerfaces requires excellent resistance to fouling from complex biological media. Thus, the prepared polymer brushes were challenged by contacting the surfaces with undiluted human serum (HS) for 15 min. SPR and QCM-D techniques were used to asses the amount of non-specifically adsorbed protein. Overall, all polymer brushes under current study perform showed good antifouling coatings (see Table 1), and we will discuss the detailed results per technique (QCM-D and SPR, respectively).

QCM-D fouling measurements for all polymer brushes, with the only exception of poly(CBMA) brushes, showed a degree of protein fouling from HS below the detection limit (Figure 5, right) Interestingly, for non-charged polymer brushes and copolymer brushes the frequency value increased reversibly upon exposure to undiluted human serum. Such a change implies a decrease in mass of the film upon exposure (Figure 5, left). The increase in frequency upon exposure to HS also was correlated with changes in the dissipation, related to the viscoelastic properties of the brush. While basically no change in the dissipation were observed for poly(HPMA), a slight increase was seen for poly(MeOEGMA), the poly(HMPA)-poly(CBMA) diblock, and the poly(HPMA)-poly(CBMA) random copolymer. These observations can be rationalized with an osmotic-pressure induced change in the water content of the polymer brush and concomitant morphological changes within the brush. Such loss of water has previously described in the literature.[37-38] Both the frequency and the dissipation returned to their pre-exposure levels for all non-changed brushes after washing with PBS, thus indicating that no loss or gain of the covalently bound mass of the brush had occurred, in line with the reversibly changeable water content. Only with pure CBMA and uncoated Au fouling occurred, as seen from a decrease in frequency, i.e. increase of mass due to adsorbed protein. These findings were substantiated by our SPR measurements, which displayed a lower limit of detection.

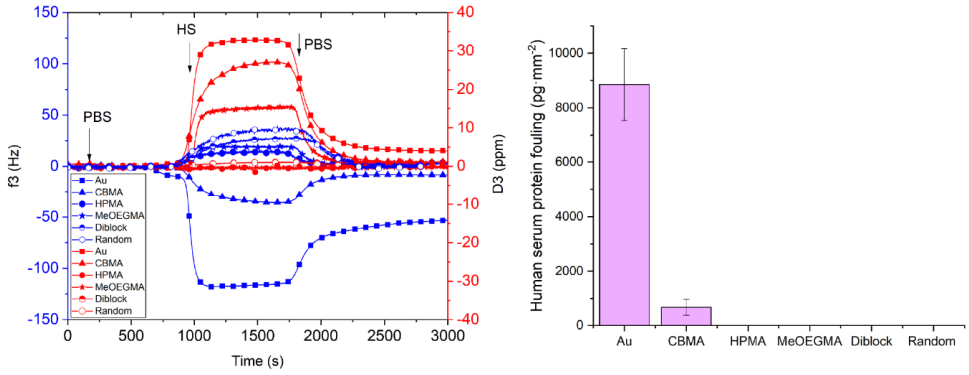

Figure 5. QCM-D data showing the change in mass upon exposure to undiluted human serum (HS) for the various coatings.

The SPR measurements provided more detailed information about the antifouling properties of the layers, due to the overall higher sensitivity of SPR analysis as an method to

determine protein fouling. This allowed to show small but significant significant differences between the various brushes: poly(HPMA) (10 ± 3 pg·mm^{-2}) poly(MeOEGMA) (126 ± 31 pg·mm^{-2}) and poly(CBMA) (55 ± 23 pg·mm^{-2}) brushes. Despite the overall similar sensitivity factors of SPR and QCM-D machines. SPR allows more detailed and thorough investigation of the fouling in contrast to confocal laser scanning microscopy or QCM-D techniques. The slightly higher fouling than previously reported for the random poly(HPMA)-poly(CBMA), poly(MeOEGMA) brushes by SPR, and poly(CBMA) by QCM-D created by other techniques such as ATRP can be related to possible lower grafting density of the coatings. It can be further explained by the two-step immobilization of the RAFT agent. The protein fouling on the diblock and random copolymer brushes from undiluted HS was determined to be 40 ± 18 pg·mm^{-2} and 53 ± 35 pg·mm^{-2}, respectively. It also should be noted that we observed significant differences in the extent of fouling on the blanc bare gold surface as measurements in SPR and QCM-D. This may be related to a different type of gold in chips and difference in actual sensitivity of both methods.

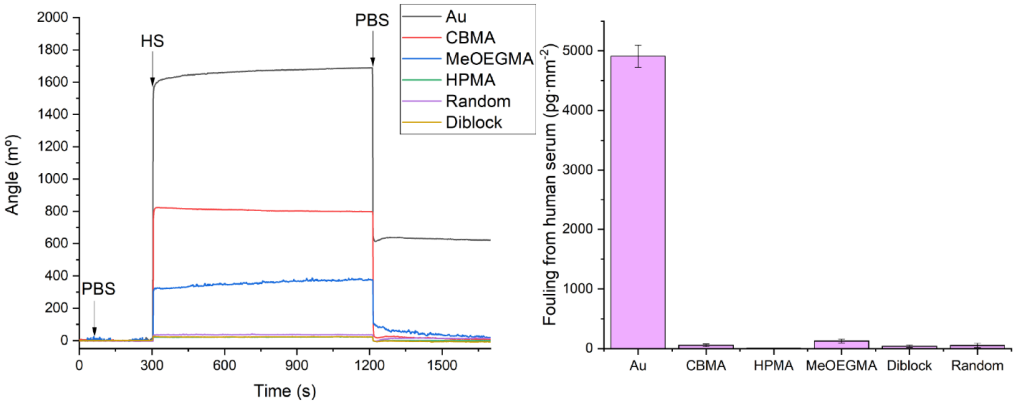

Figure 6. The SPR sensorgram of the change in angle upon contact with undiluted HS on bare gold and gold coated with various polymer brushes (left), irreversible fouling from HS obtained from SPR measurements (right).

Conclusions

We applied surface-initiated photoinduced electron transfer–reversible addition-fragmentation chain transfer (SI-PET-RAFT) technique for the creation of well-defined antifouling polymer brushes based on oligo(ethylene glycol) methacrylate, *N*-(2-hydroxypropyl)methacrylamide, and carboxybetaine methacrylamide. Furthermore, the synthesis of random and diblock polymer brushes based on *N*-(2-hydroxypropyl)methacrylamide and carboxybetaine methacrylamide was demonstrated. Thus, providing a route for the application of SI-PET-RAFT for the creations of biofunctional antifouling surfaces. All created coatings showed good antifouling properties towards the undiluted human serum. Due to the simple overall approach of producing these antifouling and functional surfaces, we envision that they can be efficiently used in biosensing devices, tissue engineering, and other applications of bioactive surfaces.

Acknowledgment

Sevil Şahin is acknowledged for assistance with the QCM-D measurements. This research is carried out under project number C16030a in the framework of the Research Program of the Materials innovation institute M2I.

References

1. Yu, Q.; Zhang, Y.; Wang, H.; Brash, J.; Chen, H., Anti-fouling Bioactive Surfaces. *Acta Biomaterialia* **2011,** *7* (4), 1550-1557.

2. Williams, D. F., On the Nature of Biomaterials. *Biomaterials* **2009,** *30* (30), 5897-5909.

3. Wischerhoff, E.; Badi, N.; Lutz, J.-F.; Laschewsky, A., Smart Bioactive Surfaces. *Soft Matter* **2010,** *6* (4), 705-713.

4. Rodriguez Emmenegger, C.; Brynda, E.; Riedel, T.; Sedlakova, Z.; Houska, M.; Alles, A. B., Interaction of Blood Plasma with Antifouling Surfaces. *Langmuir* **2009,** *25* (11), 6328-6333.

5. Rodriguez-Emmenegger, C.; Avramenko, O. A.; Brynda, E.; Skvor, J.; Alles, A. B., Poly(HEMA) Brushes Emerging as a New Platform for Direct Detection of Food Pathogen in Milk Samples. *Biosensors and Bioelectronics* **2011,** *26* (11), 4545-4551.

6. Baggerman, J.; Smulders, M. M. J.; Zuilhof, H., Romantic Surfaces: A Systematic Overview of Stable, Biospecific, and Antifouling Zwitterionic Surfaces. *Langmuir* **2019,** *35* (5), 1072-1084.

7. Le-Clech, P., Protein Fouling. In *Encyclopedia of Membranes*, Drioli, E.; Giorno, L., Eds. Springer Berlin Heidelberg: Berlin, Heidelberg, 2015; pp 1-2.

8. Le-Clech, P., Protein Fouling Mechanisms. In *Encyclopedia of Membranes*, Drioli, E.; Giorno, L., Eds. Springer Berlin Heidelberg: Berlin, Heidelberg, 2015; pp 1-2.

9. Kotlarek, D.; Vorobii, M.; Ogieglo, W.; Knoll, W.; Rodriguez-Emmenegger, C.; Dostálek, J., Compact Grating-Coupled Biosensor for the Analysis of Thrombin. *ACS Sensors* **2019,** *4* (8), 2109-2116.

10. Kotlarek, D.; Curti, F.; Vorobii, M.; Corradini, R.; Careri, M.; Knoll, W.; Rodriguez-Emmenegger, C.; Dostálek, J., Surface plasmon resonance-based aptasensor for direct monitoring of thrombin in a minimally processed human blood. *Sensors and Actuators B: Chemical* **2020,** *320*, 128380.

11. Kuzmyn, A. R.; de los Santos Pereira, A.; Pop-Georgievski, O.; Bruns, M.; Brynda, E.; Rodriguez-Emmenegger, C., Exploiting End Group Functionalization for the Design of Antifouling Bioactive Brushes. *Polymer Chemistry* **2014,** *5* (13), 4124-4131.

12. Roeven, E.; Kuzmyn, A. R.; Scheres, L.; Baggerman, J.; Smulders, M. M. J.; Zuilhof, H., PLL–Poly(HPMA) Bottlebrush-Based Antifouling Coatings: Three Grafting Routes. *Langmuir* **2020,** *36* (34), 10187-10199.

13. Vaisocherová-Lísalová, H.; Surman, F.; Víšová, I.; Vala, M.; Špringer, T.; Ermini, M. L.; Šípová, H.; Šedivák, P.; Houska, M.; Riedel, T.; Pop-Georgievski, O.; Brynda, E.; Homola, J., Copolymer Brush-Based Ultralow-Fouling Biorecognition Surface Platform for Food Safety. *Analytical Chemistry* **2016,** *88* (21), 10533-10539.

14. van Andel, E.; Lange, S. C.; Pujari, S. P.; Tijhaar, E. J.; Smulders, M. M. J.; Savelkoul, H. F. J.; Zuilhof, H., Systematic Comparison of Zwitterionic and Non-Zwitterionic Antifouling Polymer Brushes on a Bead-Based Platform. *Langmuir* **2019,** *35* (5), 1181-1191.

15. Morgese, G.; Benetti, E. M., Polyoxazoline Biointerfaces by Surface Grafting. *European Polymer Journal* **2017,** *88*, 470-485.

16. Michalek, L.; Barner, L.; Barner-Kowollik, C., Polymer on Top: Current Limits and Future Perspectives of Quantitatively Evaluating Surface Grafting. *Advanced Materials* **2018,** *30* (21), 1706321.

17. Lísalová, H.; Brynda, E.; Houska, M.; Víšová, I.; Mrkvová, K.; Song, X. C.; Gedeonová, E.; Surman, F.; Riedel, T.; Pop-Georgievski, O.; Homola, J., Ultralow-Fouling Behavior of Biorecognition Coatings Based on Carboxy-Functional Brushes of Zwitterionic Homo- and Copolymers in Blood Plasma: Functionalization Matters. *Analytical Chemistry* **2017,** *89* (6), 3524-3531.

18. Kuzmyn, A. R.; Nguyen, A. T.; Zuilhof, H.; Baggerman, J., Bioactive Antifouling Surfaces by Visible-Light-Triggered Polymerization. *Advanced Materials Interfaces* **2019,** *6* (12), 1900351.

19. Nguyen, A. T.; Baggerman, J.; Paulusse, J. M. J.; van Rijn, C. J. M.; Zuilhof, H., Stable Protein-Repellent Zwitterionic Polymer Brushes Grafted from Silicon Nitride. *Langmuir* **2011,** *27* (6), 2587-2594.

20. Zoppe, J. O.; Ataman, N. C.; Mocny, P.; Wang, J.; Moraes, J.; Klok, H.-A., Surface-Initiated Controlled Radical Polymerization: State-of-the-Art, Opportunities, and Challenges in Surface and Interface Engineering with Polymer Brushes. *Chemical Reviews* **2017,** *117* (3), 1105-1318.

21. de los Santos Pereira, A.; Rodriguez-Emmenegger, C.; Surman, F.; Riedel, T.; Alles, A. B.; Brynda, E., Use of Pooled Blood Plasmas in the Assessment of Fouling Resistance. *RSC Advances* **2014,** *4* (5), 2318-2321.

22. Vorobii, M.; de los Santos Pereira, A.; Pop-Georgievski, O.; Kostina, N. Y.; Rodriguez-Emmenegger, C.; Percec, V., Synthesis of Non-fouling poly[N-(2-hydroxypropyl)methacrylamide] Brushes by Photoinduced SET-LRP. *Polymer Chemistry* **2015,** *6* (23), 4210-4220.

23. Zamfir, M.; Rodriguez-Emmenegger, C.; Bauer, S.; Barner, L.; Rosenhahn, A.; Barner-Kowollik, C., Controlled Growth of Protein Resistant PHEMA Brushes via S-RAFT Polymerization. *Journal of Materials Chemistry B* **2013,** *1* (44), 6027-6034.

24. Kuzmyn, A. R.; Nguyen, A. T.; Teunissen, L. W.; Zuilhof, H.; Baggerman, J., Antifouling Polymer Brushes via Oxygen-Tolerant Surface-Initiated PET-RAFT. *Langmuir* **2020,** *36* (16), 4439-4446.

25. Li, M.; Fromel, M.; Ranaweera, D.; Rocha, S.; Boyer, C.; Pester, C. W., SI-PET-RAFT: Surface-Initiated Photoinduced Electron Transfer-Reversible Addition–Fragmentation Chain Transfer Polymerization. *ACS Macro Letters* **2019,** *8* (4), 374-380.

26. Lueckerath, T.; Strauch, T.; Koynov, K.; Barner-Kowollik, C.; Ng, D. Y. W.; Weil, T., DNA–Polymer Conjugates by Photoinduced RAFT Polymerization. *Biomacromolecules* **2019,** *20* (1), 212-221.

27. Niu, J.; Lunn, D. J.; Pusuluri, A.; Yoo, J. I.; O'Malley, M. A.; Mitragotri, S.; Soh, H. T.; Hawker, C. J., Engineering Live Cell Surfaces with Functional Polymers via Cytocompatible Controlled Radical Polymerization. *Nature Chemistry* **2017,** *9*, 537.

28. Vaisocherová, H.; Ševců, V.; Adam, P.; Špačková, B.; Hegnerová, K.; de los Santos Pereira, A.; Rodriguez-Emmenegger, C.; Riedel, T.; Houska, M.; Brynda, E.; Homola, J., Functionalized Ultra-low Fouling Carboxy- and Hydroxy-functional Surface Platforms: Functionalization Capacity, Biorecognition Capability and Resistance to Fouling from Undiluted Biological Media. *Biosensors and Bioelectronics* **2014,** *51*, 150-157.

29. Nguyen, A. T.; Baggerman, J.; Paulusse, J. M. J.; Zuilhof, H.; van Rijn, C. J. M., Bioconjugation of Protein-Repellent Zwitterionic Polymer Brushes Grafted from Silicon Nitride. *Langmuir* **2012,** *28* (1), 604-610.

30. Lange, S. C.; van Andel, E.; Smulders, M. M. J.; Zuilhof, H., Efficient and Tunable Three-Dimensional Functionalization of Fully Zwitterionic Antifouling Surface Coatings. *Langmuir* **2016,** *32* (40), 10199-10205.

31. de los Santos Pereira, A.; Riedel, T.; Brynda, E.; Rodriguez-Emmenegger, C., Hierarchical Antifouling Brushes for Biosensing Applications. *Sensors and Actuators B: Chemical* **2014,** *202*, 1313-1321.

32. Sittel, K.; Rouse, P. E.; Bailey, E. D., Method for Determining the Viscoelastic Properties of Dilute Polymer Solutions at Audio-Frequencies. *Journal of Applied Physics* **1954,** *25* (10), 1312-1320.

33. Rodahl, M.; Kasemo, B., A Simple Setup to Simultaneously Measure the Resonant Frequency and the Absolute Dissipation Factor of a Quartz Crystal Microbalance. *Review of Scientific Instruments* **1996,** *67* (9), 3238-3241.

34. Harewood, K.; Wolff, J. S., A rapid electrophoretic procedure for the detection of SDS-released oncorna-viral RNA using polyacrylamide-agarose gels. *Analytical Biochemistry* **1973,** *55* (2), 573-581.

35. Penfold, J.; Staples, E.; Tucker, I.; Thomas, R. K., Adsorption of Mixed Anionic and Nonionic Surfactants at the Hydrophilic Silicon Surface. *Langmuir* **2002,** *18* (15), 5755-5760.

36. Sauerbrey, G., Verwendung von Schwingquarzen zur Wägung dünner Schichten und zur Mikrowägung. *Zeitschrift für Physik* **1959,** *155* (2), 206-222.

37. Banerjee, I.; Pangule, R. C.; Kane, R. S., Antifouling Coatings: Recent Developments in the Design of Surfaces That Prevent Fouling by Proteins, Bacteria, and Marine Organisms. *Advanced Materials* **2011,** *23* (6), 690-718.

38. Jeon, S. I.; Andrade, J. D., Protein—surface Interactions in the Presence of Polyethylene Oxide: II. Effect of Protein Size. *Journal of Colloid and Interface Science* **1991,** *142* (1), 159-166.

Chapter 6

General Discussion and Future prospects

General Discussion

Numerous antifouling surfaces were designed and extensively studied for various applications.[1-7] The dramatic increase in research publications on the antifouling and bioactive surfaces highlights the importance of this area of research. In this thesis, the main focus was on creating light-tunable and, in further stages, oxygen-tolerant and heavy-metal free methods for achieving antifouling, functional and bioactive surfaces.

In the strive towards simple and versatile techniques for the creation of antifouling bioactive and functional coatings, two main techniques were developed: surface-initiated visible-light-triggered living radical polymerization (LT-LRP) (explored in chapter 2)[8] and Surface-Initiated Photoinduced Electron Transfer-Reversible Addition–Fragmentation Chain Transfer Polymerization (SI-PET-RAFT) (explored in Chapters 3,4,5).[9-10] The LT-LRP technique allowed polymer brushes synthesis with an unparalleled level of control and tunability by light. Those aspects thus allowed the creation of precisely controlled three-dimensional, bioactive poly(HPMA)-poly(CBMA) diblock architectures on the surfaces. On the other hand, the SI-PET-RAFT – that provided average control of the polymerization – provided a highly desirable oxygen-tolerant and heavy-metal free polymerization method. The requirements of more traditional techniques – such as surface-initiated atom transfer radical polymerization (SI-ATRP)[3, 11] – of an oxygen-free environment and, in some cases, the use of Schlenk lines to create antifouling coatings, make such techniques hard to apply for non-specialists and seriously hampers mass manufacturing. Thus, one of the crucial aspects of the SI-PET-RAFT technique is oxygen-tolerance. It will allow non-specialists use with almost no special equipment needed and can, in principle, even be scaled up further to ship's hull coatings and mass production of next-generation diagnostic devices. We have conducted an additional experiment utilizing the most successful antifouling monomer by this technique described in Chapters 3-5 by just sunlight, yielding thickness 23 nm after 15 min of polymerizations. (Figure 1)

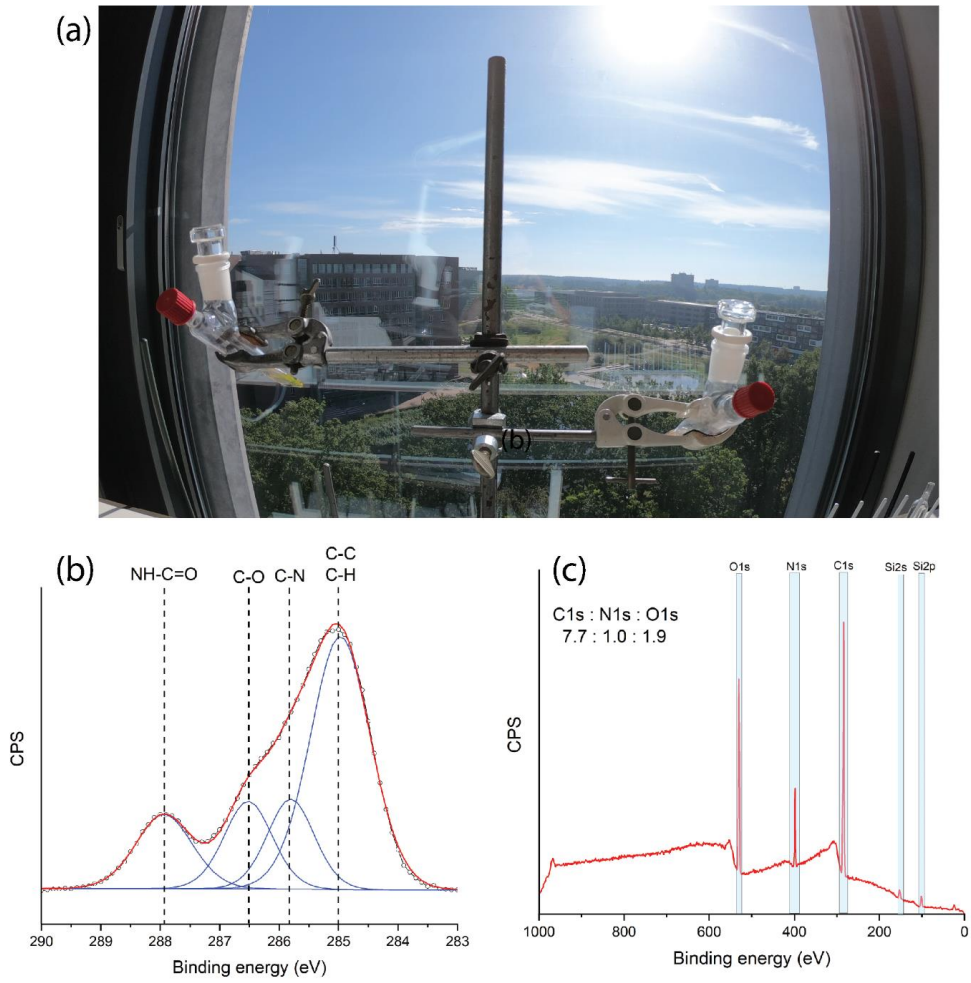

Figure 1. SI-PET-RAFT polymerization of HPMA on silicon surface by sunlight (a) experimental setup in 8040 lab in Helix building in Wageningen University. (b) XPS narrow C1s scan of obtained poly(HPMA) brush. (c) XPS wide scan of poly(HPMA) after 15 min of polymerization.

The control over the polymerization grafting density, overall structure, and homogeneity over the surfaces are important aspects of creating antifouling polymer brushes.[12] The roughness, grafting density, and overall structure and homogeneity affects the antifouling performance of polymer brushes.[12-13] Another aspect of the controlled polymerizations is their living nature. This property allows the formation of more complex architectures on the surface, in particular diblock copolymer brushes. Those structures have a unique potential to

combine the best possible antifouling properties with a high loading of bioactive moieties at the top of the coating, which is ideal for developing bioactive surfaces.[8, 14]

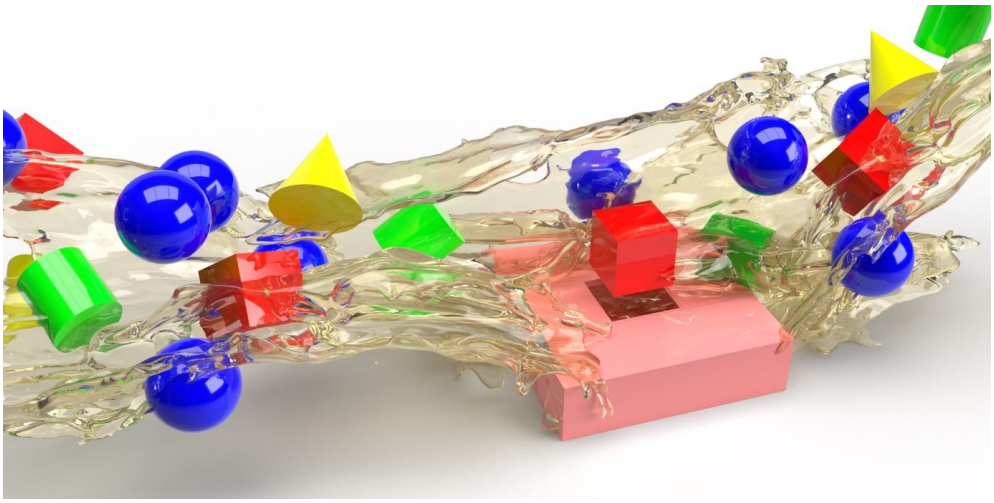

Figure 2. Schematic depiction of bioactive antifouling surfaces that interact specifically only with certain biomolecules.

The antifouling surfaces can have numerous applications on their own, but the true summit of their capabilities is for them to be an integral part of bioactive surfaces.[15] Those surfaces play a crucial role in biosensors and tissue engineering, interacting specifically only with certain biomolecules or cells (Figure 2). This means that the introduction of the bioactive moiety in the antifouling polymer brush is the second challenging task. It has become quite obvious that using the side chains of the whole brush for attaching biomolecules affects the antifouling properties of the system (Figure 3). Solving the problem of polymer brush biofunctionalization has, therefore, been attempted by combining two main aspects: chemical and architectural control. The chemistry of the attachment of biomolecules to the polymer brushes has utilized many different approaches, such as “click” chemistries based on azide-alkyne cycloadditions,[16] (inverse electron-demand) Diels–Alder cycloadditions and derived chemistries,[12] active ester chemistries such as NHS/EDC,[5-6, 8], etc. While the oldest of these, active ether NHS/EDC chemistry has stayed the most popular post-polymerization modification of polymer brushes, likely given its easy application for a wide range of compounds. This can be easily explained by the near-ubiquitous presence of amine groups in bioactive agents, such as antibodies, peptides, and proteins. The architecture approaches aim

to focus on only some of the polymer brush's side groups, using a post-polymerization modification of side chains, to obtain either of the four options: uniform monoblock modifications, random or diblock copolymer approaches that allow functionalizing part of the brush, or end chain functionalization (Figure 3). The aspect of creating random and diblock copolymer brushes was explored in chapters 2 and 4, 5. The degree of functionalization, the resulting bioactivity, and the effects on the antifouling properties were investigated in more detail in chapter 2. Our research has confirmed that the use of diblock polymer brushes provides the possibility for a high capture of model analytes, and actually even higher than full side-chain functionalization of a single block of CBMA based polymer brush. We further explored the possibility of introducing a CBMA moiety using SI-PET-RAFT in poly(HPMA) diblock and random copolymers.

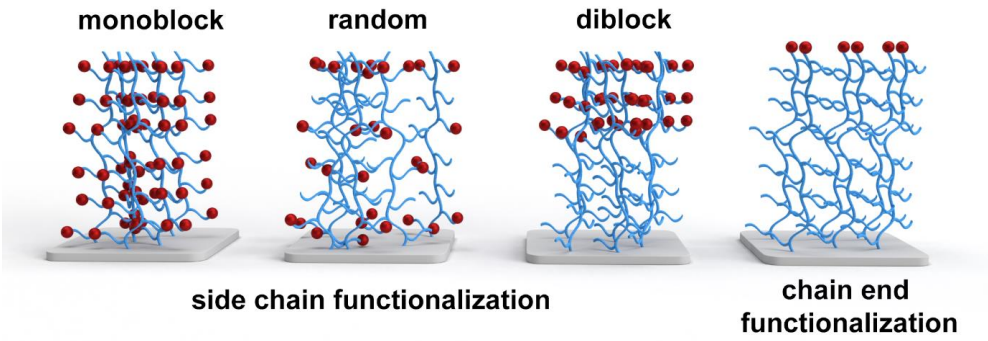

Figure 3. Different architectural pathways for the functionalization of polymer brushes.

The “grafted-from” polymer brush as a complex polymer system caused many debates around the question “What is actually on the surface?”. It also induced a search for “grafted-to” alternatives for the creation of polymer brush systems. The search for a method to build a high grafting-density polymer brush system in one step via a “grafted-to” approach may have some successes. Still, for now, the grafting density of “grafted-from” polymer systems and architecture was not fully reproduced by “grafted-to” attempts.[17-18] One of such attempts towards a “grafted-to” approach was further explored with bottle brush structures based on PLL-HPMA in chapter 4. The one-step immobilization of PLL-HPMA bottle brushes achieved by this technique did not achieve the thickness and grafting densities of “grafted-from”

polymer brushes – as e.g. observed from XPS and ellipsometry measurements – yet they displayed good antifouling properties against single-protein solutions.

The *N*-(2-Hydroxypropyl) methacrylamide or HPMA monomer was the favorite monomer throughout this thesis for the construction of antifouling layers, and it was applied in all chapters of this thesis. The research on HPMA-based antifouling coatings evidenced that little is known about the complex behavior of even more complex biological matrixes such as human serum and bovine serum on different types of antifouling surfaces. The question about the mechanisms of fouling resistance on the overall non-zwitterionic, non-charged coatings and, to some extent, zwitterionic coatings remain open. The antifouling mechanisms of non-charged polymer brushes like poly-HPMA and zwitterionic polymer brushes may be significantly different, e.g. because the water affinity and interactions between polymer chains are significantly different. The full understanding of the interactions of complex biological media with artificially created bioactive antifouling coatings will open new horizons for biosensing, tissue engineering, implants, drug delivery, and biomimetic research.

Future prospects

The antifouling polymer brush-based coatings have demonstrated, in both the work described in this thesis and in many other publications, remarkable antifouling capabilities close to 0 pg·mm^2, or more correctly: close to the detection limit of the fouling monitoring technique.[4, 7, 11] In the lab environment, those coatings were applied as bases of bioactive surfaces for numerous biosensors. Nevertheless, those coatings are not used in the mass manufacturing of biosensing or tissue engineering devices. Likely, the complexity of the synthesis of those coatings plays a big part in the lack of large-scale applications. We claim that this is about to change with the techniques developed in this thesis: SI-PET-RAFT is the first of the techniques that may bring covalently bound polymer brushes towards mass manufacturing as it is both robust, easy to use, and highly scalable.

Search for the perfect monomer to create antifouling and, more importantly, bioactive antifouling coatings is still ongoing. Initially, it has long been considered that highly hydrophobic coatings (water contact angle much higher than 100°)[19-20] would provide effective antifouling properties. Next, hydrophilic self-assembled monolayers were introduced in the 1990s. Those layers provided good resistance to single-protein solutions but poor resistance towards complex biological media. The introduction of polyethylene glycol

and highly hydrophilic zwitterionic layers (water contact angle < 20 °) provided a remarkable resistance towards fouling from complex biological liquids.[4-5, 21-23] The next step was HPMA monomer that broke a paradigm of highly hydrophilic layers with water contact angle ranging from 40 to 45°.[4, 7, 11] Do we make an almost full circle? From hydrophobic to hydrophilic to less hydrophilic layers? Will the next best antifouling monomer be superhydrophobic? The interactions with water and attempts to mimic nature will be crucial aspects for the next antifouling monomer design. The other aspect that will be considered is the easy biofunctionalization of monomers. Thus, the monomer hybrid of HPMA with an oligoethylene bridge to the carboxyl group for easy functionalization may be an interesting option. The oligoethylene bridge may provide the necessary gap between the antifouling part that interacts and the water structure and the biofunctionazable part (Figure 4).

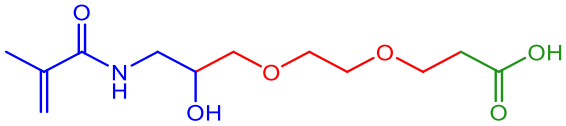

Figure 4. Suggested structure of next-generation antifouling and biofunctionalizable monomers for the creation of bioactive surfaces based on HPMA (full name: 3-(2-(2-hydroxy-3-methacrylamidopropoxy)ethoxy)propanoic acid).

Most of the work described in this thesis was done on silicon, silicon nitride or gold surfaces. The functionalization of those layers is performed by different types of chemistries, such as silane-based chemistry for silicon,[21, 23] thiol-based attachment for gold,[5-6, 12] etc. It is no secret that the structure of the initial monolayers of initiators and RAFT agents is slightly different from the surface to surface. It also should be noted that antifouling and bioactive coatings are required on different types of surfaces. Thus, another future research direction in this area may thus focus on the application of surface-independent approaches, for example, based on dopamine and tannic acid for grafted-to or grafted-from polymer brush growth. Progress in that direction was made utilizing dopamine as an anchoring layer for antifouling layers[24] or by the creation of dopamine-zwitterionic structures for the one-step immobilization of antifouling or bioactive coatings on the surface.[18] This approach may provide a viable alternative to the SI-PET-RAFT technique. While finally, since "one size fits all" - solutions in science are rare, it may be feasible and/or necessary to combine such a

surface-independent approach with SI-PET-RAFT, and as far as I can imagine this is the future of the research in and applications of antifouling bioactive coatings.

References

1. Williams, D. F., On the Nature of Biomaterials. *Biomaterials* **2009,** *30* (30), 5897-5909.

2. Rodriguez-Emmenegger, C.; Avramenko, O. A.; Brynda, E.; Skvor, J.; Alles, A. B., Poly(HEMA) Brushes Emerging as a New Platform for Direct Detection of Food Pathogen in Milk Samples. *Biosensors and Bioelectronics* **2011,** *26* (11), 4545-4551.

3. Baggerman, J.; Smulders, M. M. J.; Zuilhof, H., Romantic Surfaces: A Systematic Overview of Stable, Biospecific, and Antifouling Zwitterionic Surfaces. *Langmuir* **2019,** *35* (5), 1072-1084.

4. van Andel, E.; Lange, S. C.; Pujari, S. P.; Tijhaar, E. J.; Smulders, M. M. J.; Savelkoul, H. F. J.; Zuilhof, H., Systematic Comparison of Zwitterionic and Non-Zwitterionic Antifouling Polymer Brushes on a Bead-Based Platform. *Langmuir* **2019,** *35* (5), 1181-1191.

5. Lísalová, H.; Brynda, E.; Houska, M.; Víšová, I.; Mrkvová, K.; Song, X. C.; Gedeonová, E.; Surman, F.; Riedel, T.; Pop-Georgievski, O.; Homola, J., Ultralow-Fouling Behavior of Biorecognition Coatings Based on Carboxy-Functional Brushes of Zwitterionic Homo- and Copolymers in Blood Plasma: Functionalization Matters. *Analytical Chemistry* **2017,** *89* (6), 3524-3531.

6. Jiang, S.; Cao, Z., Ultralow-Fouling, Functionalizable, and Hydrolyzable Zwitterionic Materials and Their Derivatives for Biological Applications. *Advanced Materials* **2010,** *22* (9), 920-932.

7. de los Santos Pereira, A.; Rodriguez-Emmenegger, C.; Surman, F.; Riedel, T.; Alles, A. B.; Brynda, E., Use of Pooled Blood Plasmas in the Assessment of Fouling Resistance. *RSC Advances* **2014,** *4* (5), 2318-2321.

8. Kuzmyn, A. R.; Nguyen, A. T.; Zuilhof, H.; Baggerman, J., Bioactive Antifouling Surfaces by Visible-Light-Triggered Polymerization. *Advanced Materials Interfaces* **2019,** *6* (12), 1900351.

9. Kuzmyn, A. R.; Nguyen, A. T.; Teunissen, L. W.; Zuilhof, H.; Baggerman, J., Antifouling Polymer Brushes via Oxygen-Tolerant Surface-Initiated PET-RAFT. *Langmuir* **2020,** *36* (16), 4439-4446.

10. Roeven, E.; Kuzmyn, A. R.; Scheres, L.; Baggerman, J.; Smulders, M. M. J.; Zuilhof, H., PLL–Poly(HPMA) Bottlebrush-Based Antifouling Coatings: Three Grafting Routes. *Langmuir* **2020,** *36* (34), 10187-10199.

11. Rodriguez-Emmenegger, C.; Brynda, E.; Riedel, T.; Houska, M.; Šubr, V.; Alles, A. B.; Hasan, E.; Gautrot, J. E.; Huck, W. T. S., Polymer Brushes Showing Non-Fouling in Blood Plasma Challenge the Currently Accepted Design of Protein Resistant Surfaces. *Macromolecular Rapid Communications* **2011,** *32* (13), 952-957.

12. Kuzmyn, A. R.; de los Santos Pereira, A.; Pop-Georgievski, O.; Bruns, M.; Brynda, E.; Rodriguez-Emmenegger, C., Exploiting End Group Functionalization for the Design of Antifouling Bioactive Brushes. *Polymer Chemistry* **2014,** *5* (13), 4124-4131.

13. Ahmed, S. T.; Leckband, D. E., Protein Adsorption on Grafted Zwitterionic Polymers Depends on Chain Density and Molecular Weight. *Advanced Functional Materials* **2020,** *30* (30), 2000757.

14. de los Santos Pereira, A.; Riedel, T.; Brynda, E.; Rodriguez-Emmenegger, C., Hierarchical Antifouling Brushes for Biosensing Applications. *Sensors and Actuators B: Chemical* **2014,** *202*, 1313-1321.

15. Yu, Q.; Zhang, Y.; Wang, H.; Brash, J.; Chen, H., Anti-fouling Bioactive Surfaces. *Acta Biomaterialia* **2011,** *7* (4), 1550-1557.

16. Lange, S. C.; van Andel, E.; Smulders, M. M. J.; Zuilhof, H., Efficient and Tunable Three-Dimensional Functionalization of Fully Zwitterionic Antifouling Surface Coatings. *Langmuir* **2016,** *32* (40), 10199-10205.

17. Morgese, G.; Benetti, E. M., Polyoxazoline Biointerfaces by Surface Grafting. *European Polymer Journal* **2017,** *88*, 470-485.

18. Sun, F.; Wu, K.; Hung, H.-C.; Zhang, P.; Che, X.; Smith, J.; Lin, X.; Li, B.; Jain, P.; Yu, Q.; Jiang, S., Paper Sensor Coated with a Poly(carboxybetaine)-Multiple DOPA Conjugate via Dip-Coating for Biosensing in Complex Media. *Analytical Chemistry* **2017,** *89* (20), 10999-11004.

19. Zhang, H.; Chiao, M., Anti-fouling Coatings of Poly(dimethylsiloxane) Devices for Biological and Biomedical Applications. *Journal of Medical and Biological Engineering* **2015,** *35* (2), 143-155.

20. Molena, E.; Credi, C.; De Marco, C.; Levi, M.; Turri, S.; Simeone, G., Protein Antifouling and Fouling-release in Perfluoropolyether Surfaces. *Applied Surface Science* **2014,** *309*, 160-167.

21. Nguyen, A. T.; Baggerman, J.; Paulusse, J. M. J.; Zuilhof, H.; van Rijn, C. J. M., Bioconjugation of Protein-Repellent Zwitterionic Polymer Brushes Grafted from Silicon Nitride. *Langmuir* **2012,** *28* (1), 604-610.

22. Laschewsky, A.; Rosenhahn, A., Molecular Design of Zwitterionic Polymer Interfaces: Searching for the Difference. *Langmuir* **2019,** *35* (5), 1056-1071.

23. Nguyen, A. T.; Baggerman, J.; Paulusse, J. M. J.; van Rijn, C. J. M.; Zuilhof, H., Stable Protein-Repellent Zwitterionic Polymer Brushes Grafted from Silicon Nitride. *Langmuir* **2011,** *27* (6), 2587-2594.

24. Pop-Georgievski, O.; Rodriguez-Emmenegger, C.; Pereira, A. d. l. S.; Proks, V.; Brynda, E.; Rypáček, F., Biomimetic Non-fouling Surfaces: Extending the Concepts. *Journal of Materials Chemistry B* **2013,** *1* (22), 2859-2867.

Summary

This thesis centered on the study and development of control light-triggered techniques for the creation of polymer brushes. The designed structures are applied as antifouling and bioactive coatings.

Chapter 1 provides a general introduction to the problem of protein fouling and ways to curb it. This chapter focuses on the antifouling polymer brushes and on methods and techniques to create those structures on the surface. This chapter also dives into mechanisms of the control polymerizations such as ATRP and RAFT as main techniques for the creation of polymer brushes. The light-triggered control polymerization mechanism and techniques applied in the next chapters are also discussed in detail.

Hierarchical bioactive surfaces are introduced in ***Chapter 2*** for future application in biosensing and tissue engineering. Those surfaces are created by visible light-induced surface-initiated living radical polymerization employing tris[2-phenylpyridinato-C2,N]iridium(III) as a photocatalyst. The hierarchical antifouling diblock copolymer structures consist of *N*-(2-hydroxypropyl)-methacrylamide (HPMA; first block) and carboxybetaine methacrylate (CBMA; second block). The living nature of the polymerization is shown by a linear increase in layer thickness over time (as measured by atomic force microscopy, AFM), and by the possibility for reinitiation of the polymerization to create a patterned second block of the polymer. The chemical structure of the brushes is confirmed by X-ray photoelectron spectroscopy (XPS) and attenuated total reflection infrared spectroscopy (IRRAS) measurements. The block copolymer brushes demonstrate excellent antifouling properties when exposed to single-protein solutions or to bovine serum. The second carboxybetaine block of the hierarchical antifouling structures can effectively be biofunctionalized with an anti-fibrinogen antibody. The coated surfaces show a high affinity and specificity to fibrinogen while preventing non-specific adsorption from other proteins in bovine serum.

We used the gained knowledge of controlled photopolymerization for further exploration of applications of surface-initiated photoinduced electron transfer–reversible addition-fragmentation chain transfer (SI-PET-RAFT) polymerization in water (***Chapter 3***). This novel process proceeds in an aqueous environment under atmospheric conditions without any prior degassing, and without the use of heavy metal catalysts, with Eosin Y and triethanolamine as catalysts for the synthesis of antifouling polymer brushes. The versatility of the method is shown by using three chemically different monomers: oligo(ethylene glycol) methacrylate,

HPMA, and CBMA. In addition, the light-triggered nature of the polymerization allows the creation of complex three-dimensional structures. The composition and topological structuring of the brushes is confirmed by XPS and AFM. The kinetics of the polymerizations are followed by measuring the layer thickness with ellipsometry. The polymer brushes demonstrate excellent antifouling properties when exposed to single-protein solutions and complex biological matrices such as diluted bovine serum. This method thus presents a new simple and robust approach for the manufacturing of antifouling coatings for biomedical and biotechnological applications.

We further push the SI-PET-RAFT boundaries for the creation of PLL-HPMA bottlebrushes as antifouling coatings in ***Chapter 4***. The poly(HPMA) side chains, grown by PET-RAFT polymerization, provide antifouling properties to the surface. In this chapter such brushes are prepared in three different ways, and subsequently investigated for their antifouling potential. First, the PLL-HPMA coatings are synthesized in a bottom-up fashion through a grafting-from approach. In this route, the PLL is self-assembled onto a surface, after which a polymerization agent is immobilized, and finally HPMA is polymerized from the surface. In the second explored route the PLL is modified in solution by a RAFT agent to create a macroinitiator. After self-assembly of this macroinitiator, the HPMA is polymerized from the surface by RAFT. In the third and last route, the whole PLL-HPMA bottlebrush is synthesized in solution. To this end, HPMA is polymerized from the macroinitiator in solution and the PLL-HPMA is then self-assembled onto the surface in just one step (grafting-to). Additionally, in this third route, we also design and synthesize a bottlebrush polymer with a PLL backbone and HPMA side chains that contain 5% CBMA monomers that allow for additional (bio)functionalization in solution or after surface immobilization.

These three routes are evaluated with respect to the following terms: ease of synthesis, scalability, ease of characterization, and a preliminary investigation of their antifouling performance. All three coating procedures result in coatings that show good antifouling properties in single-protein antifouling tests. This method thus presents a new, simple, versatile, and highly scalable approach for the manufacturing of PLL-based bottlebrush coatings that can be synthesized partly or completely on the surface or in solution, depending on the desired production process and/or application.

In ***Chapter 5***, SI-PET-RAFT was applied for the creation of antifouling polymer brushes on gold surfaces. The living nature of this method allowed the creation of random and diblock copolymer brushes based on HPMA and CBMA. The introduction of the CBMA into the polymer brushes opens the route for further brush functionalization by versatile active ester chemistry. The chemical composition of the brushes was confirmed by XPS, and the polymer brush thickness was determined by spectroscopic ellipsometry. The polymer brushes demonstrate good antifouling properties against undiluted human serum monitored by quartz crystal microbalance with dissipation (QCMD-D) and surface plasmon resonance (SPR) spectroscopy in real-time. This approach further widens the road towards building highly antifouling and still functional copolymer brushes in a scalable, robust, oxygen-tolerant, and the heavy metal-free way that opens up applications in biosensing and tissue engineering.

Chapter 6 discusses and highlightes previous chapters with a focus on open questions in antifouling, polymer brushes, and surface modification research. It also looks at the future of this research, in particular to perfect antifouling and functional monomers, and surface-independent approaches for the surfaces modification.

Acknowledgment

Acknowledgment

Science is never done alone. One way or another, we are part of a complex interconnected network of people. The COVID-19 pandemic and its social distancing measures are further proof of this statement. Decisions, actions, achievements, and failings of one ultimately will affect another. We move seamlessly alone through the path of life with some occasional interaction with family, friends, colleagues, and even random strangers. But in those particular moments, those small things make a huge course correction to our life path, some of which we will understand in many further stages of our lifepaths. Thus, this lengthy acknowledgment will allow me to thank many people who contributed to my life and scientific path.

Wow! I'm actually writing this part hah 😊 *I thought we would never reach this part ahah… So Welcome to the season finale!...* 😊

First and foremost, incredible thank you to my parents *Anna (Анна)* and *Roman (Роман)*. My sister *Olia (Оля)* who became a constant source of strength and understanding. Incredible thank you to my family and grandparents *(Дідові Богдан, Бабі Наді, Дідові Богдану і Бабі Миросі Дякую!!!)* for allowing me to build a minilab in my own room during my teenage years where different types of questionable experiments with copper salts were conducted. Ten years on from then I used similar copper salts in Prague for fancy ATRP polymerizations.

Taras and *Olia Danysh (Тарас* і *Оля Даниш)* are acknowledged for allowing me to count white blood cells at the Institute of Blood Pathology and transfusion medicine as part of my high school research projects. 6 years on from that time this work inspired a UNESCO/IUPAC application for a research program in blood antifouling surfaces.

Taras Skorokhoda (Тарас Скорохода), *Anna Riabtseva, Olena Fedorova (Федорова Олена Валеріївна)*, *Volodymyr Novikov (Новіков Володимир Павлович)* and *Zoryana Gubriy (Губрій Зоряна Василівна)* are thanked for inspiring me to do a research career and in particular polymer chemistry research. Also, *Taras* for encouraging me to do science in a foreign country and application for UNESCO/IUPAC course. *Viktor Zvarych (Віктор Зварич)* for being a great friend and our numerous scientific discussions that inspired many interesting ideas and many to come. *Solomiya Tymtsiv (Соломія Тимців)*, *Natalia Fudyga* (*Наталя Фундига/Василів*) and *Olena Gumenna (Олена Гуменна)* are acknowledged for numerous support moments.

Eduard Brynda for being a great mentor and providing me the opportunity to start my research career as a UNESCO/IUPAC student in the Institute of Macromolecular Chemistry in Prague. Thank you!

Cesar Rodriguez-Emmenegger, *Andres de los Santos Pereira*, and *Nina Yu. Kostina* are acknowledged for the life and scientific lessons and experience that you have provided me.

Ognen Pop-Georgievski, thank you for the introduction and insights to numerous surface analysis techniques, in particular ellipsometry! 🍾😊

Special thanks to the team of the Institute of Macromolecular Chemistry in Prague and Christopher Barner-Kowollik and his team in Karlsruhe Institute of Technology!

Ilya Kotelnikov (Илья Котельников) is acknowledged for being a great friend and colleague for your scientific and non-scientific advice.

Ірина Миколаївна Тихонська, Дякую!

After my research in Prague, I ended up in many IT companies. In parallel, I was applying for many, many PhD vacancies. Numerous cool ideas, some of which ended up in my papers years from that time, were born in this awesome non-researcher and non-chemical environment. My incredible thanks to *Volodymyr Artiukh [Alan], Olena Artiukh [Harmony], Michael Brasiuk [James], Ihor Hevko [Wayne],* and many others. Thank you for the many laughs that we had.

Yaroslav Stetsko [Sheldon] for being an awesome friend and a grounding rod of my numerous adventures. As well as cheering up me after numerous failed attempts to get a PhD position. Thank you, mate! *Дякую друже!*

OctenWeb Team in particular *Sergii Zhuravlov*, thank you! *Дякую!*

Ingvar Gudmundsson, Mikhail Benkovich, Elena Minakova, Helena Riabchenko, Elina Zaytseva, and all SimplyBook.me team, you are awesome! SimplyLove.it! 😊 Special thanks to *Ingvar* and *Elina* for encouraging a final push towards applying one more time for a PhD position that ended up in the next line:

Jacob Baggerman, Cees van Rijn, Michel Nielen for saying "Yes" to do a PhD in Wageningen. It was a true honor. Thank you!

Gina Ross and *Vincent O'Brien* for welcoming me to the Netherlands!

Vincent O'Brien for being a great friend and English grammar check of this acknowledgment😊 We had many clever discussions fueled by Irish whiskey. Thank you, mate!

Pepijn Beekman for an initial introduction to ORC and many jokes. Your incredible choice of music during road trips, in particular, one to Israel. Thank you!

DJ (Digvijay Gahtory) for the great collaboration in my first year of my PhD. Thank you!

Master and bachelor students that stayed in 8055 office: *Reamon Bouman, Michael Hoekstra, Margaux Tellez, Sophie van Lange, Axel Kampfraath, David Broekhuijsen, Mees Vos* and many others. Thank you, it was a true joy! In particular, *Michael Hoekstra* for encouraging the use of LED lamps in my first project (Chapter 2) that proved to be super beneficial.

Reamon Bouman, for many scientific discussions, non-scientific discussions, and in particular teaching me so many Dutch swear words. Thank you, mate! ... Teering ! 😊

Mees Vos for many awesome beers and discussions. Thank you!

Thomas Kodger thank you for the initial advice on fluorescence measurement and clever discussions.

My students *Justin Weerink, Jessie van Doesburg, Eva Hebers* for the great work that you have done for my numerous projects 😊 Thank you!

Michel de Haan for being a great friend and helping in one of my career's toughest moments. As well as numerous Avalon, Among Us, and other games played. Thank you!

Esther van Andel thank you for your advice and help in more biological matters of my project and providing different biological liquids. Thank you!

Sjoerd Slagman is acknowledged for many inspiring trumpeting songs that were heard in my lab 😊. Thank you!

Jordi Keijzer and *Ian de Bus* for an awesome PhD trip to Israel, many jokes and an awesome time! *Dank je wel !*

Han Zuilhof, our first meeting was an argument, or as you refer to it in the Netherlands a "discussion". We talked about good antifouling coatings, where I claimed that poly(HPMA) brushes were better than polyzwitterionic brushes. The constant discussion, in Ukraine, we would call it a "battle", was a true "endeavor". As once you told me, "endeavor" from French is an enjoyable journey. It was a tough but engaging journey for the next three years for me. Thank you for sticking and standing with me until the very end! It is truly appreciated! *Dank je wel!*

Elly Geurtsen, for pushing the boundaries of what's possible by bending the spacetime continuum in scheduling my meetings with *Han Zuilhof*. Thank you!

Lucas Teunissen my best buddy in polymer brushes. Thank you for being my critic, collaborator, colleague, and great friend. Many, many more awesome projects, discussions, and drinks to come! *Dank je wel, kerel!*

Sybren Schoustra, mate, for being an awesome friend. Your help in dragging me out from the most tricky and sensitive situations ever was most welcome. Great advice in organic chemistry matters. Our numerous drinks and discussions on science and far, far beyond 😊 Your accepting and cheery nature helped me a lot. Many, many scientific and non-scientific adventures to come. *Dank je wel, kerel!*

Ellen Dautzenberg thank you for the help and many scientific and non-scientific discussion that we had 😊, as well as accepting and surviving the true jerkiness of my character! Thank you!

Sevil Sahin, for surviving numerous non-pizza evening meetings at the beginning of our PhDs *heh*. 😊 Thank you for trying our unsuccessful collaborative project and many fun scientific and non-scientific discussions. Thank you!

Jay (Jayaruwan Gamaethiralalage), for many great smiling photos of me and long discussions about everything. Thank you!

Alice Guarneri, thank you for being a great friend. You are an explosion of positive energy and an amazing person that dragged me from so many lows of my PhD, and there were a lot of those. I will never understand enzymes as much as you will never understand my love for pineapple on pizza 😊. Nevertheless, I am deeply happy to have you around. Thank you for allowing me to annoy you for so long 😊.

Also, a special thank you to *Lucas* and *Sybren* for going through this whole thesis*. Ellen, Jay, Lucas, Sybren,* and *Alice* for the constructive criticism of my cover and opinions on my propositions. In particular, *Ellen* for providing the most detailed critic😊. Thank you!

Jorick Bruins, for being a great friend and providing many nice discussions that we had, as well as unsolicited cleaning of my lab. Thank you!

Dong-Dong Liang, for numerous advice and discussion on pure organic chemistry. Thank you!

Pina Fritz, for help with SPR and many laughs during Dutch class. Thank you!

Esther Roeven, for being a great friend and collaborator! We have survived the category five hurricane with our shared chapter (in this thesis chapter 4). Your support and understanding were much needed and really appreciated! *Dank je wel!*

Maarten Smulders, incredible and huge thank you for your help and your contribution to Chapter 4 and Chapter 5. Your help, advice, and understanding of my undiplomatic and straightforward character were most welcome and needed. Thank you!

Tu-Nan Gao, for allowing me to move to his office and being quiet. That provided me with the opportunity to finish chapters 1,5,6. Also our numerous debates on what is better, totalitarianism or democracy 😊 Thank you!

Natassa, for providing me with detailed knowledge of how and where to purchase different discount perfumes. Without this information chapters 1 and 6 would not be the same 😊 Thank you!

Sidhu (Sidharam Pujari), for measuring numerous XPS samples for me in the beginning of my PhD and showing me most of the equipment. Thank you!

Alyssa van den Boom, for the advice and insights in my boss's mind, particularly when to be quiet 😊. Thank you!

Simon van Hurne, for the many laughs that we had and your great clever and insightful jokes, and many discussions on polymer chemistry 😊 *Dank je wel!*

Julian Engelhardt, for surviving numerous work distractions from me. Thank you!

Ariadni Geballa Koukoula, thank you for surviving Belfast with me. Your positive and cheering character always brightened my day. It is nice to have you around! Thank you!

Judith Firet, for initial lab training and teaching advice and a lot of patience. Thank you!

Hans Beijleveld for help and advice on GPC technique. Super Thank you!

Frank Claassen for providing me with MS training every year of my PhD as I forget what to do with that machine each time, thank you for your patience!

Yuri Damen for numerous discussions and advice on hardcore organic synthesis! Thank you! *Dank je wel!*

Kaustub Singh a truly awesome time that we had teaching numerous practical courses together. Thank you!

Barend van Lagen, for introduction to most of the equipment and knighting me in order of XPS knight users. Thank you!

VLAG team and particular *Vesna Prsic* for making this PhD possible! Thank you!

… and many, many others, thank you!

Special thanks to all members of ORC for surviving my totalitarian regime of "Good Morning!"

A huge thanks to the opponents of my thesis André Laschewsky, Sissi de Beer, Axel Rosenhahn, Jasper van der Gucht, for agreeing to evaluate my thesis! Thank you!

Andriy | *Andrij* | *Андрій*

Overview of Completed Training Activities

Discipline specific activities	***Organizer***	***Year***
Summer school on Smartphone-based Assay Development & Open Science	VLAG | RIKILT	2017
Summer school on Food Applications, QA/QC and Validation	UCT	2018
FoodSmartphone Midterm review	RIKILT	2019
Dutch Polymer Days 2019	PTN | KNCV | NWO | CW-MM	2019
2019 MCAA General Assembly Annual Conference	MCAA	2019
Organic Chemistry National Symposium 2019	KNCV | NWO	2019
The 13th International Conference on "Advanced Polymers via Macromolecular Engineering" (APME 2019)	Stellenbosch University	2019
CHAINS 2019	NWO	2019
ICBZM 2019 4th International Conference on Bioinspired and Zwitterionic Materials	UT | WUR	2019
2019 #RSCPoster Twitter Conference	RCS	2019
2020 #RSCPoster Twitter Conference	RCS	2020

General course		
VLAG PhD week	VLAG	2018
Presenting with Impact	WGS	2018
Scientific Writing	WGS	2019
Summer school on Software Design and FoodSmartphone Exploitation	QUB	2019

Optionals		
Preparation of research proposal	ORC WUR	2017
PhDs study trip to Israel	ORC WUR	2019
Weekly group meetings	ORC WUR	2017-2021
Organization of PhD trip to Israel	ORC WUR	2018-2019

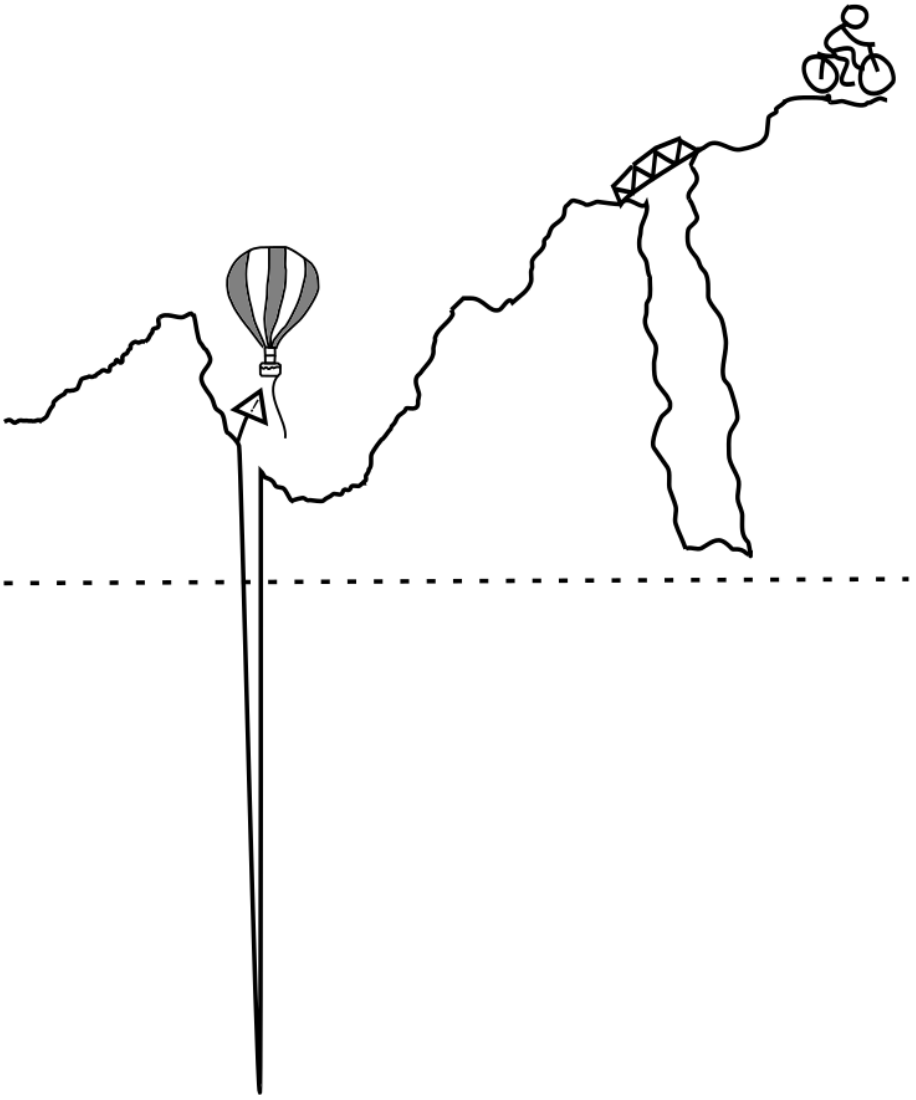

Financial support from Wageningen University for printing this thesis is gratefully acknowledged.